2015

Gold Nanomolecules : Developing Synthetic Protocols, Characterization And Investigation Of Ligand Effects On Structure And Properties

Praneeth Reddy Nimmala
University of Mississippi

GOLD NANOMOLECULES: DEVELOPING SYNTHETIC PROTOCOLS, CHARACTERIZATION AND INVESTIGATING THE LIGAND EFFECTS ON STRUCTURE AND PROPERTIES

A Dissertation presented for the Doctor of Philosophy Degree

The University of Mississippi

Praneeth Reddy Nimmala

May 2015

ABSTRACT / ORGANIZATION OF DISSERTATION

The term "Nano" in chemistry refers to particles/molecules in the size range 1 to 100 nm. Gold nanoparticles were used in ancient times in making decorative glass as they produce vibrant, size dependent, colors upon interaction with light. Gold is a preferred choice of metal for the synthesis of nanoparticles mainly due to its inertness to atmospheric conditions and most chemicals. Gold thiolate nanomolecules, which is the primary focus of this dissertation research, are chemical molecules with a fixed number of gold atoms and organo-thiolate ligands. They are of the form $Au_x(SR)_y$ and possess molecule-like properties as a result of distinctive quantum confinement effects occurring at the nanoscale size. The optical and electronic properties of these molecules change as a function of "x" and "y" in the formulation $Au_x(SR)_y$. The stability of these nanomolecules can be attributed due in part to their symmetrical geometry as evidenced by the X-ray crystallography.

Recent research in the field has focused on exploiting the size-dependent properties of gold nanomolecules in applications like nano-electronics, biological sensing and catalysis. But much of the hindrance to these advances come from the lack of established protocols to synthesize monodisperse nanomolecules in high yields. Brust-schiffrin protocol for the synthesis of nanomolecules yields stable products in a two-phase system which can be dried and re-dispersed without affecting the stability. But the protocol has a major drawback of producing a polydisperse mixture of different sizes of nanomolecules. A major portion of my dissertation focuses on addressing this issue of polydispersity of products. In this regard, I have investigated

the one-phase synthesis protocol for synthesis of gold-thiolate nanomolecules wherein the gold salt and the capping ligands are essentially dissolved in a single solvent system. This protocol is peculiar in that it yields various sizes which are otherwise not observed.

Chapter 2 of this dissertation details one such synthesis involving $Au_{67}(SR)_{35}$ nanomolecule. The synthetic protocol was optimized to maximize the yield of Au_{67} in the product. As the product of the synthesis contains multiple sizes, I developed solvent-fractionation separation protocol to isolate Au_{67} in its pure form. It involves a systematic size-based precipitation of nanomolecules by the addition of a non-solvent (methanol) to a solvent system (nanomolecules in toluene) containing polydisperse mixtures. 50+ mg of the pure Au_{67} was isolated for the first time using the above designed protocols. The high yields of the product has enabled its complete characterization using mass spectrometric techniques of MALDI (Matrix-assisted Laser Desorption Ionization) and ESI (Electro-spray Ionization), optical spectroscopy, NMR spectroscopy (Nuclear Magnetic Resonance), powder-XRD (X-ray Diffraction) and electrochemistry.

Chapter 3 of the dissertation describes the synthesis and characterization of $Au_{103\text{-}105}$ nanomolecules. It was called "103-105" as the product in this size range contains multiple species as observed in the high resolution mass spectra. The isolation and purification of this compound was achieved using size exclusion chromatography (SEC) which has proved to be highly reproducible and less laborious than solvent fractionation. After learning the basic technique from our collaborators in University of Geneva, I have optimized the process and applied it to a variety of ligands and a wide-variety of sizes (25 to 1000 Au-atom) at UM-Dass laboratory. SEC can be used to purify nanomolecules from a wide size distribution. It has now

become a method of choice in our laboratory for separation of nanomolecules like Au_{67} and $Au_{\sim 103}$.

Chapter 4 of the dissertation highlights the protocols of "etching" and "core size conversion" as a way to minimize the polydispersity of nanomolecules. In an etching reaction, a polydisperse nanomolecule mixture is treated in excess thiol at higher temperature. The less stable sizes in the mixture are decomposed while the more stable ones survive. In some cases, it is observed that some of these meta-stable sizes convert to a smaller, more stable nanomolecule. This process is termed core conversion. The phenomenon was used to study the formation of stable Au_{38} and Au_{40} nanomolecules from a mixture of larger sizes. The two sizes mentioned were always observed to co-exist in etching reactions. To understand why that happens, we have etched single-sized nanomolecules and followed the reactions with mass spectrometry. The results were interesting; Au_{38} was observed to be forming from core size conversion of nanomolecules < 15 kDa while Au_{40} was formed from the core size conversion of Au_{67} and $Au_{103\text{-}105}$. These protocols can be used to exclusively synthesize highly stable Au_{38} and Au_{40} sizes.

Chapter 5 of my dissertation highlights the role of capping ligands in determining the properties of nanomolecules; a factor which is typically overlooked in this field. We performed hundreds of etching and core conversion reactions using phenylethanethiol and observed formation of $Au_{38}(SCH_2CH_2Ph)_{24}$ or $Au_{40}(SCH_2CH_2Ph)_{24}$. But when an aromatic ligand thiophenol was used in the etching reaction, we observed the formation of $Au_{36}(SPh)_{24}$. The optical and electrochemical properties of Au_{36} were totally different from those of Au_{38}. The results indicated that aromatic ligands protect the gold core in a different way compared to the

commonly used phenylethanethiol. Ligands induce functionality to the nanomolecule while the $Au_x(SR)_y$ motif dictates the optical and electronic properties. Therefore it cannot be assumed that all ligands behave similarly on the $Au_x(SR)_y$ motif. It is also important to investigate how different ligands influence the size, geometry and properties of the nanomolecules. These studies constitute a significant part of my dissertation.

DEDICATION

I would like to take this opportunity to thank and dedicate my dissertation to all the people in my life who supported me get here. I would like to start with my parents who have worked really hard to put me in the best school available in my place; my grandfather and uncle who have always encouraged and supported me in all my endeavors; my younger brother and friends who were there by me in my good and bad times; my school teachers, professors during my undergraduate and graduate education who have selflessly supported me. Last but not the least, I would like to thank my doctoral research advisor Dr Amala Dass who has taught me great professional and personal lessons that I would keep in mind for the rest of my life.

TABLE OF CONTENTS

Contents

LIST OF FIGURES

LIST OF SCHEMES

CHAPTER I

INTRODUCTION

1.1 Gold nanoparticles

Gold nanoparticles are chemical entities composed of gold in the size range of 1-100 nm. There are multiple reasons why gold is a preferred metal of choice for the synthesis of nanoparticles; prominent ones being its inertness to atmospheric oxidation and most chemicals, and its high affinity to ligands like thiols, phosphines and citrates.[1-3] Though the scientific interest on gold nanoparticles came only in the 19th century, the use of colloidal gold for decoration and jewelry dates back to 5th century. In 1857, Michael Faraday prepared gold colloids and also discovered that a mere change in the size of the gold particles resulted in various brilliant colors of their colloidal solutions, stimulating research on the optical properties of gold nanoparticles.[4] In 20th century, Gustav Mie solved the Maxwell's equations to explain the optical properties of gold nanoparticles. The reason for these size dependent optical properties was attributed to the collective response of the conduction electrons to light.[5] Much of the current research is focused on the practical applications of gold nanoparticles in the fields of nano-electronics[6,7], biological sensing, catalysis[8,9] and medicine.[10]

1.2 Gold nanomolecules

My research work is primarily focused on the gold nanomolecules, which are ultra-small gold nanoparticles that are <2 nm in size and passivated with organo-thiolate ligands. Nanomolecules are often misconceived as nanoclusters and hence it is important to mention the

difference between these terms. Clusters do not possess a fixed composition or size and is a term commonly used to describe nano-sized polydisperse gas phase clusters which range from a few hundred to a few thousand atoms, i.e., there is often a *distribution of sizes*.[11] Some examples of clusters include molecular clusters like ammonia clusters and atomic clusters like sodium clusters. Thiolate protected gold nanomolecules on the other hand possess an exact molecular composition with a specific molecular weight, see Scheme 1.1.[12] Some of the examples of these nanomolecules include $Au_{25}(SCH_2CH_2Ph)_{18}$, $Au_{36}(SPh)_{24}$ and $Au_{144}(SC_6H_{13})_{60}$. $Au_{25}(SR)_{18}$ contains 25 Au atoms and 18 SR ligands with a error/deviation of 0 atoms.

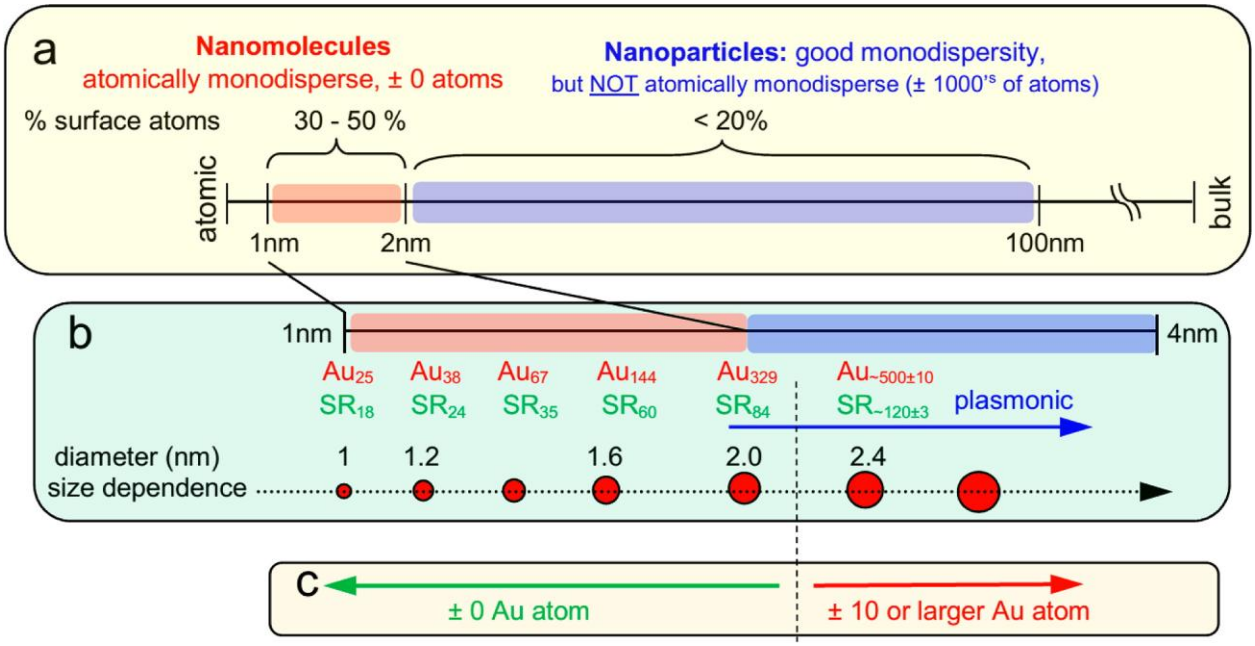

Scheme 1.1. (a) The 1−100 nm regime with nanomolecules in the 1−2 nm region, and nanoparticles in the 2−100 nm regime (where very good monodispersity has been achieved, but the size distribution is still ±1000's of atoms or a few nanometers). (b) Thiolated gold nanomolecules, such as Au_{25}, Au_{38}, Au_{67}, Au_{144}, and Au_{329} with a precise number of metal atoms

and organic ligands and $Au_{\sim 500\pm 10}(SR)_{\sim 120\pm 3}$. (c) The dashed line, between 329−and 500−atom sizes, indicating the transition between the fixed composition containing nanomolecules region, with±0 Au atom variation versus polydisperse $Au_{\sim 500\pm 10}(SR_{)\sim 120\pm 3}$ particles, with a ±10 Au atom variation. Reprinted with permission from Journal of American Chemical Society, **2014**, *136* (20), pp 7410–7417. Copyright 2014 American Chemical Society.

The unique size-dependent properties of gold nanomolecules draws great attention to this field of research. These gold nanomolecules are chemically different from their larger analogues like bulk gold or colloidal nanoparticles. Nanomolecules possess molecule-like properties, which are a result of distinctive quantum confinement effects induced by their ultra-small size.[13,14]. Sizes like $Au_{25}(SCH_2CH_2Ph)_{18}$ have a large HOMO-LUMO gap and distinct optical absorption bands in the UV-vis region, which are typical of small organic molecules. The distinct optical properties are a result of the quantum confinement effects. [15,16] The large gold nanocrystals (>2nm) on the other end show surface plasmon resonance (SPR) band in the UV-vis region near ~530 nm. SPR is the result of the collective response of conduction electrons to the incoming radiation. Within the size range of 0 to 2 nm, gold nanomolecules with different combinations of gold and ligands are observed and can be represented in the form $Au_x(SR)_y$. The optical and electronic properties of gold nanomolecules change as "x", the number of gold atoms and "y", the number of ligands change.

1.3 Structure of gold nanomolecules

Recent advances in the X-ray crystallography provide an understanding of the three-dimensional arrangement of gold atoms and ligands in the structure of gold nanomolecules. The atomic structure is key in understanding the stability of certain combinations of gold atoms and

ligands over others. It is also interesting to compare how the atomic structure varies with the size of the nanomolecules. The basic structure of the gold-thiolate nanomolecules comprises a highly symmetric central Au core surrounded by staple motifs. Two of the commonly observed staple motifs are: a) short staples of the form -SR-Au-SR- and b) long staples of the form -SR-Au-SR-Au-SR-. With evolving research in this area, there are many new motifs being added to this list.[17]

The most commonly used ligands in the synthesis of gold nanomolecules are phenylethanethiol ($PhCH_2CH_2SH$). Although crystal structures of smaller nanomolecules like $Au_{25}(SR)_{18}$ and $Au_{38}(SR)_{24}$ have been obtained using phenylethanethiol and hexanethiol ligands, it is still a major challenge to grow X-ray quality crystals of larger nanomolecules. Au_{102}(p-MBA)$_{44}$ (where p-MBA = SPhCOOH) reported by Kornberg's group in 2007 is by far the largest nanomolecule to be crystallized.[18] We anticipate that capping the Au_{102} nanomolecule with an aromatic ligand like p-MBA imparts rigidity to the structure thereby favoring crystal formation. The role of aromatic ligands in obtaining X-ray quality crystals of gold nanomolecules is discussed in detail in chapter 5.

1.4 Developing synthetic protocols for gold thiolate nanomolecules

Synthesis of highly monodisperse nanomolecules with high yields is a key issue that requires much attention and research. Gold thiolate nanomolecules exhibit interesting size-dependent optical and electrochemical properties. For example, $Au_{25}(SCH_2CH_2Ph)_{18}$ is only ~0.2 nm less in diameter than $Au_{38}(SCH_2CH_2Ph)_{24}$ but the properties of both are totally distinct. In order to develop potential applications, it is important to establish protocols for synthesizing different nanomolecules sizes in a robust and easy to scale up approach. Unlike the clusters that are synthesized in gas-phase, these nanomolecules are synthesized via a wet chemistry approach,

which demands optimization of several parameters at different steps in the synthesis.

Brust et al. established the basic route for the synthesis of ultrasmall gold thiolate nanomolecules in 1994, stimulating tremendous interest in this area. Later, the Brust-Schiffrin method was modified and a simple one-phase synthetic protocol was developed. These two protocols are still the most widely used techniques owing to their reproducibility and ease of synthesis.[19,20]

1.4.1 Brust Schiffrin method

Reported in 1994 and often referred to as the Brust Schiffrin two phase synthesis[19], it is the first wet chemical approach to synthesize ultra-small gold nanomolecules of the size <2 nm. Prior to this, there were protocols for the synthesis of gold colloid solutions in two-phase systems. Faraday synthesized colloidal solutions of gold in a two phase system by reducing gold salt with phosphorous in carbon disulfide and obtained a ruby colored aqueous colloidal solution. Deriving inspiration from this and the recent developments in self-assembled monolayers of thiols on gold, Brust et al. developed a synthetic scheme which produced ultra-small gold nanomolecules. Unlike the colloids, the gold nanomolecules have the advantage of high stability in solutions and in dried forms.

The Brust-Schiffrin protocol involves synthesizing the gold nanomolecule cores in two-phase solutions in the presence of the passivating ligands to cap the Au cores. Au in the form of $HAuCl_4.3H_2O$ (Tetrachloroauric acid trihydrate) salt is dissolved in an aqueous phase and transferred to an organic phase using a phase-transfer agent like TOABr (tetraoctylammonium bromide). This solution is reduced with a cold aqueous solution of $NaBH_4$ (sodium borohydride, the source of electrons). Up on addition of sodium borohydride, the color of the solution turns to

black within seconds indicating the formation of gold nanomolecules in the reaction mixture. The reaction is sensitive to the ratio of ligands to gold (y:x, where y is for ligands and x is for the Au)). It is observed that higher the y/x ratio, smaller the size of the resulting nanomolecules. Sodium borohydride is the source of electrons for the reduction and is added in excess quantities (~10x of Au concentration) in this reaction. These initial reactions were successful in synthesizing ultra-small and highly stable nanomolecules, which could be isolated in dried form and re-dispersed in solutions. This reaction also paved the way for many new protocols that exist in the literature today.

1.4.2 One-phase synthesis

As discussed above, the surfactant has a key role in transferring the Au from aqueous to organic phase in a two-phase synthesis. The one-phase synthesis[20], as opposed to the two-phase synthesis, involves a surfactant-free synthesis of gold nanomolecules in one solvent, single phase system. The ingredients of the reaction are typically dissolved in a single solvent system like dichloromethane or tetrahydrofuran. When dichloromethane is used as the reaction solvent, the need for TOABr is eliminated by dissolving $HAuCl_4.3H_2O$ salt in a small volume (~1% of total reaction volume) of ethanol.[20] When using THF as the reaction solvent, there is no need for other solvents as the gold salt is completely soluble in THF. There are advantages as well as challenges associated with the one-phase synthetic approach. The key advantage is the ability to produce certain core sizes of nanomolecules that are otherwise not easily synthesized and isolated. For example, it is extremely difficult to synthesize isolable quantities of Au_{67} and $Au_{103-105}$ nanomolecules with the two phase approach whereas in this case, it is possible to isolate ~100mg scale quantities of these nanomolecules which possess unique and interesting optical

and electrochemical properties. Perhaps the reason for this change in size distribution could be attributed to the surfactant, which is adsorbed to the Au^{3+} ions with its bulky hydrophobic chains, could alter the solubility of the intermediates in the gold nanomolecule formation.[20]

Following the course of the one phase reaction with MALDI mass spectrometry gave interesting insights into the size evolution of the products after the addition of $NaBH_4$. At earlier reaction times, a mixture of Au_{25}, Au_{38}, Au_{67} and $Au_{103\text{-}105}$ are observed in the reaction mixture. As time progresses, the large clusters of $Au_{103\text{-}105}$, Au_{67} and Au_{38} appear to convert to Au_{25}. Instead, data suggested that all these higher clusters decompose and only Au_{25} remains stable after 3 days. More challenges are involved when Au_{67} and $Au_{\sim 103\text{-}105}$ are the desired products. It is difficult to isolate Au_{67} and $Au_{103\text{-}105}$ from this synthesis. The first challenge is that one-phase reactions are highly sensitive to the gold to thiol ratio. It is critical to maintain an accurate ratio of gold to thiol for obtaining desired products. The second challenge, as mentioned above, is that the nanomolecule size distribution in the product changes significantly with time after the addition of reducing agent. For example, when the goal of the one phase synthesis is to obtain Au_{67} and $Au_{103\text{-}105}$ in high yields, it is important to stop the reaction exactly 5 minutes after the addition of $NaBH_4$. Every minute after that, the size distribution of the product shifts to lower mass. Nevertheless, this approach of synthesis has proven to be of high value in all my projects and will be discussed repeatedly.

1.4.3 Post synthetic separation of polydisperse products

The major drawback associated with most of the synthetic techniques is the polydispersity of the resulting product, which means that there is more than a single sized nanomolecule in it. Polydispersity creates ambiguity when we are trying to study the

characteristics of a certain component present in the mixture. In the literature, Au_{25} is the only nanomolecule that can be obtained in monodisperse form using a one-phase approach without any post-synthetic treatment. All the other nanomolecules require either a post synthetic separation/purification or etching procedure. There are two basic separation techniques employed in the separation/purification of nanomolecules, namely solvent fractionation and size exclusion chromatography. Mechanical methods like centrifugation could separate nanomolecules when the components are separated by a high mass value. For example, centrifugation can separate sizes of Au_{25} (~7000 Da) and Au_{144} (~36000 Da) but not Au_{67} (18000 Da) and $Au_{\sim 103}$ (27 kDa).

1.4.3.1 Solvent fractionation of gold nanomolecules

Solvent fractionation procedure was a vital part of this dissertation research as it was applied in isolation and characterization of nanomolecules like Au_{67} and $Au_{103\text{-}105}$ in ~100mg quantities for the first time. It is a systematic size-based precipitation of nanomolecules by the addition of a non-solvent to a solution of nanomolecule mixture. We exploit the size-dependent solubility properties of gold nanomolecules in solvent fractionation. The process starts by *complete* dissolution the polydisperse nanomolecules in a solvent and adding a non-solvent to facilitate the precipitation of the largest sized nanomolecule. The soluble fraction is separated from the insoluble fraction and analyzed using MALDI mass spectrometry.[12]

Figure 1.1 shows the systematic separation of $Au_{103\text{-}105}$ from a mixture of Au_{25}, Au_{67} and $Au_{103\text{-}105}$. The polydisperse mixture was dissolved in toluene, which gives a completely soluble solution. To this solution, a non-solvent, methanol, was added drop wise. As observed in the mass spectra, the largest component $Au_{\sim 103\text{-}105}$ systematically precipitated with subsequent

fractionations. $Au_{103\text{-}105}(SCH_2CH_2Ph)_{44\text{-}46}$ is the largest component in the mixture with the highest number of the non-polar ligands in this case. Non-polar nature makes this nanomolecule soluble in a non-polar solvent like toluene/dichloromethane. In this case, due to the highest non-polar nature, it is the first size to precipitate as the polar solvent (non-solvent) is added to this mixture.

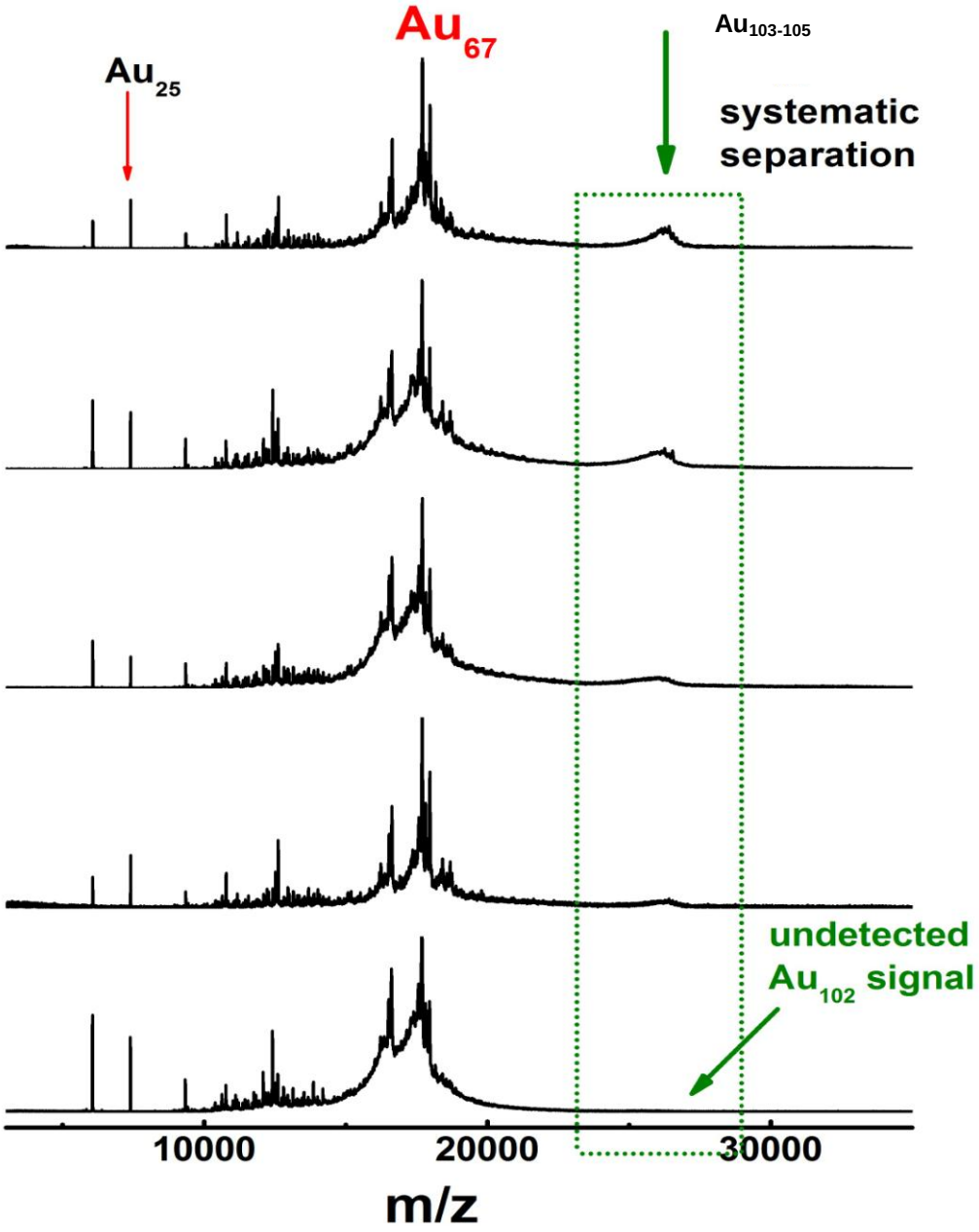

Figure 1.1: Illustration of a solvent fractionation procedure. MALDI spectra showing the systematic precipitation of $Au_{103-105}$ from a polydisperse mixture of Au_{25}, Au_{67} and $Au_{103-105}$. The top spectrum in the figure has peaks at mass of ~27000 Da, whose intensity decreases with each fractionation until it is not detected in the bottom spectra. From top to bottom each spectrum corresponds to the soluble portions obtained from consecutive fractionation steps.

1.4.3.2 Size exclusion chromatography

Size exclusion chromatography for purification of gold nanomolecules is a very recent development. It is a chromatographic process that employs porous beads to separate nanomolecules based on the size.[21]

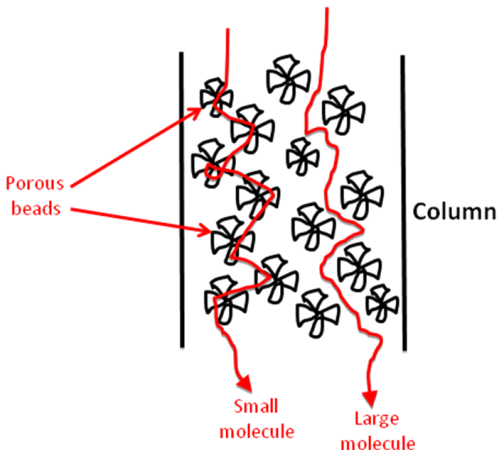

Figure 1.2: Illustration of a size exclusion chromatographic separation. Smaller molecules pass through multiple pores and hence elute last.

As depicted in the figure 1.2 above, a glass column is packed with the porous beads in

THF solvent. These commercially available beads are made of polystyrene divinylbenzene and are soaked in the solvent overnight and packed into the glass column for separation. When a polydisperse nanomolecule sample is loaded on the column bed, it travels through the column along with the solvent used as eluent. THF is the best choice of solvent, as many of the nanomolecules are soluble in it.[22] As the column is packed with beads of certain pore size, the molecules smaller than the pore size tend to pass through many pores on their way down and elute last. On the other hand, the larger molecules do not pass through the bead pores and escape through the spaces between the beads to elute faster. Hence, when a mixture of Au_{25}, Au_{67} and $Au_{103\text{-}105}$ are loaded on the column, the $Au_{103\text{-}105}$ band elutes first followed by Au_{67} which is followed by Au_{25} all in a single column run. These fractions are collected and analyzed for their size distribution using mass spectrometry.

In our laboratory, the SEC procedure was established in 2012 in collaboration with Stefan Knoppe from University of Geneva, Switzerland. This technique has proved to be very effective in purifying gold nanomolecules such that it has a) replaced the solvent fractionation technique, which involves more labor compared to SEC and b) it has become a routinely applied technique by all the researchers in our laboratory.

1.4.4 Etching

As discussed in the previous sections, crude products from the syntheses are generally polydisperse and need post-synthetic treatment. Etching is one such post-synthetic process, where a crude product with a large size distribution is subjected to harsh chemical conditions of excess thiolate ligands and high temperatures.[23] Under the etching conditions, stable sizes survive through the reaction while the metastable sizes decompose to gold-thiolate polymers,

observed as insoluble material in the reaction flask. Thus etching acts a size selective process.

In some cases, when a mixture of different sizes is etched super-stable nanomolecules with smaller core masses are formed. This process of larger sizes converting to smaller sizes is called as *core size conversion.* The exact mechanism of core conversion reaction is unknown but it is presumed that Au atoms are removed from the outermost surface of the larger less stable nanomolecules. In a typical etching reaction, 50-100mg of the crude mixture of nanomolecules is dissolved in 0.5 to 2ml of thiol (>50 times the amount of crude mixture) and heated to ~80°C for several hours depending on the ligand used. The total reaction time is decided based on the MALDI mass spectrum of the aliquots taken from the reaction at systematic intervals.

1.4.5 Ligand exchange reactions

The interesting properties of nanomolecules come from their two structural components a) the Au core and b) the capping ligands. The core determines the optical and electronic properties of the nanomolecules and can be tuned. On the other hand, the ligands that cap the nanomolecule determines its chemical properties such as solubility and binding affinity.[24] Therefore, ligands play a key role in incorporating functionality to the nanomolecules. For example, it is possible to synthesize a water-soluble nanomolecule by incorporating polar ligands like glutathione in a chemical synthesis. However, there are challenges and limitations to ligand exchange reactions like a) exchanging the ligands without changing the core size and composition of the nanomolecule b) exchanging charged ligands and c) driving the exchange to completion.[25]

Nevertheless, these exchange reactions are employed in the thiolate stabilized gold nanomolecule by researchers in different countries. The ligand exchange reaction involves two

reaction steps. The first step includes preparation of highly monodisperse nanomolecules and the second step is exchanging the surface ligands from first step with the ligand of interest. The studies performed by Murray et al. on the dynamics of the ligand exchange reactions suggest an SN2-type mechanism in which the incoming thiol protonates an already bound thiolate ligand in the rate determining step. This is evidenced by the fact that the rate of ligand exchange decreases with increasing length and bulkiness of the incoming thiol.[25,26]

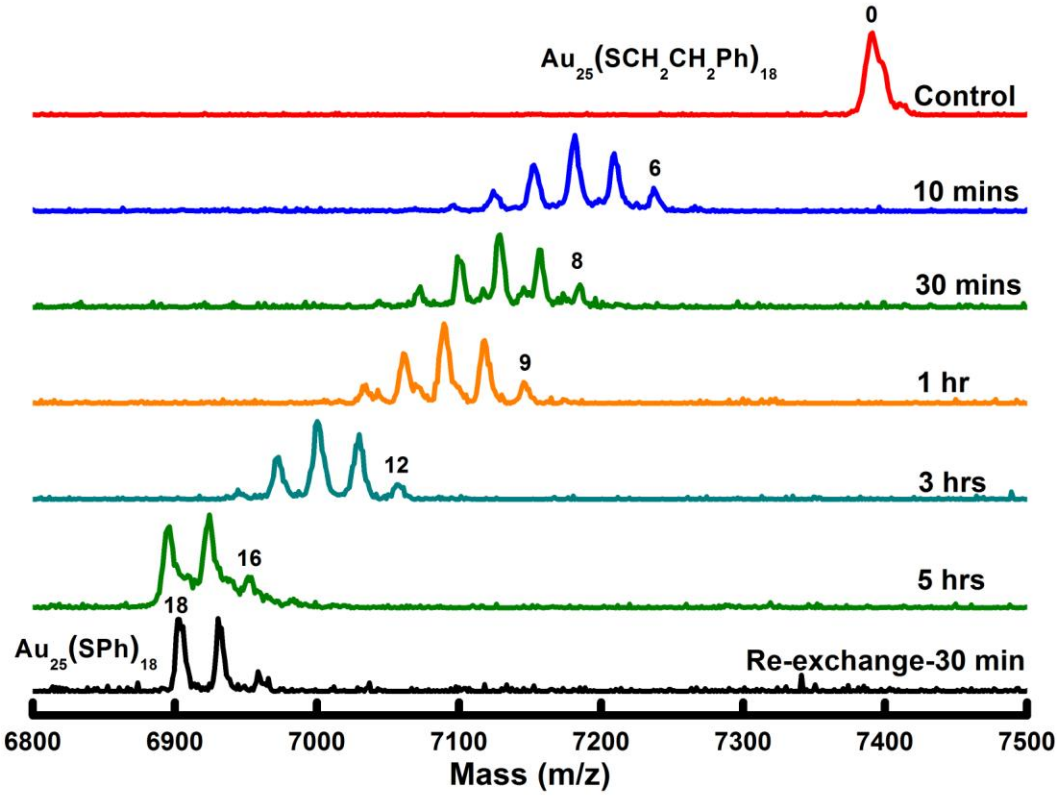

Figure 1.3. ESI mass spectrum illustrating a ligand process where $Au_{25}(SCH_2CH_2Ph)_{18}$ is exchanged completely by thiophenol (C_6H_5SH) to form $Au_{25}(SPh)_{18}$. 5 mg control Au_{25} was dissolved in 0.5 ml toluene and 0.5 ml PhSH ans stirred at room temperature.

The ligand exchange reactions on gold nanomolecules are typically monitored by mass spectrometry. Figure 1.3 illustrates a typical example of ligand exchange reaction. The control or the starting material was $Au_{25}(SCH_2CH_2Ph)_{18}$. The mass of phenylethanethiol and thiophenol are 137 Da and 107 Da respectively. Thus, when a phenylethanethiol ligand on the nanomolecule is replaced with thiophenol, the mass of the resulting nanomolecule decreases by ~(30*18) Da, where the molecular weight difference between phenylethanethiol and thiophenol was 30 Da adn there were 18 ligands on Au_{25}. This difference can be manifested as a different peak in the mass spectrum as show in figure 1.5. When the calculated amount of thiophenol was added to the nanomolecule solution in toluene and stirred at room temperature, all the 18 phenylethanethiol ligands were replaced with thiophenol. The progress of ligand exchange reaction can be seen in the mass spectra of the samples collected at different time intervals as shown in figure 1.5. Each of the consecutive peaks (moving from left to right) corresponds to an additional exchange with thiophenol. In certain cases, as shown in figure 1.4, the core of the nanomolecule is not stable upon ligand exchange. When $Au_{38}(SCH_2CH_2Ph)_{24}$ was exchanged with thiophenol, it is possible to exchange all the 24 ligands in a controlled fashion. In this case, the biicosahedral core of Au_{38} is no longer stable and starts transforming into a more stable FCC core in $Au_{36}(SPh)_{24}$ as proven by the known crystal structures of Au_{38} and Au_{36}.[27-29] This is discussed in detail in chapter five.

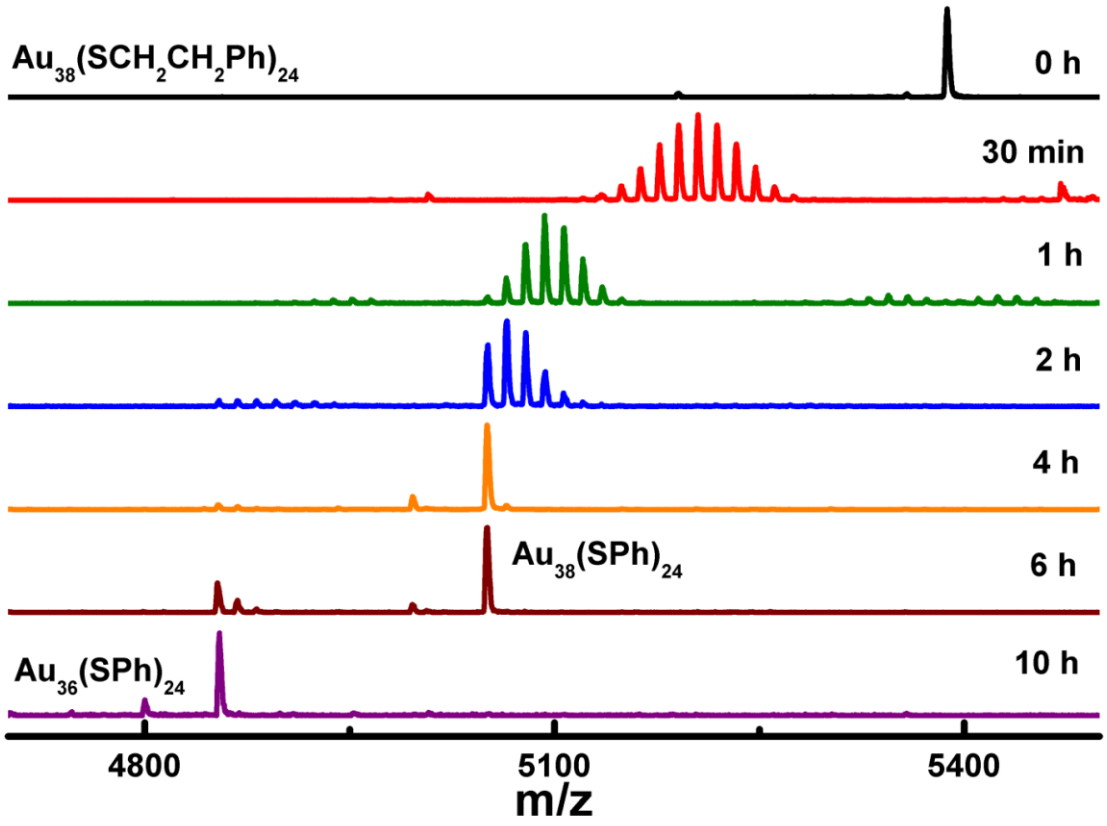

Figure 1.4. ESI mass spectrum illustrating a ligand process where the core of $Au_{38}(SCH_2CH_2Ph)_{24}$ is transformed to $Au_{36}(SPh)_{24}$ when exchanged with thiophenol. 5 mg control Au_{38} was dissolved in 0.5 ml toluene and 0.5 ml PhSH ans stirred at room temperature.

1.5 Analytical Characterization of gold nanomolecules

After the synthesis of gold nanomolecules, it is crucial to characterize their composition and key properties like optical, electronic and electrochemical properties. Over the last two decades since the Brust-Schiffrin synthesis was first introduced, several advances have been reported in the

characterization of these materials. The key characterization techniques like mass spectrometry and optical spectroscopy used in this dissertation work are introduced below.

1.5.1 Mass spectrometry

The discussion on mass spectrometry here pertains to the techniques of MALDI (Matrix Assisted Laser Desorption Ionization) and ESI (Electrospray Ionization) mass spectrometry and how they have revolutionized the field of gold nanomolecules in the recent times. Prior to the introduction of mass spectrometry techniques, gold thiolate nanomolecules were previously characterized for size and composition using TEM, optical spectroscopy and powder X-ray diffraction techniques, which only provided a general idea of an average diameter. LDI (Laser Desorption Ionization) mass spectrometry was the first mass spectrometric technique introduced for the compositional characterization of gold nanomolecules by Whetten and coworkers in their seminal work on ultra-small and highly stable thiolate capped gold nanomolecules.[1,30] The technique was useful in identifying the core sizes (like 8, 14 and 29 kDa cores) of different nanomolecules by their mass. But the major drawback of the LDI was the extensive fragmentation of the surface Au and ligand molecules from the nanomolecule cores. This fragmentation made it difficult to interpret the parent ion and the exact composition of the synthesized nanomolecules. To address the issue of fragmentation and obtain an exact molecular assignment of these nanomolecules, we use MALDI-MS (Matrix assisted laser desorption ionization mass spectrometry) and ESI-MS (electro-spray ionization mass spectrometry) techniques. The mechanism of ionization in these techniques, their advantages and disadvantages are discussed in detail in the sections below.

1.5.1.1 MALDI-TOF mass spectrometry

As discussed above, MALDI mass spectrometry was introduced keeping in view the drawbacks

of the LDI in extensively fragmenting the surface Au and ligands from the nanomolecule. This technique proved to be highly effective in eliminating that problem. For this dissertation work, Bruker Autoflex I is used to obtain MALDI MS results. In this instrument, the molecular ions are generated using a nitrogen laser operating at 337 nm. It is coupled with a TOF (Time of flight) mass analyzer, maintained at high vacuum, where the generated ions are separated based on their mass to charge values. All the ions are accelerated with the same kinetic energy, which makes smaller ions travel faster compared to the larger ions thereby separating them from each other in the TOF tube.

Dass et al[31] introduced the MALDI TOF MS technique for gold nanomolecules using DCTB (trans-2-[3-(4-tert-butylphenyl)-2-methyl-2-propenylidene]-malononitrile) matrix, which at optimal laser power produces minimal fragmentation (or sometimes unfragmented, in case of lower mass nanomolecules) enabling the determination of true molecular ion mass, thereby facilitating the compositional assignment.. The two critical parameters that influence the outcome of a MALDI mass spectrometer are a) *the laser fluence* and b) *the choice of matrix*. Systematic variation of the *laser fluence* shows a corresponding change in the resulting spectrum.

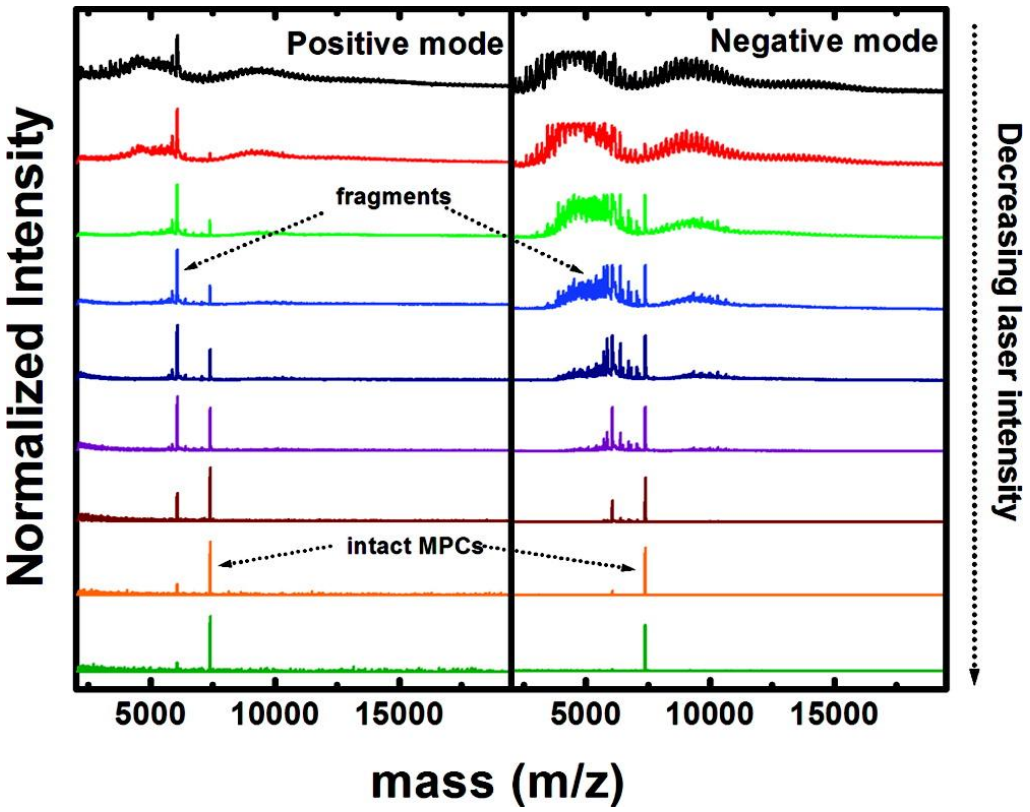

Figure 1.5. MALDI-TOF-MS spectra (Applied Biosystems Voyager-DE Pro) of $Au_{25}(SCH_2CH_2Ph)_{18}$ in DCTB matrix with varying laser intensity delineating the molecular ions from fragment ions in positive and negative linear mode. Some spectra here are clipped at the top; see Supporting Information for complete spectra examples. Reprinted with permission from Ref 31. Copyright 2008 American Chemical Society.

As illustrated in figure 1.5, increasing the laser fluence leads to greater fragmentation of the ligands from the nanomolecules making it difficult to make an exact molecular composition assignment. It has to be operated at a threshold laser fluence, which is just enough to ionize the nanomolecule but prevent fragmentation. On the other hand, if the laser fluence is reduced below the threshold, there is no ionization of the nanomolecule and as a result, no peaks are observed in the mass spectrum. The second critical parameter influencing the outcome from a MALDI is *the*

choice of the matrix. This is highly crucial in obtaining a clean, unfragmented molecular ion peak for a nanomolecule.

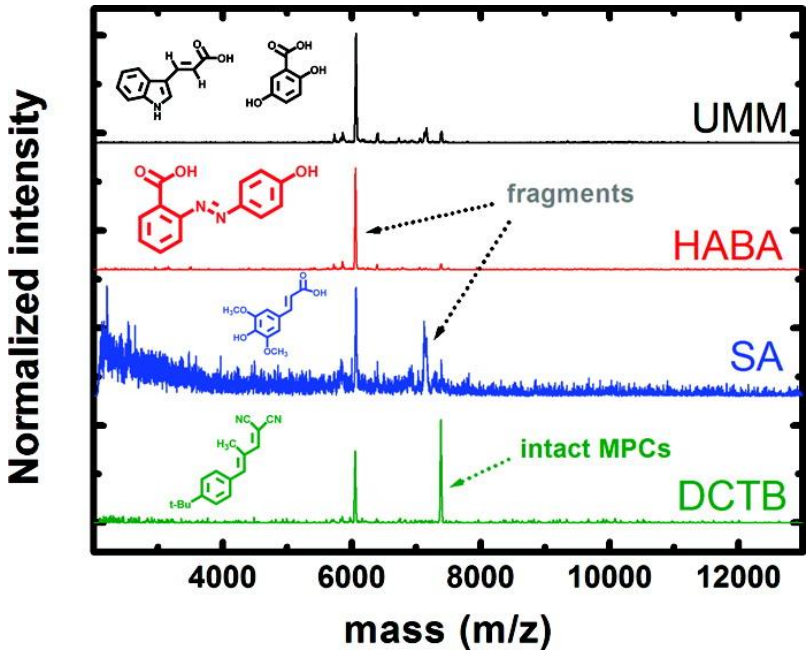

Figure 1.6. MALDI mass spectrum illustrating the influence of different matrices on the fragmentation of the nanomolecules.[31] Reprinted with permission from Ref 31. Copyright 2008 American Chemical Society.

There are experimental results obtained from tests on different matrices using sinapinic acid (SA), 4′-hydroxy -azobenzene-2-carboxylic acid (HABA), and "Universal MALDI Matrix", UMM (1:1 mixture of dihydroxybenzoic acid and R-cyano-4-hydroxycinnamic acid) all operated at threshold laser fluence. The evidence, as shown in figure 1.6, points to the fact that only the mass spectra acquired using DCTB matrix show intact molecular ion peaks while all other spectra are dominated by the fragment ion peaks. Nevertheless, MALDI-MS has proven to be

instrumental in analyzing the nanomolecules produced in synthesis, isolation and etching reactions.

1.5.1.2 ESI mass spectrometry

ESI (electrospray ionization) mass spectrometry and MALDI-MS use different sample introduction technique and different ionization mechanisms. Nanomolecule sample is introduced as a solution and passed through a high voltage capillary. Charged droplets of nanomolecule solution are dissipated from the capillary, which then loose the solvent to shrink in size due to the desolvation temperatures applied. Eventually, these charged droplets burst into small gas phase ions, which are then directed into the mass analyzer. Waters Synapt G2 ESI-MS in our lab uses a quadrupole mass analyzer coupled with TOF mass analyzer, there by yielding high resolution data suitable for the compositional assignment of nanomolecules. Murray's group first reported ESI-MS of gold nanomolecules. [109] Later, Tsukuda and coworkers introduced a homemade ESI instrument in the analysis of glutathione capped gold nanomolecules.[32] ESI mechanism allows the formation of multiply charged ions due to large charge density on the solvent droplets prior to ionization. These multiply charged ions appear at a lower mass that are better resolved there by resulting in high resolution data.

When analyzing gold nanomolecules below a mass of ~15000 Da, both MALDI and ESI mass spectrometers are capable of generating intact parent ion peaks. Generally, MALDI MS is a fast robust method, and less sample consuming compared to ESI MS. But when analyzing nanomolecules of mass >15000 Da, MALDI peaks start to fragment (only 1+ peaks are generated in MALDI) resulting in broad peaks unsuitable for compositional assignment. In such cases, it is required to use ESI in generating multiple charge states of the parent ion with high

resolution.

1.5.2 Optical spectroscopy

At a fundamental level, optical absorption spectra provide information on the electronic structure of gold nanomolecules. It is interesting to explore how properties of nanomolecules evolve from bulk to molecule. Most small metallic nanoparticles are characterized by a broad absorption peak in the visible region due to the surface plasmon resonance. It is the collective oscillation of conducting electrons in response to optical excitation. The shift in the SPR band with size of the nanoparticles is the reason for different colors of different sizes. In case of ultra small nanomolecules, discrete electronic structure and molecule like properties of HOMO-LUMO gap are observed. It would be interesting to determine the approximate size at which the quantization dominates the absorption spectrum compared to the SPR. Using the free-electron model in metal clusters, we can calculate the average spacing (δ) of electronic energy levels.[13,15,33,34]

$\delta = E_f/N$, E_f is the fermi energy and N is the number of Au atoms

As the size decreases, N value decreases and δ value increases as observed in the UV-vis spectrum of the nanomolecules. When we take thermal energy (K_BT) as criterion, electronic energy quantization becomes distinct when δ is $\geq K_BT$. Substituting in $K_B = 8.6*10^{-5}$ and Ef = 5.5eV we get a N value of 212 atoms. The relation between N and volume of atoms is

$N = 59$ atoms/nm^3 * Volume, which gives

Volume = $3.59nm^3$ and

Diameter = 1.53nm

Hence the critical diameter at which the electronic energy quantization occurs is *1.53 nm*.

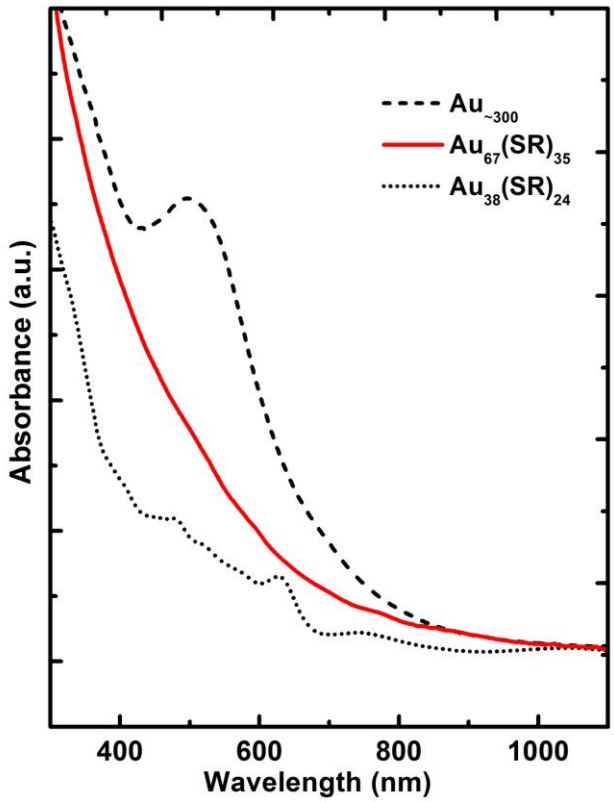

Figure 1.7 : Size-dependant UV-vis absorption spectra of gold nanomolecules performed in toluene solutions.

The electronic energy quantization is clearly illustrated in figure 1.7. $Au_{\sim 300}$ atom shows SPR peak at 530 nm while Au_{67} and Au_{38} show discrete absorption bands. It is also clear that as the size decreases from Au_{67} to Au_{38}, the energy gap or the HOMO-LUMO gap increases.

1.6 Ligand effects of aromatic thiols

Research on gold-thiolate nanomolecules over the past decade was focused on aliphatic thiols (C_nH_{2n+1}-SH) as capping ligands. Besides aliphatic thiol, one of the more widely used ligand was phenylethanethiol ($C_6H_5CH_2CH_2SH$). This was due to the fact that this ligand, like aliphatic ligands, yields same core sizes of Au_{25}, Au_{38}, Au_{67}, $Au_{103\text{-}105}$ and Au_{144} in synthesis and etching

reactions. Therefore, phenylethanethiol was grouped with aliphatic ligands in distinguishing the ligands based on their effects on the size and geometry of nanomolecules. Herein, I have investigated a new group of ligands called aromatic thiols, which has a profound effect on the geometry and properties of nanomolecules. In our first report[35] on using aromatic thiols, when a polydisperse mixture of Au_{67} and $Au_{103\text{-}105}$ was etched in thiophenol, an aromatic ligand, we observed a new core $Au_{36}(SPh)_{24}$. The fact that it was not one of the known series of magic stabilized clusters has drawn tremendous interest. Further investigations on the properties of this new nanomolecule revealed that it does not follow the trends of geometry and electrochemical gap shared by other magic stabilized clusters. It is also been reported that it holds a *fcc* geometry when compared to Au_{38} which holds a biicosahedral geometry, although they differ only by two Au atoms.[27-29] All these findings and questions whether it is an effect of bulkiness of the ligand or the aromaticity have spurred an in-depth investigation into the effects of aromatic ligands on the structure and properties of gold nanomolecules.

CHAPTER TWO

$Au_{67}(SR)_{35}$ NANOMOLECULES : UNIQUE SIZE-DEPENDENT OPTICAL, ELECTROCHEMICAL, STRUCTURAL PROPERTIES AND THEORETICAL ANALYSIS

Part of the text and figures in this chapter are extracted from the following publication:
Praneeth Reddy Nimmala,[†] Bokwon Yoon,[‡] Robert L. Whetten,[§] Uzi Landman,[‡] Amala Dass[†,]*
J. Am. Chem. Soc. **2011**, *133*, 20258.

CHAPTER TWO

$Au_{67}(SR)_{35}$ NANOMOLECULES : UNIQUE SIZE-DEPENDENT OPTICAL, ELECTROCHEMICAL, STRUCTURAL PROPERTIES AND THEORETICAL ANALYSIS

2.1 Abstract

Isolation of distinct thiolate protected gold nanomolecules has been a major challenge for over a decade. $Au_{25}(SR)_{18}$, $Au_{38}(SR)_{24}$, and $Au_{144}(SR)_{60}$ are the most studied sizes due to the reproducible high yield synthesis and well established isolation methods. The synthesis and isolation of other core sizes has been less successful as the yield of pure compounds was rather low. The main goal of this project was to develop a procedure to prepare $Au_{67}(SCH_2CH_2Ph)_{35}$ compound in high yield and high purity. A three-step synthesis involved synthesis of a crude procuct, mild thermochemical treatment and isolation resulted in yields on an average of 35% (which is a high considering the previous yields). The product purity was assessed at each stage by rapid MALDI-TOF-MS. The highly reproducible synthesis was applied to two distinct thiolate ligands, $Au_{67}(SCH_2CH_2Ph)_{35}$ and $Au_{67}(SC_6H_{13})_{35}$, and for each case the compositions were established by high-resolution ESI-MS. The electronic properties of the pure compounds were investigated using optical absorption spectroscopy (UV-visible-NIR regions) and voltammetry (0.50 eV HOMO-LUMO gap estimated from the DPV). The ligand-core interface

was explored by NMR (^{13}C and ^{1}H); and the structural characteristics of the nanomolecule core were investigated by powder XRD measurements. This composition and structural evidence suggested a model featuring a Au_{17} Marks-decahedral type central core encapsulated by the 30 anchoring atoms of 15 staple-motif units. These staple motifs are organized as two polar caps of five staples each, as in the totally determined structure of $Au_{102}(pMBA)_{44}$, plus an equatorial belt comprised of five long staple units. The hollow Au_{17} core rationalizes a 32-electron shell closing for the neutral cluster.

Author Contributions

Praneeth Nimmala developed the protocols for synthesis and isolation of $Au_{67}(SCH_2CH_2Ph)_{35}$ and $Au_{67}(SC_6H_{13})_{35}$, characterized the compounds using optical spectroscopy, mass spectrometry, electrochemistry, powder-XRD and NMR spectroscopy. Bokwon Yoon provided the first-principles theoretical analysis on the title compound.

2.2 Introduction

Gold nanomolecules are ultra-small (< 2 nm) gold nanoparticles of molecular definition and atomic monodispersity, with molecular formulae $Au_{25}(SR)_{18}$, $Au_{38}(SR)_{24}$ and $Au_{144}(SR)_{60}$. They contain a distinct number of gold atoms protected by distinct number of thiolate ligands, similar to organic and inorganic molecular compounds. They differ in certain respects from their larger metallic, or plasmonic, counterparts which have core diameters > 2 nm (~ 200 atoms). For example, they show discrete, molecule-like electronic properties with a enhanced electrochemical and optical HOMO-LUMO gap.[1,36,37] These size-dependent electronic properties are due to the transitions among the energy levels of the bulk conduction or valence band, as modified by the ligand bonding. The interesting size dependent optical and electronic properties

of these nanomolecules can be attributed to their quantum confinement effects and to the atomic packing.[38,39] Their stability can be explained by electronic[40] and geometric[41] effects. Beyond a size of 2 nm or ~ 300 atoms[42,43] there emerges a strong, broad peak ~500 nm called the surface plasmon resonance (SPR) that results from the collective response of the conduction electrons to the excitation. The 76.3 kDa atomically monodisperse, giant gold nanomolecule, named Faradaurates,[42] in honor of Michael Faraday's seminal 1857 work,[44] is the smallest size that supports the SPR peak. The clusters below 2 nm show unique features in the absorption spectrum with a common inflection at 1.7 eV for most of them. These unique features are assigned to single electron excitations rather than collective responses. Research in this field has also crossed a milestone of determining the atomic structure by single crystal total structure methods, first in the case of Au_{102}(p-MBA)$_{44}$ (p-MBA refers to para-mercapto benzoic acid) followed closely by $Au_{25}(SCH_2CH_2Ph)_{18}$.[45-48] Certain conclusions about the structure-property relations in these clusters have been drawn from their atomic packing in the cluster core (or kernel) and also the Au-S bonding at the surface. This has indeed accelerated research in this field considerably but the high yield synthesis of monodisperse gold thiolate nanomolecules remains as a major challenge hindering the use of these clusters in practical applications.

So far, only a few such gold nanomolecules with core masses of 5, 8, 14, 22, 29 and 76 kDa have been synthesized and identified.[38] The kDa values represent the mass of the inorganic core atoms only based on earlier laser desorption ionization(LDI) studies and correspond to 25, 38, 67, 102, 144 and ~300 total gold atoms respectively. For example, the 5 kDa referred to $Au_{25}(SR)_{18}$ with a parent ion mass of 7.394 kDa for phenylethane thiolate.[49] It is essential that we classify these nanomolecules on the basis of their mass and composition as it can be justified

from the differences they exhibit with varying gold to thiolate ligand numbers. Of these compounds, the 5, 8 and 29 kDa sizes ($Au_{25}(SR)_{18}$, $Au_{38}(SR)_{24}$ and $Au_{144}(SR)_{60}$ respectively; hereafter referred to as Au_{25}, Au_{38} and Au_{144}) are stable under harsh thermochemical treatment,[50] rendering the synthesis-isolation procedures manageable. Consequently experimental and theoretical[40,51-55] reports on the selected 25, 38 and 144 abound – reproducible reports have come from various continents, spanning over the past 15 years.[56] Organic soluble versions of other core sizes, such as $Au_{\sim 68}$ (14 kDa) and Au_{102} (22 kDa), however, are not well studied. The 22 kDa species have been studied well from the crystal structure of its water-soluble analog[57] .

The title compound was first reported as 14 kDa clusters with ~75 Au atoms based on LDI mass spectra,[38,58]with the x-ray scattering data showing Marks-decahedral motif,[59] its voltammetry,[36] and optical band gap of ~0.6 eV.[39] Recently some of us reported the preparation of 14 kDa species enriched sample (containing minor amounts of 25- and 102-atom clusters) and assigned its composition as $Au_{68}(SR)_{34}$ on the basis of matrix assisted laser desorption ionization (MALDI) mass spectra.[60] It was then regarded merely as an intermediate product[61] and its characterization remained incomplete due to lack of methods to isolate this cluster in its purest form in sufficient quantities. In this project, we developed methods for the high-yield synthesis and isolation of the pure title compound, and identify its composition as $Au_{67}(SR)_{35}$ using high resolution electrospray (ESI) mass spectrometry on two different thiolate groups, namely, 2-phenylethane thiol and n-hexanethiol. The compound displayed a HOMO-LUMO gap of 0.74 V in electrochemical experiments that is consistent with size dependent behavior of earlier results on Au_{25}, Au_{38} and Au_{144} nanomolecules. Further characterization was performed using UV-visible spectroscopy, NMR spectroscopy, powder XRD measurements, which permit a

discussion of its likely structural characteristics.

2.3 Experimental methods

2.3.1Chemicals

Phenylethanemercaptan (Sigma aldrich, ≥ 98%), sodium borohydride (Acros, 99%), trans-2-[3-(4-tert-butylphenyl)-2-methyl-2-propenylidene]malononitrile (DCTB matrix) (Fluka, ≥ 99%) were purchased from Aldrich. Tetrahydrofuran (Acros anhydrous, stabilized 99.9%) and other solvents like toluene, methanol, acetonitrile and acetone were used from Fisher as received.

2.3.2 Equipment

UV-Visible absorption spectra were recorded in toluene on a Shimadzu UV-1601 instrument. Matrix assisted laser desorption time-of-flight (MALDI TOF) mass spectra were collected on a Bruker Autoflex 1 mass spectrometer in linear positive mode using a nitrogen laser (337 nm) with DCTB as a matrix. ESI-MS spectra were acquired on Waters SYNAPT HDMS instrument either with or without cesium acetate as an electrolyte. NMR spectra were recorded on a Bruker AC-300 NMR spectrometer at ~10mg/mL concentration. Electrochemical measurements were performed on a CHI 620 instrument using 5mg of title compound in 5mL of THF solution with 0.5mM $TBAPF_6$ as supporting electrolyte under nitrogen atmosphere. Powder XRD measurements were performed on Bruker D8-Focus XRD instrument on a quartz substrate. 10mg of sample was dissolved in minimal amount of toluene and deposited on the substrate and air-dried.

2.3.3 Theoretical Methods:

Insights into the electronic structure and stability of the protected gold cluster studied here have been gained through first-principles calculations using the spin density-functional theory (SDFT) and employing the ab-initio Born-Oppenheimer molecular dynamics, AIBOMD, method which has been originally formulated,[62] and is especially advantageous, for treating charged systems, since it does not employ a supercell; that is, the ionic system is not periodically replicated and consequently no spurious contributions from image multipole interations are encountered. In this method the Kohn-Sham equations are solved in conjunction with non-local norm-conserving soft pseudopotentials[63] (using scalar relativistic ones for the Au atoms), with the valence $5d^{10}$ and $6s^1$ electronic states of the Au atoms, as well as the valence electrons of the S ($3s^2$, $3p^4$), C ($2s^2$,$2p^2$) and hydrogen atoms of the protecting layer, expanded in a plane-wave basis with a 62 Ry kinetic energy cutoff. The Perdew-Burke-Ernzerhof (PBE) functional is employed in the generalized gradient approximation (GGA) to the exchange-correlation corrections.[64]

2.4 Synthesis and isolation of Au_{67}

Briefly, the synthesis and isolation of $Au_{67}(SCH_2CH_2Ph)_{35}$ (abbreviated as Au_{67}) proceeds via three stages. The first stage being a one phase reaction using THF as a solvent,[20,60,61] to produce a mixture of 14 kDa clusters and 22 kDa clusters, the mass being that of the core. The second stage involves mild thermochemical treatment of the polydisperse mixture obtained from the previous stage, in the presence of excess thiol,[58] to form distinct peaks at 14 and 22 kDa with a good baseline separation (see methods section below; figure 6). The third and final stage involves multiple separation steps, to remove the 22 kDa and any other

species present in the product of second stage, to isolate pure Au_{67}. We exploited the solubility properties of different sized gold nanoclusters through solvent fractionations[38] in order to isolate the 14 kDa cluster. Understanding this property allowed for a neat separation of any single cluster from a mixture of Au_{102}, Au_{67}, Au_{38} and Au_{25}. We observed that toluene and acetone solvent mixtures in certain proportions, precipitates Au_{102} leaving Au_{67} in the soluble part (for details see methods below). Similarly, the THF and methanol mixture in certain proportions precipitated Au_{67} and leaves lower clusters like Au_{25} and Au_{38} in solution. In the isolation of Au_{67}, through trial and error, we observed that THF and methanol (in different proportions) was the most useful solvent mixture. The proportion of THF:methanol solvent mixture depended on the concentration of starting material mixture, drop or addition rate of the non-solvent methanol, stirring rate of the solution and polar/non-polar differences in the nature of the protecting ligand used in synthesizing the nanomolecule. For example, we dissolved 100 mg of Au_{67} and Au_{102} mixture in 1 ml THF and added 0.8 ml methanol at 1 drop/minute to precipitate out the higher cluster $Au_{102.}$ Above all, like other separation methods,[22,65] this method does not yield pure product in a single fractionation and may need multiple fractionations to obtain the pure product. This process may seem tedious but since a practical method is developed, it has become a fairly routine operation in our laboratory. As a one-step synthesis of Au_{67} is not available, this multi-step solvent fractionation can yield highly pure (mass spectrometric purity) $Au_{67}(SR)_{35}$ nanomolecules (~10 mg per batch quantities). High purity refers to the absence of other size nanomolecules within the detection limit of MALDI-TOF and ESI-Q-TOF mass spectrometers.

Step 1: Synthesis of crude product : Typically, 0.5 mmol of $HAuCl_4.3H_2O$ was dissolved in 20 ml of THF and stirred for about 10 min before adding 6 mmol of phenylethanethiol

($PhCH_2CH_2SH$). The reaction mixture started to change its color from golden yellow to turbid in about 15 mins when stirred at 500 rpm. Then, we added 5 mmol of $NaBH_4$ to the reaction mixture. The color of the reaction mixture turned black. The stirring was continued for another 5 min and then the solvent was removed from the reaction mixture by rotary evaporation as quickly as possible. Once the solvent was completely removed, the resulting product, which was adhering to the round bottom flask, was washed with methanol two or three times to remove the excess thiol and other reaction byproducts. At this stage, the MALDI mass spectrometric analysis of this crude product showed a broad peak ranging in mass.

Step 2: Mild thermo-chemical treatment of Au_{67} and Au_{102} mixture : The synthesis of crude products does not yield the final product, the MALDI-MS may show a broad peak ranging in m/z value of 15 kDa to 35 kDa. In fact, this broad peak is typical of many reactions involving synthesis of the crude mixtures in step 1.

In such cases it is difficult to proceed for solvent fractionations as the baseline between the two clusters Au_{67} (14 kDa) and $Au_{103\text{-}105}$ (22 kDa) is not perfectly resolved; in other words, there are many other metastable clusters other than Au_{67} and $Au_{103\text{-}105}$. These peaks can often be sharpened by a mild thermochemical treatment.[58] This is accomplished by heating the product from stage 1 (~100 mg) in 0.5 ml of toluene and 0.2 ml of phenylethanethiol at 60°C for one hour.[23,66] This treatment flattens the baseline (see Figure 2.1) between the stable clusters (Au_{67} and $Au_{103\text{-}105}$) and makes it suitable for solvent fractionations (step 3). Harsh chemical conditions (higher temperature or longer reaction time) should be avoided for this step, as they may result in decomposition or conversion of the species of interest.

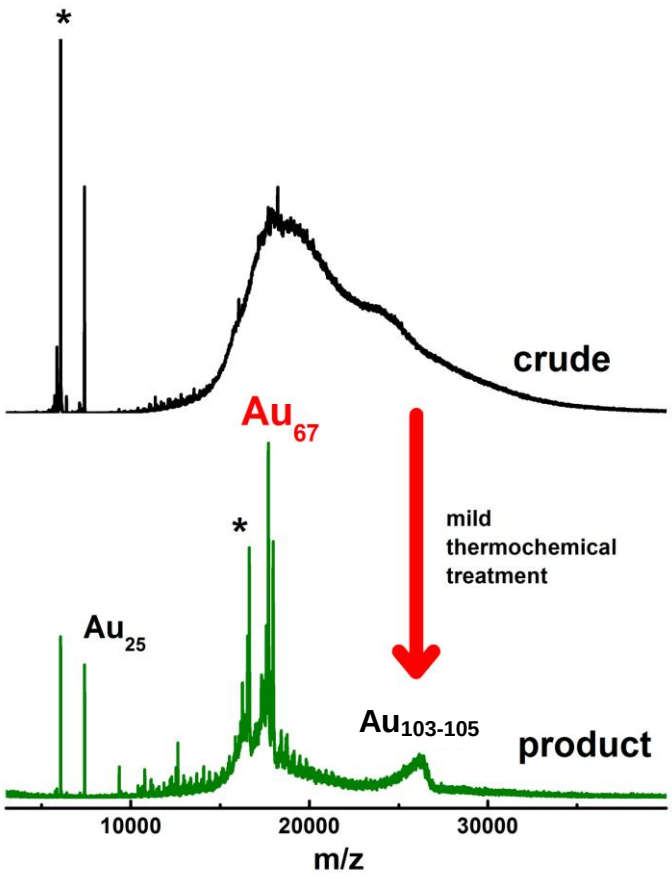

Figure 2.1. MALDI-MS spectrum of a typical reaction where the initial crude product (control – top spectrum) was subjected to mild thermo-chemical treatment to obtain a product (bottom MALDI MS spectrum) where Au_{67} is a major product and other sizes are diminished in signal. Peaks with asterisks denote fragments.

Step 3: Solvent fractionations to get pure Au_{67} : Figure 2.2 tracks the systematic isolation or removal of Au_{102} from a mixture resulting in step 2. Since Au_{102} (~ 22 kDa) is larger in size (and more non-polar ligands around it) compared to Au_{67} (~14 kDa) and other lower clusters, it can be removed successfully in a few fractionations using tetrahydrofuran and methanol. A typical solvent fractionation procedure involves dissolving the initial nanocluster

mixture in a round bottom flask in a least possible amount (~0.5 ml for 50 mg) of a nonpolar solvent like toluene or THF followed by addition of a polar solvent like methanol drop wise (~1 drop/minute). The lower the drop rate of the polar solvent, the better the separation. But slower drop rate result in longer separation times. So the parameters are adjusted as per the requirements of each fractionation. The mixture in the RBF needs to be stirred at a constant rate (typically 300 rpm) which is high enough to mix the solvents homogenously and slow enough to allow for precipitation of higher clusters. As the polarity of the mixture increases, the higher clusters (containing more nonpolar ligands) start precipitating. In general slower separation over longer time periods yield better results.

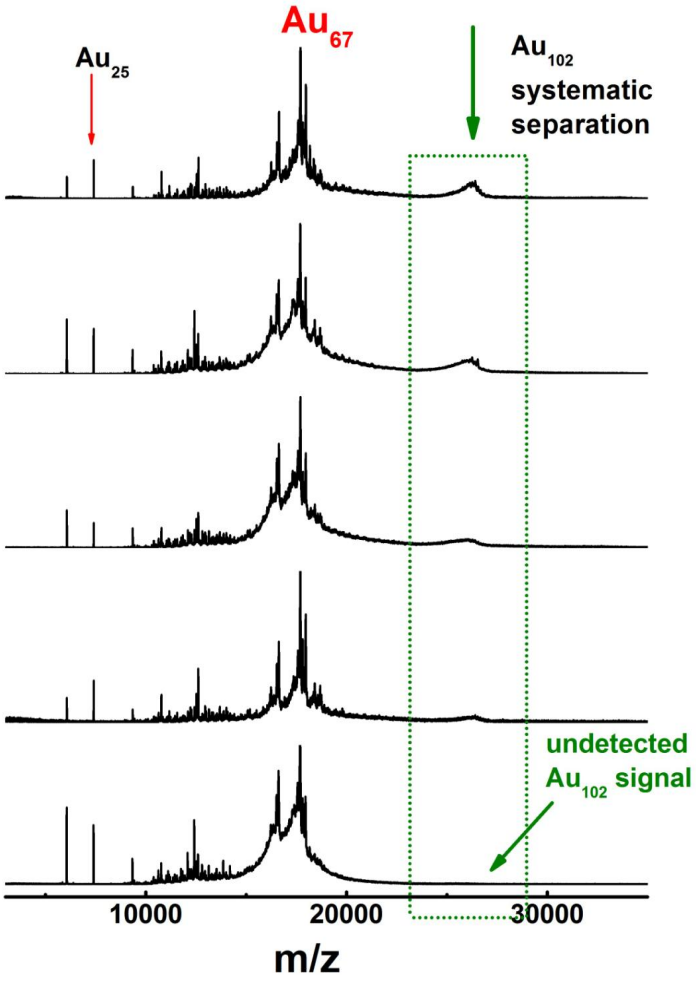

Figure 2.2. $Au_{67}(SR)_{35}$ purification separating larger clusters: MALDI spectra showing the systematic separation (top to bottom) of Au_{102} clusters from a mixture of Au_{25}, Au_{67} and $Au_{103\text{-}105}$. The final product (bottom) is further used to separate the clusters lower in mass than $Au_{67}(SR)_{35}$.

So in the mixture of $Au_{103\text{-}105}$, Au_{67} and Au_{25}, the heaviest size ($Au_{\sim 103\text{-}105}$) precipitates out first. When a considerable amount of precipitate is seen at the bottom of the round bottom flask, we stopped the stirring, allowed it to settle for a few minutes and then separate the soluble part from the insoluble part using a Pasteur pipette. We then quickly analyze both the soluble and insoluble portions by MALDI-MS to estimate the separation.

A controlled first solvent fractionation shown in figure 2.2 above would result in a soluble part with most of the Au_{67} retained in it while the precipitate would contain a major amount of $Au_{103\text{-}105}$ with a little Au_{67}. We repeated these fractionations until we reached a stage where the soluble part has no $Au_{103\text{-}105}$ at all. This final soluble part (the bottom most spectra in Figure 2.2) is further fractiontaed to remove the lower clusters and obtain pure Au_{67}. Separating lower clusters: In the schematic shown (Figure 2.3), we have systematically removed all the lower clusters (to the left of Au_{67}). Here again, solubility differences were used as that of $Au_{03\text{-}105}$ separation above, except that this time the heaviest molecule in the mixture was Au_{67}. THF was used to wet and dissolve the starting mixture and methanol was added to it so far that almost all of the mixture has precipitated. The soluble portion now looks reddish in color and is very dilute (reddish color indicates the presence of low mass species like Au_{25}). This soluble fraction was then removed from the round bottom flask and the precipitate was now ready for a second fractionation. Considering the area under the curve for each cluster in the starting material, the

total amount of lower clusters is very small compared to Au_{67}.

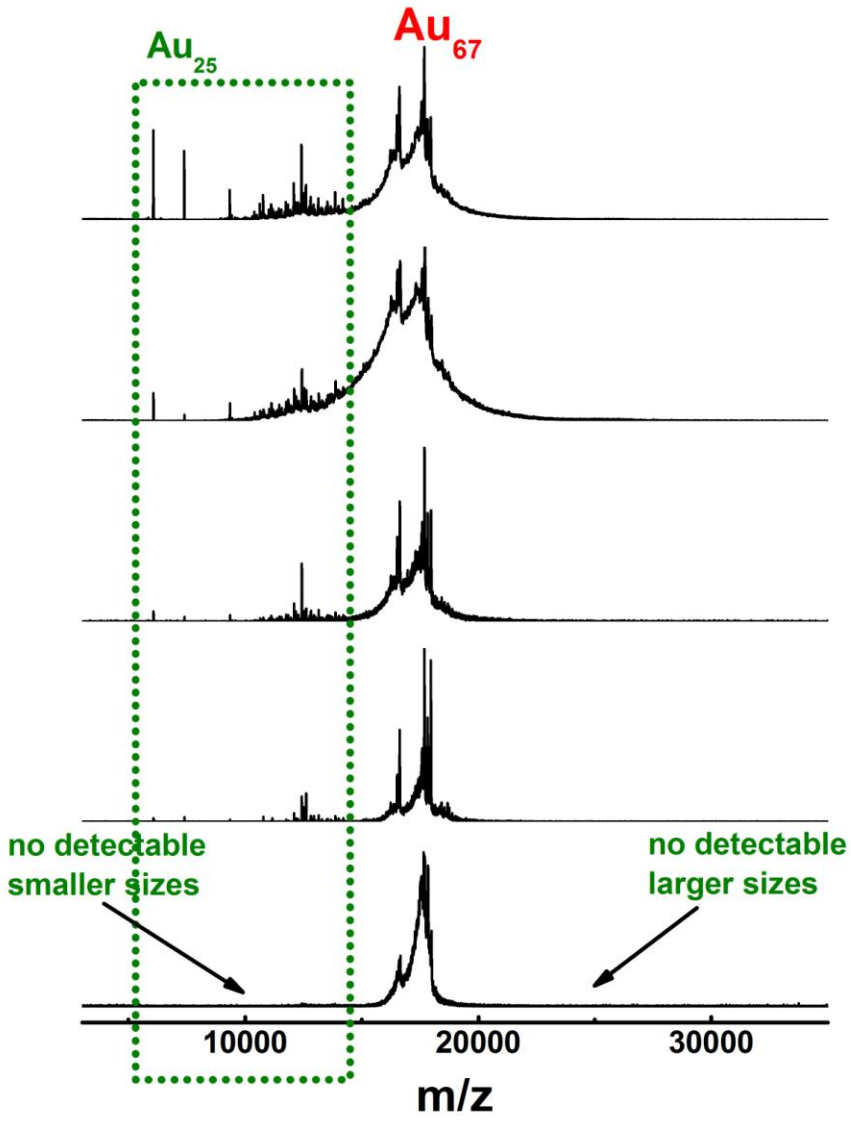

Figure 2.3. $Au_{67}(SR)_{35}$ purification separating smaller clusters: Continuation of the separation process (figure 2.2) to remove sizes smaller than $Au_{67}(SR)_{35}$. The Au_{67} at this stage is "*mass spectrometrically pure*".

This means that we need not work so carefully on the separation of lower species from

Au_{67}. The drop rate can be fast (2-3 drops/minute). Such separations, where one of the species are in minor quantities, can be fast and simple. We have repeated these fractionations until the peaks for lower species were absent in the MALDI even at high laser fluence.

2.5. Results and discussion

2.5.1 Mass spectrometry

The *size-purity* of the final products was determined principally by *MALDI-TOF mass spectrometry*. Figure 2.4 shows the MALDI-TOF mass spectra of the purified title compound showing 1+ peaks for phenylethane thiolate and n-hexanethiolate ligands. In contrast to our earlier work,[60] here the analysis of the purified sample shows negligible intensity corresponding to Au_{25} or $Au_{103\text{-}105}$, around 5 or 22 kDa mass region, respectively.

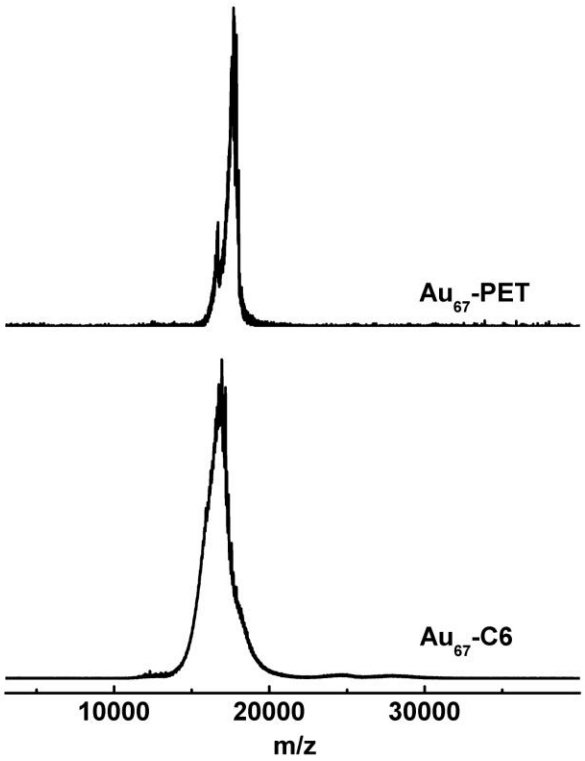

Figure 2.4. MALDI spectra of the pure $Au_{67}(SR)_{35}$ with two different ligands phenylethanethiol (top) and hexanethiol (bottom) taken at very high laser fluence. At high laser fluence, even minor amounts of impurities or other core size clusters will show higher signal intensity.

The *composition* of the clusters was determined by *ESI-MS mass spectrometry* of the phenylethane and hexane thiolate homologs. The multiply charged peaks are lower in mass-to-charge ratio compared to singly charged species, and generally have better sensitivity, resolution and accuracy. The lower mass range and better resolution due to multiply charged peaks also offers calibration check with $Au_{25}(SR)_{18}$ and $Au_{144}(SR)_{60}$, which were employed here. This is significantly different than the MALDI-TOF peak in our earlier work at 18,059 Da.[60] Figure 2.5 shows the MALDI and ESI of the $Au_{67}(SR)_{35}$ overlapped.[60]

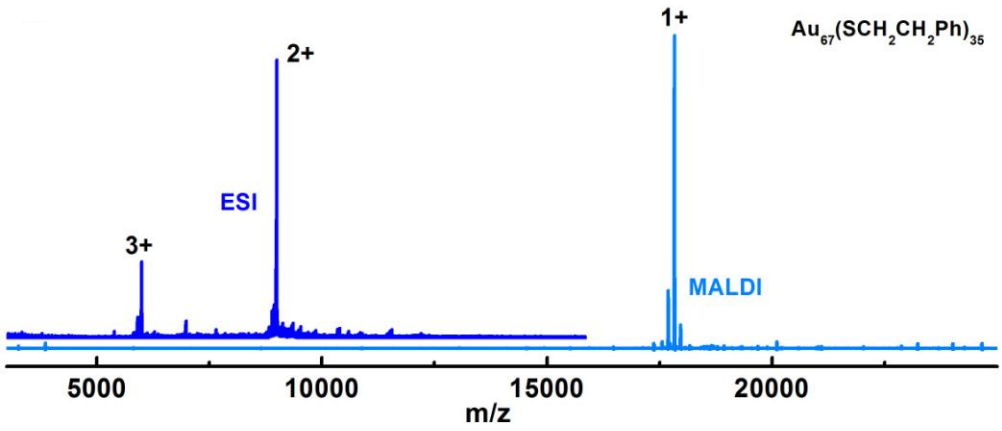

Figure 2.5. Positive mode MALDI-TOF mass spectra(MS) (in light blue) and ESI MS(dark blue) of $Au_{67}(SCH_2CH_2Ph)_{35}$ nanomolecules.

To resolve the discrepancies in compositional assignment, we $Au_{67}(SR)_{35}$ the title compound with another thiolate ligand, n-hexanethiol of different mass. If this ligand also produces the nanomolecule with identical number of Au atoms and thiolate ligands, then the

mass difference of the parent ions can be used to calculate the number of ligands.[67] Having established that the ESI mass spectra reflect ions that are free of counter ions, we used the 20-Da mass difference between 2-phenylethane thiolate (137 Da) and n-hexane thiolate (117 Da) protected nanomolecules to calculate the number of ligands. As detailed in Figure 2.6, a mass difference, Δm of 350 Da/z for the z=2 peaks would correspond to 35 ligands.[68] The unique composition (67,35) thus explains both the calibrated total mass observed and the difference (700 Da) arising from the two distinct thiolate ligands, one may regard this as a direct determination of the composition of this 14 kDa class of cluster compound.

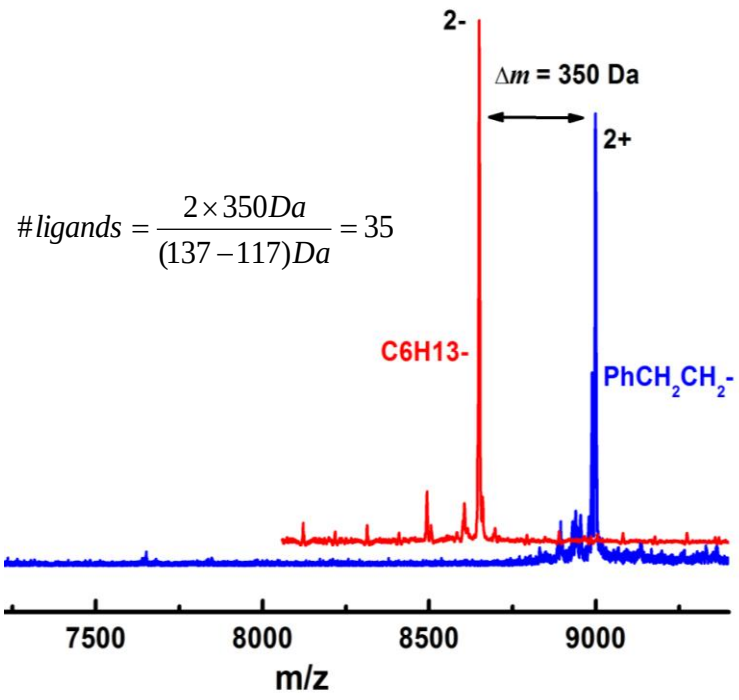

Figure 2.6. ESI mass spectra of $Au_{67}(SR)_{35}$ nanomolecules protected by phenylethane thiolate (blue) and n-hexane thiolate (ligands) showing a mass difference of 350 Da used to calculate the number of ligands in the Au_{67} to be 35.

2.5.2. Optical spectroscopy

The o*ptical spectroscopic* characterization of the purified Au_{67} compounds has principally involved linear absorption spectroscopy of the dilute solutions covering the UV-vis-NIR regions (wavelengths ranging from 300 to 1100 nm, or 1.1 – 4.0 *eV* photon energy). In Figure 2.7, a typical UV-visible spectrum of Au_{67} is compared to that of a smaller Au_{38} and also a larger Au_{329}. Under these conditions, the UV-visible spectrum of Au_{67} appears featureless overall except for a shoulder around 590 nm (2.1 eV). Clearly the onset of enhanced absorption is around 800 nm (~1.6 eV) as is expected for sizes in this group.[38,69] These features were also observed in Au_{67} protected by hexanethiol. The spectrum in Figure 2.6 is in substantial agreement with that reported by Alvarez et al.[69] as analyzed further in Chen et al. ,[36] and Wyrwas et al.[39]

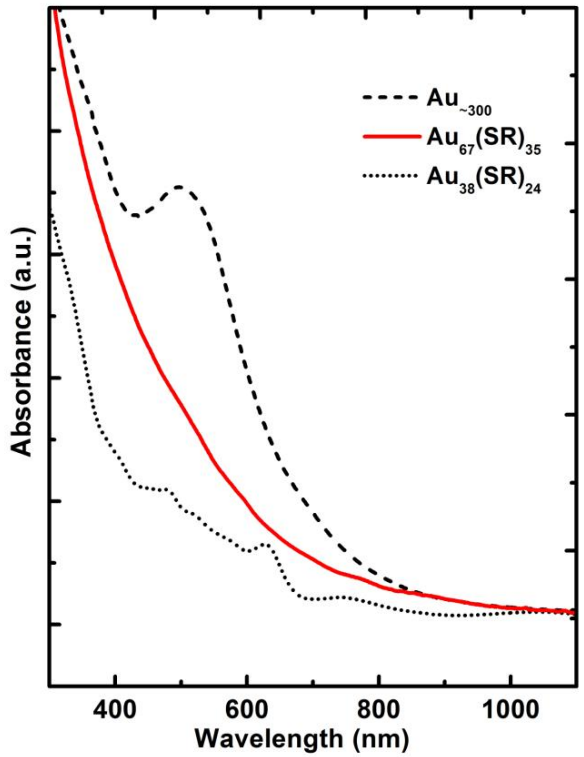

Figure 2.7**.** UV-visible optical spectrum of $Au_{67}(SR)_{35}$ nanomolecules (red) in toluene compared with a smaller cluster $Au_{38}(SR)_{24}$ (dotted) and a larger $Au_{\sim 300,}$ 76.3 kDa cluster (dashed).

2.5.3. Electrochemical characterization

The e*lectrochemical characterization* of the purified Au_{67} compounds mainly involved cyclic voltammetry and differential pulsed voltammetry. Figure 2.8 shows the differential pulse voltammogram (DPV) for $Au_{67}(SCH_2CH_2Ph)_{35}$ that features six distinct features each corresponding to reversible single-electron redox waves, spaced around a large central gap. Taking the charge-state in this region as neutral, these transitions may be regarded as three oxidation peaks (centered at +0.48, +0.70 and +0.95 eV) and three reduction peaks (-0.26, -0.53 and -1.03 eV).

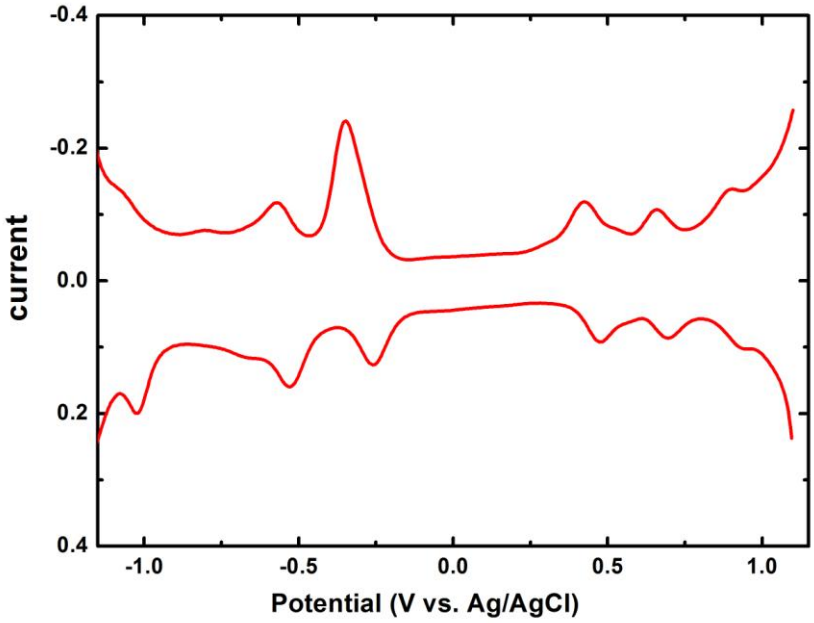

Figure 2.8. Differential pulse voltammetry of $Au_{67}(SCH_2CH_2Ph)_{35}$ nanomolecules in THF solvent / 0.5 M $TBAPF_6$ supporting electrolyte.

The potential difference between the first oxidation and first reduction peaks is

approximately 0.74 eV. The addition energy or the charging energy can be deduced from the two adjacent oxidation peaks and two reduction peaks to be 0.22 and 0.27 eV respectively. Correcting the potential difference gap for charging energy, we obtain the HOMO-LUMO gap for this molecule-like cluster to be 0.50 eV. This value is (i) consistent with Chen et. al.; [36] (ii) consistent with that deduced from optical analysis; and (iii) less when compared to the energy gaps of its smaller counterparts Au_{25} and Au_{38}, but much larger than Au_{144} . The Au_{67} size fits the size dependent trend in the calculated HOMO-LUMO gaps as reported by Murray.[37] As the core size of the nanomolecules increases, they exhibit quantized charging behavior. [70-75]

2.5.4. NMR spectroscopy

Evidence pertaining to the *ligand environments* of the phenylethane thiolate groups of the highly purified $Au_{67}(SCH_2CH_2Ph)_{35}$ has been obtained by ^1H and ^{13}C *NMR spectroscopy* in dilute solutions. The ^1H NMR of the free $PhCH_2CH_2SH$ shows distinct peaks at 2.9 ppm due to methylene protons and near 7 ppm due to aromatic protons. Corresponding features were observed in the ^1H NMR of Au_{67}. This indicates that these thiolate ligands are bound to the gold core. The methylene proton peaks at around 3 ppm are broadened, which is expected for clusters of a larger compound. The broadening of the peaks increases with increasing proximity of the methylene proton to the sulfur head group bonded to the gold surface.[76] The ^{13}C NMR spectrum similarly strengthens the case of chemisorption of thiolate groups on the gold surface. Figure 2.9 shows the carbon peaks of the compound $Au_{67}(SCH_2CH_2Ph)_{35}$ in comparison with that of the reference $PhCH_2CH_2SH$. (The triplet at around 80 ppm is due to the solvent $CDCl_3$.) The peaks in the 130 ppm range are due to the aromatic carbons. The peaks between 20 and 40 are due to the methylene carbons.

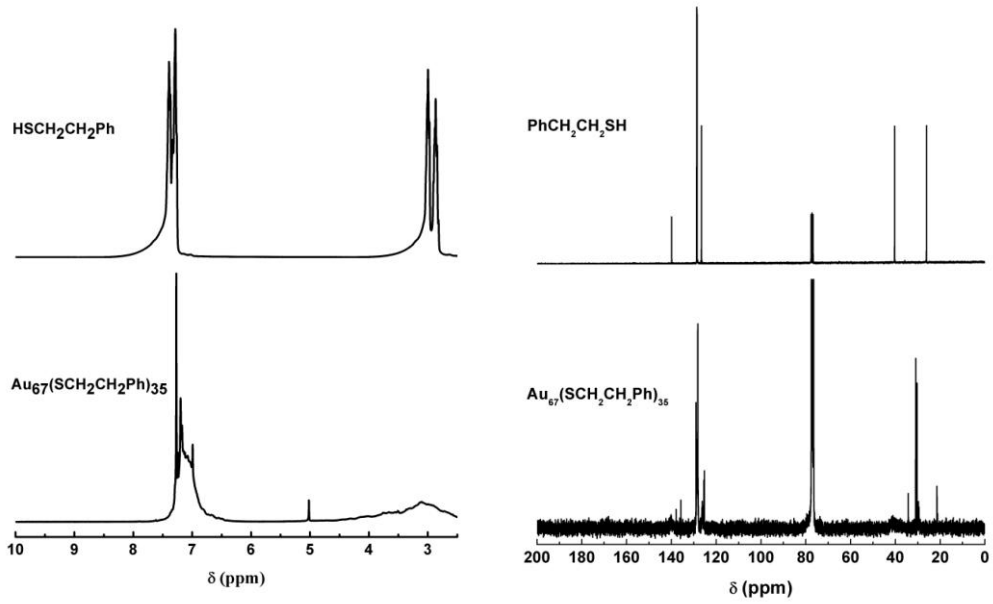

Figure 2.9. ^{1}HNMR spectra (left) of monodisperse $Au_{67}(SCH_2CH_2Ph)_{35}$ compared with that of pure thiol ($PhCH_2CH_2SH$) as reference in $CDCl_3$. ^{13}C NMR spectra (right) of monodisperse $Au_{67}(SCH_2CH_2Ph)_{35}$ compared with that of pure thiol ($PhCH_2CH_2SH$) as reference in $CDCl_3$.

These methylene carbons are the ones, which interact strongly with the gold surface and are therefore broadened or shifted much from their reference positions. NMR spectra also serve as a tool in determining the purity of the compound. Presence of compounds or starting materials that are used during the course of synthesis can be detected in the NMR spectrum. Absence of peaks corresponding to the starting materials and impurities, as in the present case, indicates good post-synthetic work up of the product.

2.5.5. Powder X-ray diffraction

Evidence relating to the *structure of the gold core* of $Au_{67}(SR)_{35}$ has been obtained by *powder X-ray diffraction*, as described in the Methods section. The XRD pattern shown in Figure

2.10 of this sample of the Au_{67} nanomolecules thus gives information on the lattice structure patterns in the gold core of the cluster when compared to the theoretically predicted models.

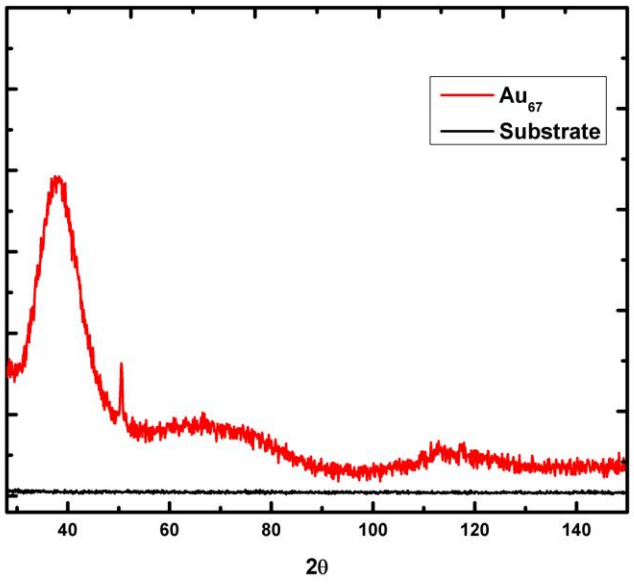

Figure 2.10. Powder X-ray diffraction pattern of $Au_{67}(SCH_2CH_2Ph)_{35}$ nanomolecules (red) in comparison with that of a blank quart substrate (black).

The observed pattern in Figure 2.10 is in substantial agreement with the one discussed by Cleveland et al.,[59] and explained in terms of a Mark's type truncated decahedral morphology and atom-packing. This feature is used in the following discussion to arrive at a plausible structural model. This pattern also gives us idea about the lattice structure transformation from fcc in pure gold to other stable Archimedean structures in the gold nanomolecules. It is reported that these clusters can take any of the three forms (in the process of energy minimization) of an icosahedron, truncated octahedral or octahedron. [59,77]

Having established a definite composition of 67 *Au* atoms and 35 thiolate groups, the question

arises as to what kind of structure and bonding this compound must have in order to account for its high stability or selective formation. Previous X-ray scattering experiments [25] on size-selected gold thiolate clusters with core-mass in the 14-kDa range were interpreted in terms of structures of the truncated-decahedral motif, which have five-fold symmetry accompanied by a certain degree of strain to which the scattering functions are quite sensitive. The particular structures proposed[59] in 1997, were of the (re-entrant, concave) Marks-decahedral (mDh) subclass (for an early description of the mDh see ref [78]), and had either 75 or 73 Au atoms, but the thiolates were assumed to be external, and might number in the 35 - 40 range. A decade later the mDh structure motif has been established for the 79-atom core of the $Au_{102}(pMBA)_{44}$ cluster (a cluster compound with a core mass of a 21 kDa), through total structure determination using single-crystal X-ray diffraction.[11]

Our construction of a structure model for the $Au_{67}(SR)_{35}$ was guided by the above findings, combining the 5-fold mDh motif for a core that is commensurably protected by staple units. The structure models considered have the following features:

(i) The inner core is a 17-atom (minimal) mDh structure, i.e. a pentagonal prism that has been capped on all seven faces; the top and bottom pentagons are, each, capped by a single atom, and one atom caps each of the five rectangular sides (see top and side views in Figure 2.11 (a,i) and 2.11 (b,i))

(ii) A 30-atom shell encapsulates this inner core. It is comprised of two pentagonal 15-atom caps, at opposite poles (top and bottom, see Figure 2.11 (a,ii) and (b,ii), in green), identical to that known for the structure of the 79-atom core of the $Au_{102}(pMBA)_{44}$ cluster. [11] This completes the core part comprised of 17 + 30 = 47 atoms.

(iii) Short stapling units are arranged in a pinwheel fashion over the two polar caps, i.e. five for each cap. These are anchored (stapled) to 10 of the 15 atoms of each cap, leaving unoccupied the remaining five from the periphery of each cap. This accounts for another 10 Au atoms, for a subtotal of 57 of the 67, as well as 20 of the 35 thiolates. See illustration in Figure 2.11 ((a,iii) and (b,iii), as well as Figure 2.11 (c); in these figures the gold atoms in the short (–S-Au-S-) staples are depicted in brown and the sulfur in bright yellow).

(iv) Long stapling units form a belt linking the two polar caps (see in particular the side views in Figure 2.11 (b,iii) and the right configuration in Figure 2.11 (c). Specifically, five such units are anchored (stapled) at each end to one of the above-mentioned peripheral Au atoms of the caps, such that all 30 surface atoms of the core serve as unique anchoring points. The five long staples account for 10 Au atoms and 15 thiolates, completing the grand total of 67 Au atoms and 35 thiolates. The shell-by-shell constructed inspired by earlier reports is shown in Figure 2.11.

Several structural variants can be constructed, all preserving the 5-fold rotational symmetry of the mDh core. Indeed, we have considered such variants, which differed in the specific *S*-anchoring of the long staples to the periphery *Au* atoms of the polar caps. All the structural variants have been optimized (relaxed to minimize the total energy) with the use of first-principles density-functional (DFT) calculations. The one displayed in figure 2.11 (which we referred to as Model I) is favored due to its low total energy, remarkably large energy gap (0.75 eV) between the highest (lowest) occupied (unoccupied) molecular orbitals, HOMO (LUMO) (see Figure 2.8, above) and the superior correspondence between the measured and calculated X-ray scattering function.

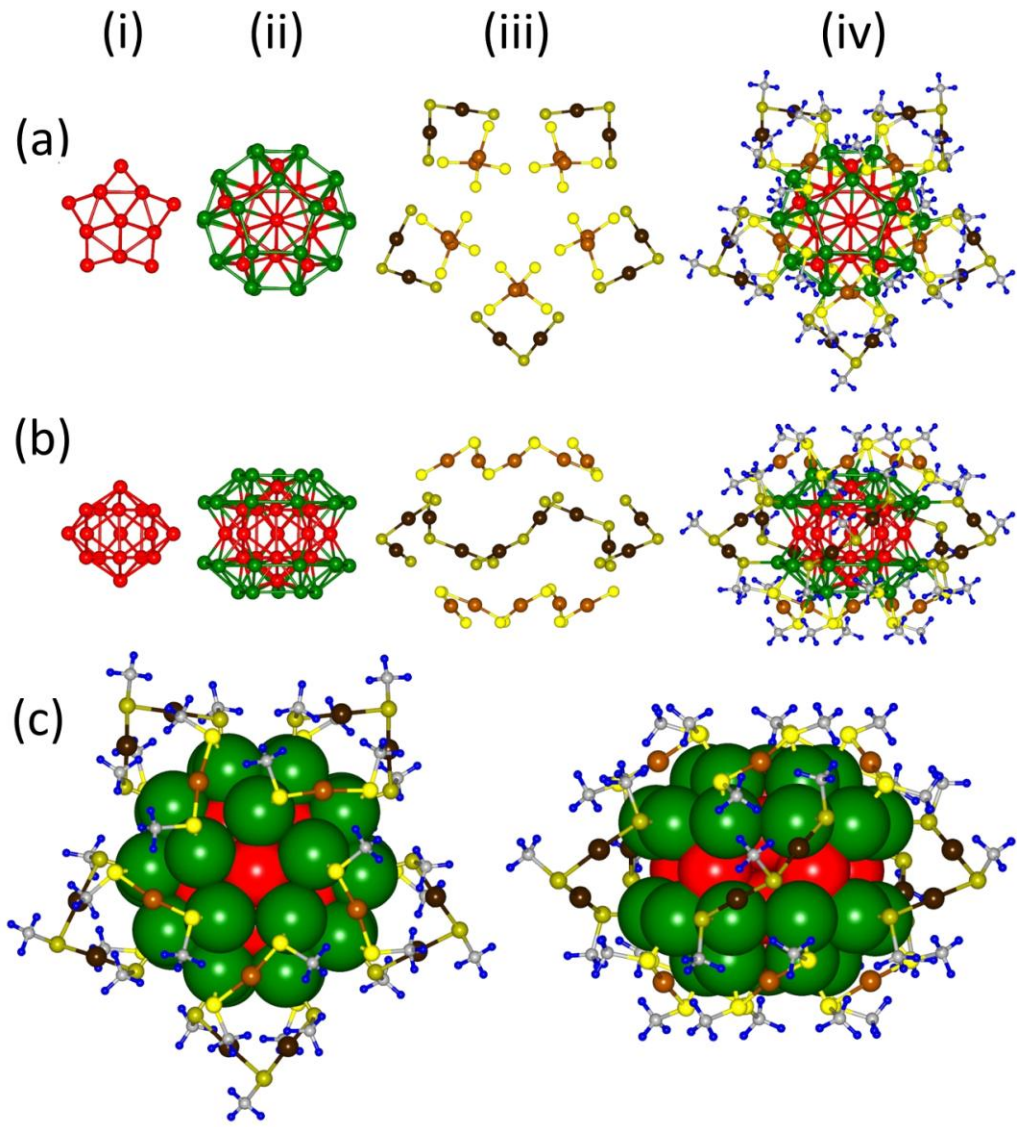

Figure 2.11. DFT- Optimized atomic structure of the $Au_{67}(SCH_3)_{35}^{2-}$. The top two rows (a and b) show two views of the shell-by-shell structures, following the model construction steps in the text. The view in (a) is along the 5-fold axis passing through the atom at the vertex of the mDh and normal to its pentagoal planes, and the view in (b) is along an axis that is normal to the one used in (a). In (i) – (iv) we display for the two views four stages in the construction of the

protected cluster, with the complete $Au_{67}(SCH_3)_{35}^{2-}$ cluster shown in column (iv), as well as in (c) where the structure on the left is the same as the one in (a,iv), and the structure on the right corresponds to that shown in (b,iv). The following structure-building elements are depicted: (i) the 17 Au atom gold mDh (gold atoms in red). (ii) The mDh with the addition of the two pentagonal 15 Au atom caps (in green), forming the Au_{47} (17+2x15 = 47) core of the protected cluster. (iii) The ten short (-S-Au-S-) staples (gold atoms in brown and sulfur in bright yellow), and five long (-S-Au-S-Au-S-) staples (gold atoms in black and sulfur in green-mustard color). In (b,iii) the long staples are located between the upper and lower rows which contain the short staples. In both (a,iii) and (b,iii) the staples are drawn in the configuration and orientation that they take when attached to the 47-Au atom core to form the protected $Au_{67}(SCH_3)_{35}^{2-}$ cluster (see (a,iv), (b,iv) and (c)). In the figures for the protected cluster the C atoms of the $–CH_3$ groups are shown as small light gray balls, and the hydrogen atoms as smaller blue spheres. For further details, including values of interatomic distances in Model I, as well as for atomic structure images for model Structure II.

2.6. Conclusions

We report the high yield synthesis and composition determination of $Au_{67}(SR)_{35}$, a nanomolecule lying between the superstable 38- and 144- metal atom cores, identified using high resolution ESI mass spectrometry. The THF solvent mediated synthesis, employing phenylethane thiolate ligand yielding the title compound has been reproduced over one hundred times in our laboratory among various researchers spanning a four year time period. Multiple techniques were used to characterize the title gold nanomolecule. Electronic properties were explored using optical absorption spectroscopy (UV-visible-NIR regions) and electrochemistry (0.74V spacing

in differential-pulsed-voltammetry), modes of ligand binding were studied by NMR spectroscopy (^{13}C and ^{1}H), and structural characteristics of the metal atom core were determined by powder X-ray measurements. The electronic structure of the cluster was analyzed using first-principles DFT calculations, interpreted within the framework the superatom shell model. The main feature in the electronic spectrum of the $Au_{67}(SCH_3)_{35}^{2-}$ cluster is the large HOMO-LUMO energy gap, $\Delta_{HL} = 0.75\ eV$, corresponding to a superatom shell closing at 34 electrons of the dianionic nanomolecule; further experimental work pertaining to the theoretically predicted charge state of the protected cluster is desirable. The observed and calculated large electrochemical gap is an indication to the high stability to the cluster with resistance to chemical attack. The definite compositional evidence and augmented structural measurements have been employed to devise structural models that might account for the singular stability and salient properties of these compounds. One of these models has been found to be superior in all these respects, and consequently its stability, electronic structure and bonding, and likely electronic transitions (optical and charging) have been investigated in further detail, to provide deeper insight into this prominent class of compounds. Structurally, the $Au_{67}(SR)_{35}$ nanomolecule is the smallest to adopt the complete truncated-decahedral motif for its core with a surface structure bearing greater similarity to the larger nanoparticles. Its aforementioned electronic energy gap (~0.75 eV) is nearly double that of the larger Au_{102} compound and it is much smaller than that of the Au_{38}.

The intermediary status of the $Au_{67}(SR)_{35}$ nanomolecule is also reflected in both its optical and electrochemical characteristics. Indeed, while Au_{144} shows quantized double-layer charging and Au_{38} exhibits molecule-like electrochemical behavior, the electrochemical band

gap and optical spectra of Au_{67} show that it is positioned below the onset of metallic behavior. Isolation and characterization of distinct nanomolecules in this size regime and development of a first-principles theoretical framework of interpretive and predictive capability, are indispensable in order to gain deep insights about the transition from ‘metallic’ to ‘molecular’ character.

CHAPTER THREE

SYNTHESIS, CHROMATOGRAPHIC ISOLATION AND CHARACTERIZATION OF 27000 Da NANOMOLECULES

Part of the text and figures in this chapter are extracted from the following publications:

Amala Dass,†,* Praneeth Reddy Nimmala†, Vijay Reddy Jupally and Nuwan Kothalawala,

Nanoscale, 2013,**5**, 12082-12085

CHAPTER THREE

SYNTHESIS, CHROMATOGRAPHIC ISOLATION AND CHARACTERIZATION OF 27 kDa NANOMOLECULES

3.1 Abstract

Gold nanomolecules possess size specific optical and electrochemical properties that make it important to develop precise and size specific synthetic protocols. In this project, I have synthesized and characterized gold nanomolecules in the 27 kDa mass range using ols and phenylethanethiol. We have employed size exclusion chromatography to isolate the title compound in high yields (~50 mg). The purity of the isolated compound was analyzed using MALDI-TOF mass spectrometry. The compositional assignments were performed by the high-resolution electrospray-ionization mass spectrometry. Unlike other compositions of Au_{25}, Au_{67} and Au_{144} which were single sized, the 27 kDa sample composed of multiple species of $Au_{103}(SR)_{45}$, $Au_{104}(SR)_{45}$, $Au_{104}(SR)_{46}$ and $Au_{105}(SR)_{46}$, where R = $-SCH_2CH_2Ph$. It is interesting to note that no $Au_{102}(SR)_{44}$ was observed in this sample which is in the same size range and the largest crystal structure reported so far (with R = -SPhCOOH)[18]. This observation might be a result of the different ligands used in the synthesis, which can influence the size and structure of the resulting nanomolecule. However, all the four species observed in this project,

with ligands of -SCH_2CH_2Ph and -SC_6H_{13} are at or near the 58 electron shell closing which is believed to be the stabilizing factor for these nanomolecules.

Author contributions

Praneeth Nimmala performed the synthesis and isolation of $Au_{103\text{-}105}$, optical spectroscopy and powder X-ray diffraction experiments. Vijay Jupally reproduced the experiments using two other ligands hexanethiol and dodecanethiol to confirm the composition of the compound. Nuwan kothalawala performed initial optical spectroscopic analysis for this compound.

3.2 Introduction

Gold thiolate nanomolecules contain a distinct number of gold atoms and thiolate groups with potential applications in the areas of catalysis, biomedicine, sensors and nano-devices. These compounds possess size specific properties making it essential to design synthetic protocols for each size. The crystal structure determination of $Au_{102}(SPhCOOH)_{44}$ in 2007 was the first of its kind and it was a breakthrough as it related the structure and properties of these compounds. Since then the research in this field has progressed rapidly. Au_{102}, with a mass of ~27 kDa was of high interest to the field, but there were no protocols to make it in large quantities. Research on gold nanomolecules until then was mainly focused on preparing Au_{25} and Au_{144} sizes as its synthesis involved only one step. Although the 27 kDa size was often observed in the mass spectra of synthesis, its isolation and characterization was hindered by issues of stability, lack of isolation techniques and low yields. With the experimental knowledge of synthesis and isolation of $Au_{67}(SR)_{35}$ described in previous chapter, we have attempted to do the

same with the 27 kDa species. One striking difference or improvement going from Au_{67} to $Au_{103-105}$ is the use of size exclusion chromatography (SEC) for the isolation instead of the solvent fractionation technique. SEC offers a less laborious, less time consuming, highly reproducible and an overall more effective separation of the compound. The detailed characterization of the compound was achieved after its isolation in large quantities.

In this report, we have synthesized the 27 kDa nanomolecules for the first time and purified it using size exclusion chromatography. The optical spectrum of the compound shows a monotonous curve with less absorption features, characteristic of nanomolecules between smaller clusters like Au_{38} and larger clusters like Au_{130}. Its purity was determined based on MALDI-MS. Using high resolution ESI-MS, it was found that it comprises multiple species namely, $Au_{103}(SR)_{45}$, $Au_{104}(SR)_{45}$, $Au_{104}(SR)_{46}$ and $Au_{105}(SR)_{46}$. Interestingly, no $Au_{102}(SR)_{44}$ peak was found in the mass spectrometry of the products with phenylethanethiol and hexanethiol. We labeled it as $Au_{103-105}(SR)_{45-46}$ for convenience. The synthesis of 27 kDa compound involves three steps, the first two are same steps employed in synthesis of Au_{67} (discussed in chapter 2). The first step involves synthesis of a crude product using one-phase THF method yielding a polydisperse mixture of Au_{25}, Au_{67} and the 27 kDa compound. The second step involves a mild thermo-chemical treatment to yield distinct peaks in a polydisperse mixture. The third and final step involves isolation of the $Au_{103-105}$ from the mixture using size exclusion chromatography.

3.3 Experimental methods

3.3.1Chemicals

Phenylethanemercaptan (Sigma aldrich, 98%), sodium borohydride (Acros, 99%), trans-

2-[3-(4-tert-butylphenyl)-2-methyl-2-propenylidene]malononitrile (DCTB matrix) (Fluka, ≥ 99%) were purchased from Aldrich. Tetrahydrofuran (Acros anhydrous, stabilized 99.9%) and other solvents like toluene, methanol, acetonitrile and acetone were used from Fisher as received. Biorad-SX1 beads from Biorad were used for the SEC according to the published literature[22]. Rubidium, potassium and sodium acetate salts used in the ESI-MS analysis were purchased commercially and used as received.

3.3.2 Equipment

UV-Visible absorption spectra were recorded in toluene on a Shimadzu UV-1601 instrument. Matrix assisted laser desorption time-of-flight (MALDI TOF) mass spectra were collected on a Bruker Autoflex 1 mass spectrometer in linear positive mode using a nitrogen laser (337 nm) with DCTB as a matrix. ESI-MS spectra were acquired on Waters SYNAPT HDMS instrument either with or without cesium acetate as an electrolyte. Powder XRD measurements were performed on Bruker D8-Focus XRD instrument on a quartz substrate. 10 mg of sample was dissolved in minimal amount of toluene and deposited on the substrate and air-dried.

3.3.3 Size exclusion chromatography

Background

Size exclusion chromatography (SEC) for separation of gold nanomolecules was first introduced by Stefan et al. at the University of Geneva in 2011.[22] They demonstrated SEC separation of Au_{38} and Au_{40} nanomolecules, which only differ by two gold atoms. In the same year, we had visited University of Geneva as a part of research collaboration with Prof. Burgi's group. As part of this visit, I had an opportunity to learn about the SEC technique. For the next

six months, I have worked on developing the technique for a wide range of applications in our laboratory. Over the last two years, the technique has matured to a great extent in our laboratory and helped expedite our research progress in many ways. This section of the chapter is dedicated to describe the minutiae of the SEC procedure for obtaining best results.

SEC Procedure

Preparation of column and sample: First step in the preparation of a SEC column is the selection of appropriate porous beads. The beads were commercially available and purchased from *Bio-rad (catalog # 152-2151)*. The beads are made of styrene divinylbenzene with 1% crosslinkage. The appropriate diameter of the pores of this particular BioradSX1 beads is 40–80 μm. They were assigned to be suitable for the separation of molecules in the mass range 600–14,000 Da. However, this number was allocated for globular proteins based on their hydrodynamic radius. But in the case of gold nanomolecules, they are seen to be effective up to 200,000 Da, probably due to the compact structure and heavy metal atoms in the nanomolecules. The beads are available in 100g bottles as well as 1 kg. About 100 g of the solid beads were soaked in ~0.5 L of THF in a 1 L beaker topped with a lid to prevent solvent evaporation. The beads need to be soaked for at least 6 hrs, preferably overnight. The beads expand in volume during this time. So initially it's a good practice to have few hundred milliliters of excess solvent when in doubt. The choice of solvent was tetrahydrofuran (stabilized with butylated hydroxy toluene or BHT) as it is compatible with the beads and dissolve the nanomolecules of a wide size distribution. The context mentioned in here is for nanomolecules capped with non-polar ligands like straight chain alkanethiols and phenylethanethiol. In case of separation of nanomolecules capped by polar/water soluble ligands like captopril and glutathione, we had different choice of beads and

solvent. After sufficient soaking, the solution looks thick and viscous and is ready to be packed into the column. The columns for SEC in our laboratory were specially ordered from chemglass with the following dimensions " *Column, Chromatography, 1.0" I.D., 40" Effective Length, 4mm Teflon Stopcock, Coarse Fritted Disc, Beaded Top*". A little cotton wool was pushed on to the fritted disc before we load the bead solution. The solution is slowly loaded through the side of the column with the stopcock open to avoid any air bubbles. At this point using excess solvent is helpful as it would eliminate the formation of air bubbles. As the beads pack in the column, the excess THF exits through the bottom. This way, the column is to be carefully packed with beads until the final level of the bed is ~4 inches from the top. Once the beads are completely packed, the stopcock is closed. It is to be made sure that the column never runs out of solvent to avoid drying of the beads. When idle, the column needs to be filled with THF solvent to 2 inches above the bed surface and capped with a lid to minimize the solvent vaporization.

Table 2.1 : List of properties of an SEC column for optimum separation in nanomolecules

Properties of SEC for optimum separation	
Column dimensions	1.0" I.D., 40" Effective Length, 4mm Teflon Stopcock, Coarse Fritted Disc, Beaded Top
Beads used	Bio-Beads S-X1 Support(#152-2151)
Amount of beads soaked	100 g in ~500 ml of solvent
Soaking time	> 6 h (preferably overnight)
Optimum amount of sample	~50 mg
Solvent/eluent	Tetrahydrofuran (stabilized with BHT)
Volume of fractions collected	~4 ml in a 20 ml preweighed vial

S*eparation using SEC:* The first step for separation using SEC column is sample preparation. The sample here is a polydisperse mixture which we intend to separate. It needs to be completely soluble in eluent solvent THF. The presence of insoluble materials in the sample disrupts the column as it sits on the bed surface permanently without any movement down the column. To ensure that there are no insoluble materials in the sample, it is a good practice to dissolve the sample in about 2-3 ml of THF and centrifuge for about ~5 mins @ 3000 rpm. Any insoluble material that may be present in the sample will precipitate. The soluble nanomolecule solution is decanted into a clean vial and dried using rotary evaporation. It is advisable to weigh the sample at this point and record the amount of sample being loaded on to the column. Typically, we load ~50 mg of samples on to the SEC column for optimum separations. The dried sample, which is ready for SEC, is dissolved in ~0.5 ml of THF and loaded on to a column.

Running a column: Before loading the sample, the first step is to bring the solvent level close to the bed surface of the beads. To do this, the stopcock was let open and solvent was allowed to elute. At the time when the solvent level reaches the bed surface, the ~0.5 ml of the nanomolecule sample was loaded on to the bed with a glass pipette. It is advisable to spread the sample throughout the surface of the column bed. Care should be taken at this time not to spill the sample on the walls of the column. Since the stopcock is open, the sample continues to flow down the column. As the samples runs down under the surface, we gently added solvent with a glass pipette through the walls of the column. Adding the solvent directly on the surface of the beads can disrupt the sample resulting in ineffective separation. About 10 pipettes (~1.5 ml THF/pipette) of solvent was added gently around the side. At this point, the sample has run down a few centimeters from the surface allowing us to fill the column with solvent using a beaker. For

best separation the nanomolecule sample should initially elute as a thin band. As the sample runs down along with the eluent, it should be made sure that there is solvent above the bed all along. With the above-mentioned dimensions of the column, the total run-time for the sample is ~45 mins.

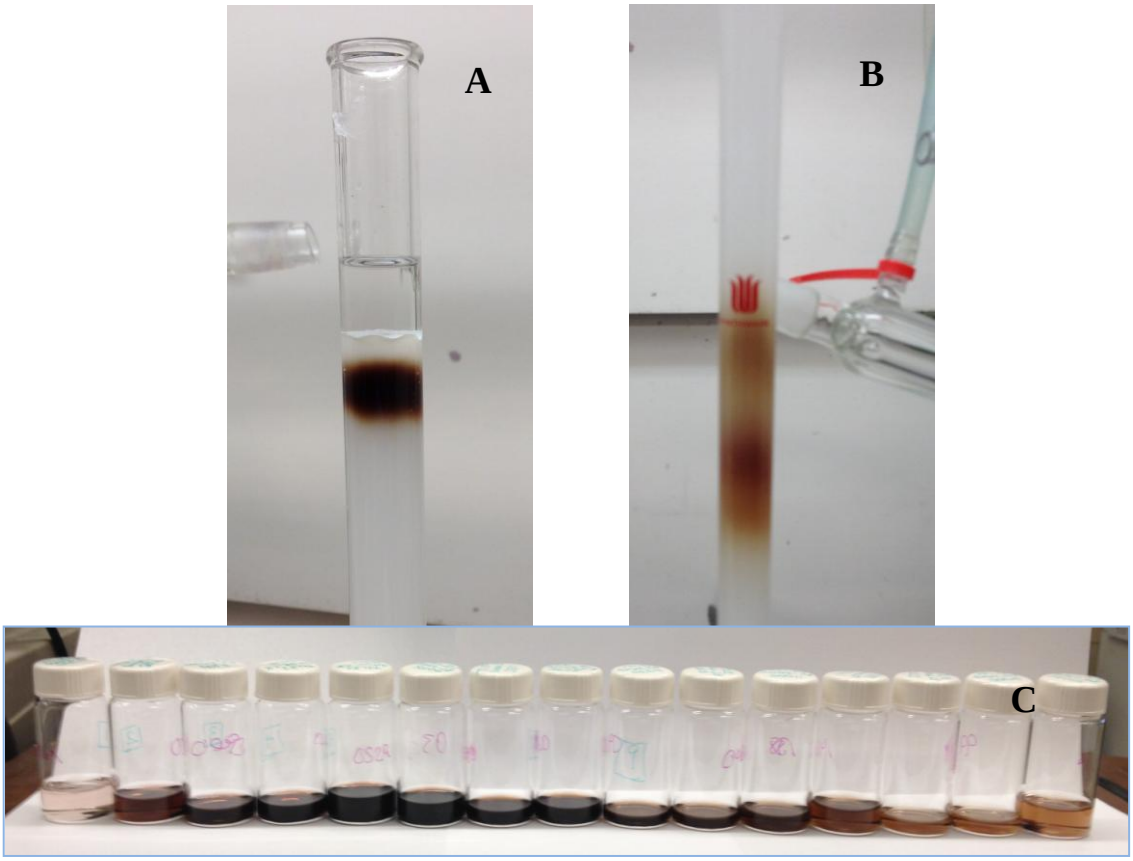

Figure 3.1. Images illustrating a typical SEC separation process. 3.1a shows the column just after loading the sample. 3.1b shows the sample mid-way down the column separating on the basis of size. 3.1c shows the 15 fractions collected in the process. Larger sizes are eluted in the initial fractions whereas smaller sizes are eluted in the later fractions.

As the sample runs down the column, the nanomolecule mixture spreads out vertically

based on the size and hydrodynamic volume. Once the sample starts eluting, fractions are collected into preweighed 20 ml glass vials. Approximately 4 ml of sample was collected in each fraction. A typical size exclusion chromatography involving ~50 mg of sample was collected in 10 to 15 fractions. The fractions collected in the chromatography were dried using rotary evaporation. Washing with ethanol three times was required to remove the BHT stabilizer present in the THF. The fractions were dried and weighed. These fractions were then analyzed using UV-vis, MALDI and ESI-MS techniques as required.

3.4 Synthesis and isolation of $Au_{103-105}(SR)_{45-46}$

$Au_{103-105}$ is produced only in a one-phase THF synthesis. It was first observed in a one-phase synthesis of Au_{25} where a polydisperse mixture containing Au_{25}, Au_{67} and $Au_{103-105}$ finally end up in a monodisperse Au_{25} product. It was from this reaction that the idea of separating Au_{67} and $Au_{103-105}$ came. The synthesis of $Au_{103-105}$ involves three steps, the first and second steps are same as Au_{67} but the third one is different in that the isolation is performed using size exclusion chromatography instead of solvent fractionation.

Step 1: Synthesis of crude product : Typically, 0.5 mmol of $HAuCl_4.3H_2O$ was dissolved in 20 ml of THF and stirred for about 10 min before adding 6 mmol of phenylethanethiol ($PhCH_2CH_2SH$). The reaction mixture changed its color from golden yellow to turbid in about 15 mins (when stirred at 500 rpm). Then, we added 5 mmol of $NaBH_4$ to the reaction mixture. The color of the reaction mixture turned black. The stirring was continued for another 5 min and then the solvent was removed from the reaction mixture by rotary evaporation as quickly as possible. Once the solvent was completely removed, the resulting product, which was adhering to the round bottom flask, was washed with methanol two or three times to remove the excess thiol and

other reaction byproducts. At this stage, the MALDI mass spectrometric analysis of this crude product shows a broad peak ranging in mass.

Step 2: Mild thermo-chemical treatment of Au_{67} and $Au_{103\text{-}105}$ mixture : The synthesis of crude products does not yield the final product, the MALDI-MS may show a broad peak ranging in m/z value of 10 kDa to 35 kDa. In fact, this broad peak is typical of many reactions involving synthesis of the crude mixtures in step 1. In such cases it is difficult to proceed for solvent fractionations as the baseline between the two clusters Au_{67} (14 kDa) and $Au_{103\text{-}105}$ (22 kDa) are not perfectly resolved; in other words, there are many other metastable clusters other than Au_{67} and $Au_{103\text{-}105}$. These peaks can often be sharpened by a mild thermochemical treatment.[58] This was accomplished by heating the product of stage 1 (≈100mg) in 0.5 ml of toluene and 0.2ml of phenylethanethiol at 60°C for one hour.[23,66] This treatment flattened the baseline (see Figure 2.1 in chapter 2) between the stable clusters (Au_{67} and $Au_{103\text{-}105}$) and made it suitable for further separation (step 3). Avoid harsh chemical conditions (higher temperature or longer reaction time) for this step, as they may result in decomposition or conversion of the species of interest.

Step 3: Size exclusion chromatography to obtain pure $Au_{103\text{-}105}$: To obtain monodisperse $Au_{103\text{-}105}$, a separation step has to be performed to remove the Au_{67} and other sizes present in the polydisperse mixture obtained from step 2. Figure 3.2 shows the MALDI mass spectrometry of systematic isolation of various nanomolecules based on the hydrodynamic volume or the size. In this case, the nanomolecule of our interest is $Au_{103\text{-}105}$ (fractions 5) but in general, the same separation also yields Au_{67} in its pure form (fractions 8). In other words, it is possible to synthesize pure Au_{67} and $Au_{103\text{-}105}$ using this protocol.

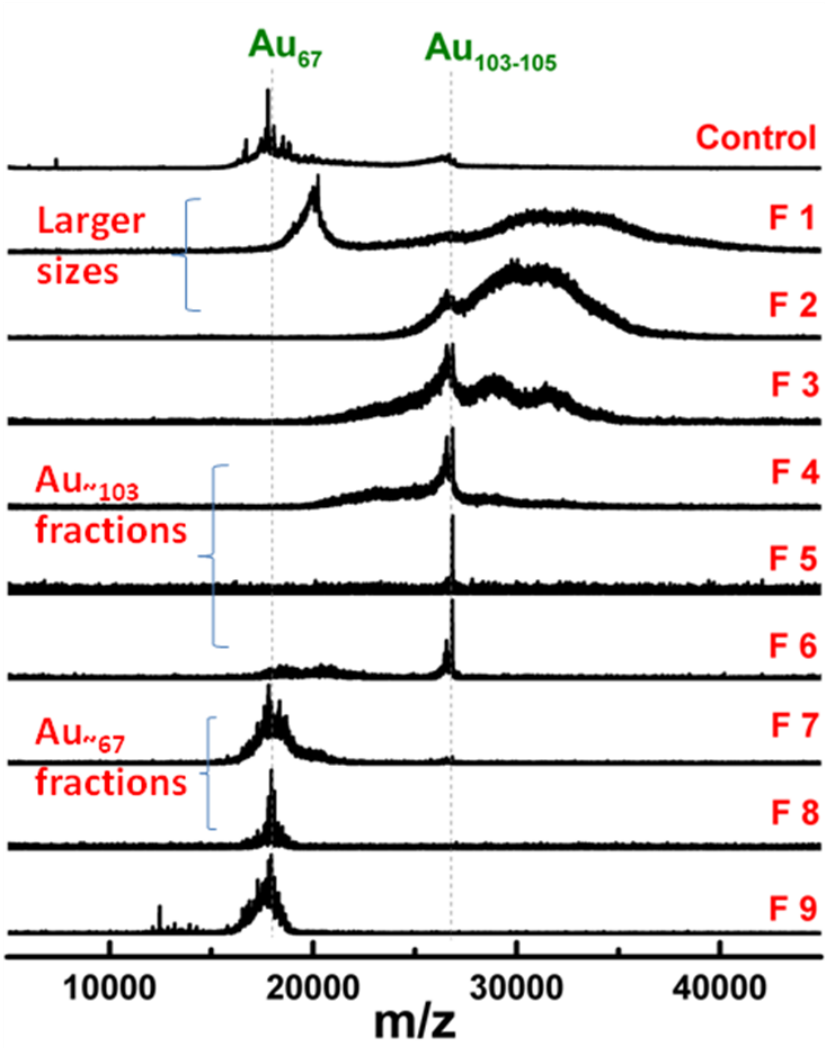

Figure 3.2. MALDI-MS monitored size exclusion chromatography of a polydisperse mixture containing Au_{67} and $Au_{103\text{-}105}$.

3.5 Results and discussion

Isolation of $Au_{103\text{-}105}$ using SEC : Obtaining pure samples of gold nanomolecules is a requirement for its characterization and applications. The use of SEC technique in isolation and purification of gold nanomolecules serves this purpose. It was first used by Stefan et al[22] University of Geneva for the separation of Au_{38} and Au_{40} nanomolecules, which differ by just two Au atoms, on a semi-preparative scale (~10 mg)[22]. It is a highly effective and versatile

technique. The beneficial features of SEC compared to solvent fractionation includes: a) more control, b) less laborious, c) highly reproducible, d) yields compounds with improved purity, e) can be used with various size distributions, f) allows for separation of multiple pure samples from a single run and g) minimum loss of nanomolecules as impure fractions. All the above-mentioned advantages of SEC far outweigh the rendered benefits of solvent fractionation. This technique developed as part of my doctoral research has become the method of choice at the UM-Dass lab for separation of nanomolecules like Au_{67} and $Au_{\sim 103}$.

The separation of nanomolecules in size exclusion chromatography is based on the hydrodynamic volume, in other words, the *size and shape* of the compounds in the mixture. Nanomolecules smaller in size compared to the pore size of the beads pass through them while those larger in size escape the bead pores. This way, the larger nanomolecules are eluted first followed by the smaller ones. The separation is affected by factors like a) amount of the polydisperse sample used for separation b) solvent used to dissolve and elute the nanomolecules and c) the sample loading technique, which comes with experience and paying attention to detail. For purification of $Au_{103\text{-}105}$ in the current case, we loaded ~100 mg of the polydisperse mixture on to the column in about 0.4 ml of tetrahydrofuran (THF). 9 fractions were collected with THF as eluent as shown in figure 3.1. 100 mg of the polydisperse sample labelled as "Control" in figure 3.1 was loaded on to the column. As the sample passes through the column, the mixture is separated into different bands based on the size. These different bands were collected as several fractions in glass vials as they exit the column. The collected fractions were analyzed using MALDI mass spectrometry. The mass spectrum of initial fractions in figure 3.1 showed the presence of larger sizes like Au_{144} along with some $Au_{103\text{-}105}$. They are followed by a few

fractions of $Au_{103-105}$, which was the compound of interest in this case. Following that were fractions of Au_{67} and other lower clusters. Overall, SEC has been an effective method in isolation and purification of gold nanomolecules and has been a routinely used technique in our laboratory. The experimental conditions for the set up of the SEC are detailed in the experimental section above.

Mass spectrometry of the 22 kDa nanomolecules : We have performed the mass spectrometric analysis of the 22 kDa nanomolecules using MALDI and ESI-MS for testing purity and assigning composition, respectively.

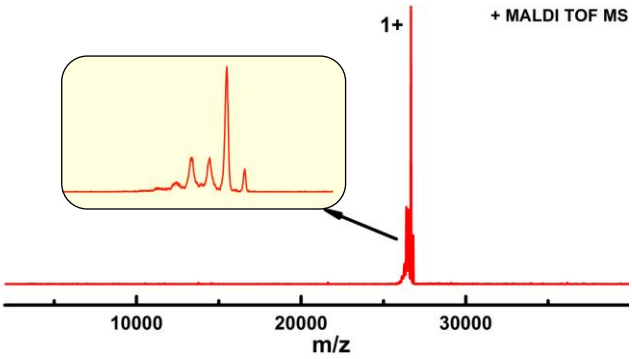

Figure 3.3. MALDI-TOF mass spectrum of the "22 kDa" nanoclusters using DCTB matrix. Inset shows the expansion of the peaks showing the presence of multiple peaks.

The MALDI mass spectrum of the 22 kDa species in figure 3.3 shows the 1+ peaks of the compound. There are no other peaks in the mass range 5 kDa to 40 kDa indicating the high purity of the sample. No assignments were made based on the MALDI data as there are no appropriate calibration standards of sufficient resolution to make accure mass measurements in this range.

High resolution ESI MS data of the 22 kDa nanoclusters in the presence of metal

acetates[79] is shown in Figure 3.3 A. Two sets of peaks corresponding to the 2+ and 3+ charge states were observed as shown in Figure 3.3 A. Analysis of the 3+ peaks, shown in Figure 3.3 B, revealed the identity of the clusters as $Au_{103}(SR)_{45}$, $Au_{104}(SR)_{45}$, $Au_{104}(SR)_{46}$, and $Au_{105}(SR)_{46}$.

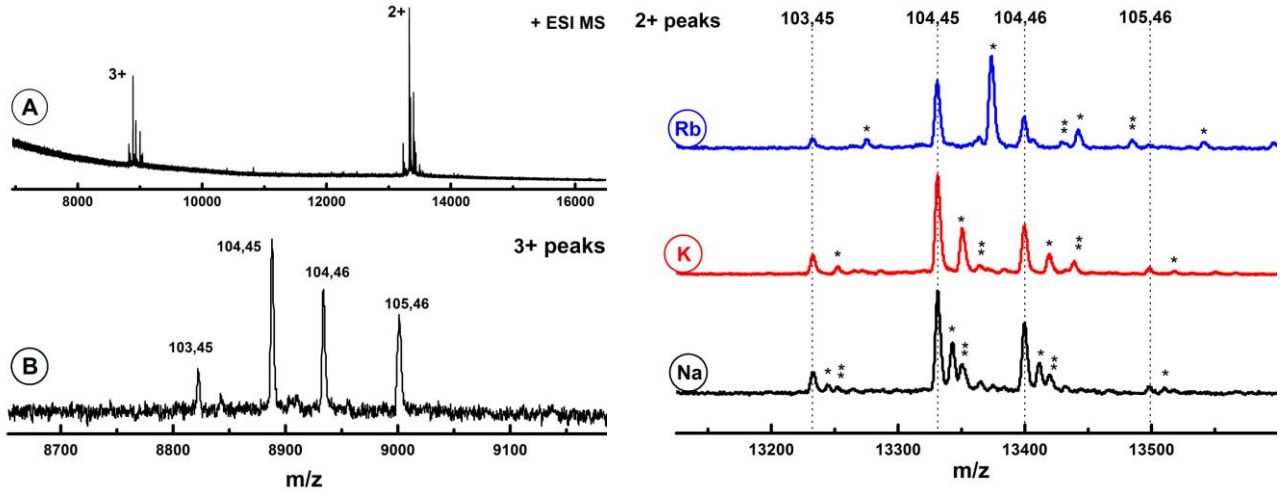

Figure 3.4. ESI mass spectra of the 22 kDa nanoclusters in 50:50 toluene:CH_3CN mixture with addition of metal acetates. (A) ESI spectra in the full mass range with KOAc and (B) expansion of 3+ peaks showing the presence of $Au_{103}(SR)_{45}$, $Au_{104}(SR)_{45}$, $Au_{104}(SR)_{46}$, $Au_{105}(SR)_{46}$. (Rb) (K) and (Na) expansion of 2+ peaks using rubidium, potassium and sodium acetate salts respectively, confirming the presence of the same set of peaks as in 3+ region. The peaks marked by one and two asterisks represent nanoclusters with one and two cationic adducts respectively, the mass difference corresponding with the cations. Notably $Au_{102}(SR)_{44}$ is not detected.

These four (103,45), (104,45), (104,46) and (105,46) peaks could be due to one single species, but appear as four peaks in mass spectra due to different adducts or fragmentation. For example, Tsukuda's work showed that due to different charges states, $Au_{25}(SR)_{18}$ can show three peaks due to adduct formation, corresponding to $Au_{25}(SR)_{18}^{+}$, $[Au_{25}(SR)_{18}.TOA]^{+}$, $[Au_{25}(SR)_{18}$.

$2TOA]^+$.[80] To rule out adduct formation, we studied the set of four peaks, by intentionally adding alkali metals salts to promote adduct formation. We did this systematically by using Na, K and Rb ions, so the shift in mass can be followed.[79] Cesium ions were intentionally avoided due to the similarity in the mass of cesium (132.9 Da) and SCH_2CH_2Ph ligand (137.2 Da). Figure 3.4 Rb, K and Na show the analysis of the 2+ peaks in the presence of rubidium, potassium and sodium acetate salts. These peaks confirmed the assignments made in Fig 3.4. This intentional metal salt adduction, including the now popular cesium acetate addition to promote the ionization of the nanocluster via [Nanocluster • $Cs]^+$ adduct formation was originally pioneered by Murray *et. al.*.[79]

In Figure 3.4 Rb, K and Na spectra, the molecular peaks denoted by the dotted lines are present at the same mass, as in the case of no salt addition. For each molecular ion, the cationic adducts containing one and two cations, marked by one or two asterisks, respectively, are also seen. The mass difference of these adducts match with the mass of the Na, K and Rb ions as seen by the increasing mass difference. A Waters Q-TOF SYNAPT was used for ESI MS and the TOF calibration was performed using CsI. Calibration check was performed using the 1+ ions of $Au_{25}(SCH_2CH_2Ph)_{18}$ and the 3+ ions of $Au_{144}(SCH_2CH_2Ph)_{60}$. In the ionization conditions used in this work, there was no fragmentation for $Au_{25}(SCH_2CH_2Ph)_{18}$ and $Au_{144}(SCH_2CH_2Ph)_{60}$ analysis. Hence, we concluded that the various clusters observed in this work - $Au_{103}(SR)_{45}$, $Au_{104}(SR)_{45}$, $Au_{104}(SR)_{46}$, and $Au_{105}(SR)_{46}$ - *are present in solution* and not a product of fragmentation in the mass spectrometer. The confidence of the *mass assignments* is of *high quality*, for the following reasons: 1) data from unique ionization methods, MALDI and ESI support the results 2) the assignment of the ions of 2+ and 3+ charge states agree with each

other; 3) three different metal adducts, namely Rb, K and Na yield systematic and expected mass shifts from the molecular ions; 4) the instrument was calibrated with well-known nanomolecules (Au_{25} and Au_{144}) and fragmentation was ruled out; 5) the results are repeated by multiple investigators over a period of 5 years. No negative ions were observed in the ESI MS analysis.

We note that $Au_{102}(SCH_2CH_2Ph)_{44}$ is not observed in this project. This could be due to the differences in the ligand. *p*-mercaptobenzoic acid is aromatic, acidic, and hydrophilic, when compared with $–SCH_2CH_2Ph$. Using an aromatic ligand, -SPh, in the synthesis leads to the formation of the 36-atom species.[35] The use of $–SCH_2CH_2Ph$ or $–SC_6H_{13}$ ligands lead to an 38-atom species. So, clearly using an aromatic ligand leads to different core sizes in some cases when compared with $–SCH_2CH_2Ph$ or $–SC_6H_{13}$ ligands. Instead of the Au_{102} core protected by aromatic core, here we observed a mixture containing $Au_{103}(SR)_{45}$, $Au_{104}(SR)_{45}$, $Au_{104}(SR)_{46}$, and $Au_{105}(SR)_{46}$ clusters.

Powder X-ray diffraction of $Au_{103\text{-}105}$: Powder X-ray diffraction (XRD) analysis was performed to study the atomic structure.

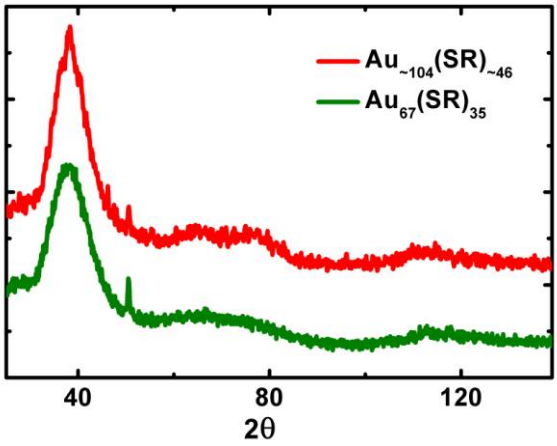

Figure 3.5. Powder XRD of the "22 kDa cluster" containing a mixture of $Au_{103}(SR)_{45}$, $Au_{104}(SR)_{45}$, $Au_{104}(SR)_{46}$, and $Au_{105}(SR)_{46}$ nanoclusters in comparison with $Au_{67}(SR)_{35}$. The

diffraction features in both the cases match, suggesting the marks decahedral structure of the samples.

Figure 3.5 shows the powder XRD pattern of the sample in comparison with $Au_{67}(SR)_{35}$.[12] The diffraction pattern resembles to that of Au_{67}, which was predicted to have Marks decahedral core.[12] The single crystal XRD structure of $Au_{102}(SC_6H_4\text{-}COOH)_{44}$, shows a Au_{79} Marks decahedral core. Therefore, we conclude that the mixture of $Au_{103}(SR)_{45}$, $Au_{104}(SR)_{45}$, $Au_{104}(SR)_{46}$, and $Au_{105}(SR)_{46}$ nanoclusters also possess similar Marks decahedral geometry. The theoretical calculations[51,81] and growing single crystals of the samples would facilitate the understanding of structures of these species.

3.6 Conclusions:

In conclusion, we report the high yield synthesis of 22 kDa nanomolecule. Isolation and purification was performed using size exclusion chromatography. This is the first time ~50 mg quantities of nanomolecules were obtained using this technique. Mass spectrometric analysis of the compound showed the presence of multiple species in this region. It was also interesting to note the absence of $Au_{102}(SCH_2CH_2Ph)_{44}$ indicating the key effect of the ligands on the size and structure of geometry. This results have lead to the investigation of processes like "core size conversion" and the effect of ligands on the structure and property of nanomolecules.

CHAPTER FOUR

CORE SIZE CONVERSION IN GOLD NANOMOLECULES AS A ROUTE TO SYNTHESIZE Au_{38} AND Au_{40}

Part of the text and figures in this chapter are extracted from the following publication:

Praneeth Reddy Nimmala†, Vijay Reddy Jupally† and Amala Dass*

Langmuir, 2014, 30 (9), pp 2490–2497

† : Authors contributed equally to the manuscript

CHAPTER FOUR

CORE SIZE CONVERSION IN GOLD NANOMOLECULES AS A ROUTE TO SYNTHESIZE Au_{38} AND Au_{40}

4.1 Abstract

Gold nanomolecules are composed of a precise number of gold atoms and organo-thiolate ligands. Most of the syntheses used for gold nanomolecules yield polydisperse mixtures. When such mixtures contain two or three different sizes, it might be possible to isolate them using the established separation protocols of solvent fractionation and size exclusion chromatography. But when the mixture is highly polydisperse, isolation protocols are not effective. In such cases, thermochemical treatment or etching is highly effective. During etching, nanomolecule mixture is subjected to higher temperatures and excess thiol thereby degrading the sizes with lower stability. In some cases, these metastable sizes convert to a stable nanomolecule. This change in core of the nanomolecules upon etching is called as *core size conversion.* When a mixture of nanomolecules with sizes <Au_{144} are etched, final product is dominated with Au_{38} and Au_{40}. But these two nanomolecules are always observed together in the etching reactions. It is important to investigate the reason behind their co-existence and also design protocols for exclusive synthesis of the two highly stable nanomolecules. In this project, we investigated this phenomenon by etching polydisperse mixtures and comparing it with etching of single-sized nanomolecules of

Au_{67} and $Au_{103\text{-}105}$. The experimental results showed that Au_{38} is formed by core size conversion of the mixtures that are <15 kDa and Au_{40} is formed by core size conversion of Au_{67} or $Au_{103\text{-}105}$. Using the core size conversion reactions developed here exclusive synthesis of Au_{38} and Au_{40} is possible, eliminating the need for tedious separation protocols.

Author contributions

Praneeth Nimmala has performed all the experiments including synthesizing the crude products and the products Au_{38} and Au_{40} via core size conversion reactions. Vijay Jupally contributed to the organisation and write-up of the manuscript.

4.2 Introduction

The two most commonly used synthetic protocols for gold nanomolecules, two-phase Brust-Schiffrin and one-phase THF method yield polydisperse products. But it is crucial to synthesize monodisperse products in high yields for characterization and practical applications. One approach known to access highly stable sizes is etching[23] or thermochemical treatment. In this process, the polydisperse mixture is etched in excess thiol at high temperatures narrowing the distribution to one or two highly stable sizes. For example, a polydisperse mixture of nanomolecules containing $Au_{67}(SCH_2CH_2Ph)_{35}$ and $Au_{103\text{-}105}(SCH_2CH_2Ph)_{35}$ when etched in excess phenylethanethiol at high temperature yields a smaller more stable $Au_{40}(SCH_2CH_2Ph)_{35}$. Etching was first introduced in the field of gold nanomolecules by Whetten and coworkers. [23] They etched the ~14 kDa polydisperse mixture capped with hexanethiol in excess dodecanethiol and observed that smaller, more stable sizes (no assignments made) were formed in the process.[23] Several reports confirmed similar observation and it became a well-established

protocol for synthesis of Au_{38}.[50,82-84] There are two possible explanations for the observed results in the etching reactions. The first explanation is that Au_{38} is present in the initial starting material and survives the etching reaction while other metastable sizes decompose. The second possible explanation is that the other metastable sizes core-convert to smaller, more stable sizes. It is important to understand which of these two processes occur in the etching of a mixture to yield stable nanomolecule.

Here we investigate the formation of Au_{38} and Au_{40} with the most commonly used ligand phenylethanethiol. These two sizes are the most dominant sizes when etching reactions are performed with phenylethanethiol. However, Au_{40} is always observed along with Au_{38} in the product[50] and requires size exclusion chromatography[22] to separate them. Considering the intrinsic stability and chirality of both these sizes[85], it would be desirable to design synthetic protocols that would result in exclusive formation of Au_{38} or Au_{40}. But this is hindered by the lack of understanding of the mechanism of the formation of these two nanomolecules in the etching reactions. We systematically investigated this mechanism by core converting "defined" starting materials. We have also studied the effect of starting material of etching on the final product. From these results, we developed protocols for exclusive synthesis of Au_{38} and Au_{40}.

4.3 Experimental methods

4.3.1Chemicals

Phenylethanethiol (Sigma Aldrich, ≥ 98%), hexanethiol (Fluka), sodium borohydride (Acros, 99%), trans-2-[3[(4-tertbutylphenyl)-2-methyl-2-propenylidene]malononitrile (DCTB matrix) (Fluka ≥ 99%) were used as received. Tetrahydrofuran (stablized), toluene, methanol,

acetonitrile and acetone were used from Fisher as received. Biorad-SX1 beads from Biorad were used for the SEC according to the literature published.[86]

4.3.2 Equipment

UV-visible absorption spectra were recorded in toluene on a Shimadzu UV-1601 spectrophotometer. Mass spectrometry analysis was performed using a Bruker Autoflex Matrix assisted laser desorption ionization (MALDI) time of flight mass spectrometer in linear positive mode using a nitrogen laser (337 nm) with DCTB as a matrix.[87]

4.4. Core size conversion experiments

Core conversion is the conversion of one nanomolecule to form another stable nanomolecule during etching reactions. The study of core conversion process involved three stages a) synthesis of crude product, b) size exclusion chromatography and c) Etching of single sized compounds. When a mixture of phenylethanethiol protected clusters smaller than ~110 metal atoms was etched, a final product with Au_{38} and Au_{40} was always observed. Primary questions that need to be addressed were; (i) is the formation of Au_{38} and Au_{40} a result of core size conversion? (ii) why are these two sizes always present as a mixture? To answer these questions we followed a three stage approach. The *first stage* involved synthesis of a crude product with $Au_{103\text{-}105}$, Au_{67} and clusters $<Au_{67}$. The *second stage* involves separation of the crude product into three different fractions containing $Au_{103\text{-}105}$, Au_{67} and clusters $<Au_{67}$ respectively using size exclusion chromatography. The *third stage* involved etching of these fractions separately to study the resulting products.

Results and discussion

Using one phase THF method, a crude product with a mixture of $Au_{103-105}$, Au_{67} and clusters $<Au_{67}$ was synthesized using a 1:6 gold:phenylethanethiol. The resulting crude product was separated into three different fractions containing $Au_{103-105}$, Au_{67} and clusters $<Au_{67}$ as illustrated in the figure 4.1. The $<Au_{67}$ was further processed to remove Au_{25} as shown in brown trace in figure 4.1.These individual fractions were further used for etching reactions. Typically 10 mg of the separated fraction was etched in ~1ml of thiol at 80°C and monitored by MALDI TOF mass spectrometry.

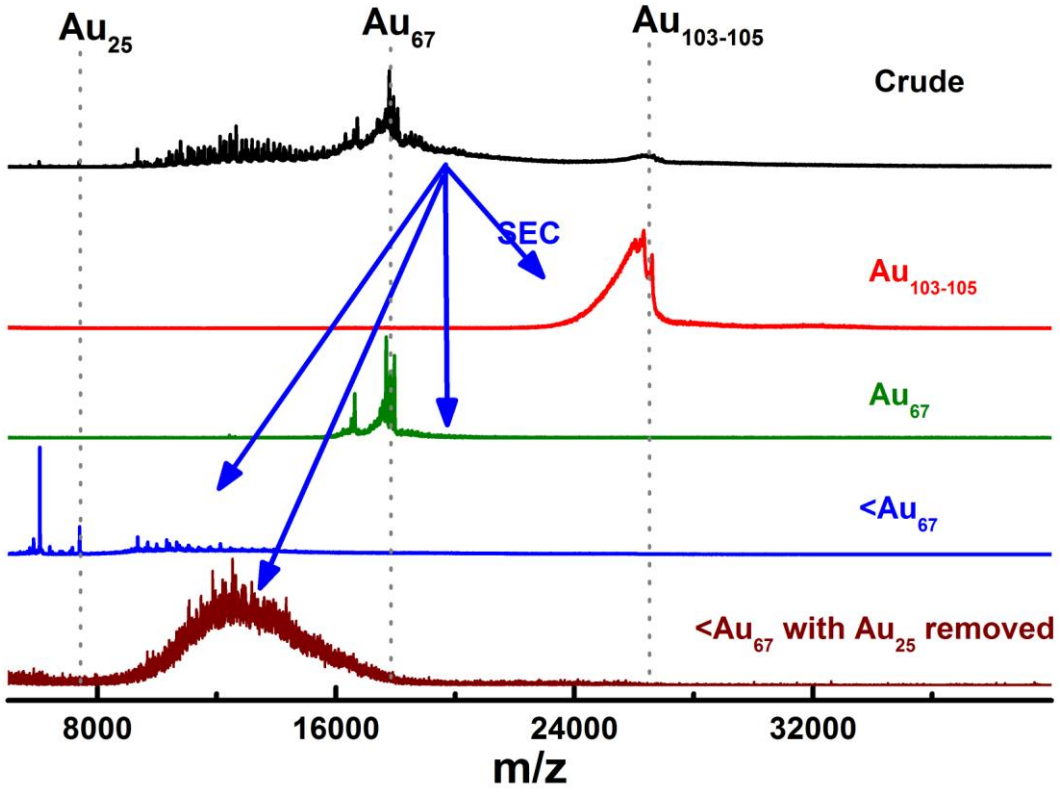

Figure 4.1. MALDI mass spectra of the fractions (red, olive and blue curves) collected from the size exclusion chromatography of the crude product (black curve) obtained from one phase THF

synthesis. The $Au_{103-105}$, Au_{67} and $<Au_{67}$ obtained here are used for core size conversion reactions.

4.4.1. Core conversion of Au_{67} to Au_{40}

The monodisperse Au_{67} obtained from SEC was used as starting material for the thermochemical treatment. Figure 4.2 shows the MALDI monitored progress of etching Au_{67}. The top spectrum (in black) in figure 4.2 shows the MALDI mass spectrum of the control material used for etching. The peak is broad as a result of the fragmentation in MALDI. In the ESI-MS, which is a soft ionization technique, single sharp peaks were observed for the same sample. Upon etching, the Au_{67} was converted to Au_{40}. By 10 h (red spectrum), most of the Au_{67} was converted to intermediate, metastable species between 13 and 17 kDa. Also at this point, Au_{40} was observed in small quantities as indicated by the low intensity peaks in this region. It is important to note that no Au_{40} was present in the starting material and hence it is reasonable to assume at this point that all the Au_{40} was being formed from Au_{67}. The 23 and 39 h samples showed a trend where the metastable species are decreasing and Au_{40} was increasing in proportion. After 50 h, $Au_{40}(SR)_{24}$ was the predominant product in the reaction mixture. There was no Au_{38} at this point indicating that Au_{40} was the major product formed by core conversion of Au_{67}. Typical yield of this core size conversion reaction was ~55% when compared to the amount of starting material Au_{67} used.

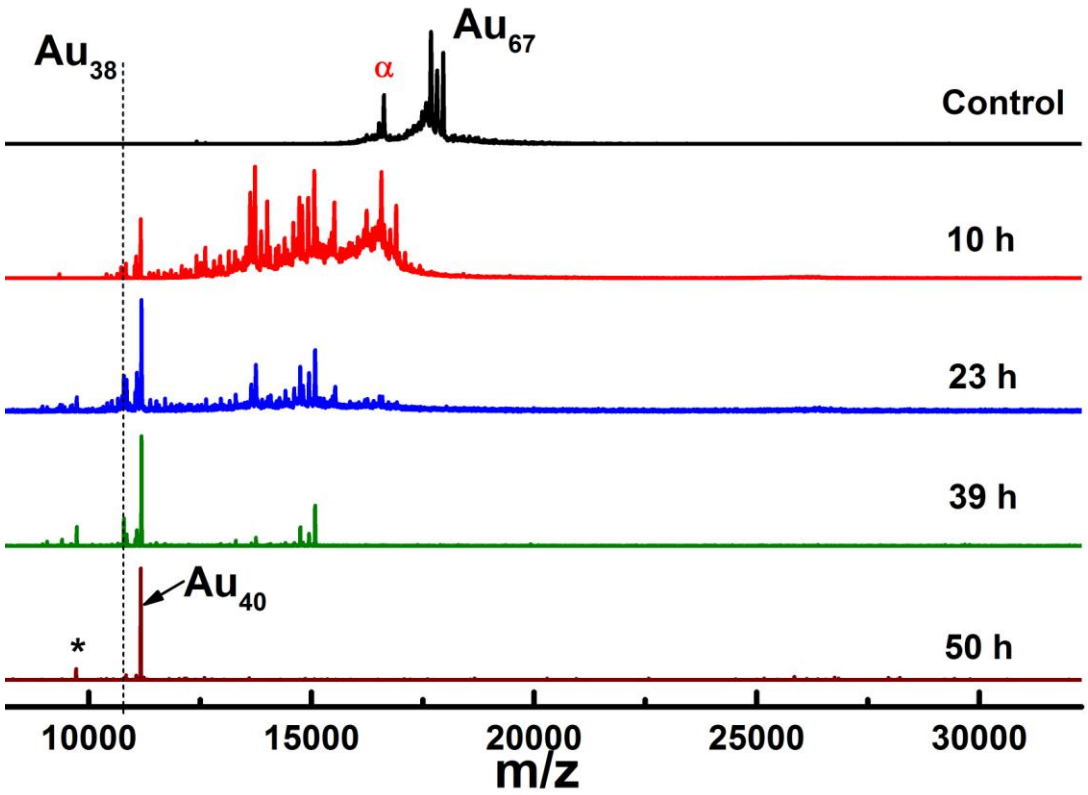

Figure 4.2. Positive MALDI mass spectra of the samples collected from etching of pure Au_{67} in the presence of excess thiol. After 50 hrs of etching, there is only Au_{40} left in the solution. Peak marked with "α" is a result of fragmentation of $Au_{67}(SR)_{35}$ with a loss of Au_4L_4. Similarly the peak marked with an asterisk in the 50 h sample indicates a fragment peak for $Au_{34}(SR)_{22}$. Please note that $Au_{40}(SR)_{24}$ is *absent* in the initial sample. This indicates that $Au_{40}(SR)_{24}$ is exclusive formed via a core size conversion process from Au_{67}. A dotted line is shown at 10778 Da, which is the molecular weight of $Au_{38}(SCH_2CH_2Ph)_{24}$, to denote its absence.

4.4.2. Core conversion of $Au_{103-105}$ to Au_{40}

Monodisperse $Au_{103-105}$ was isolated by SEC and used as a starting material in core conversion reactions. Figure 4.3 shows the MALDI TOF mass spectra of aliquots collected at different time intervals from the etching of $Au_{103-105}$.

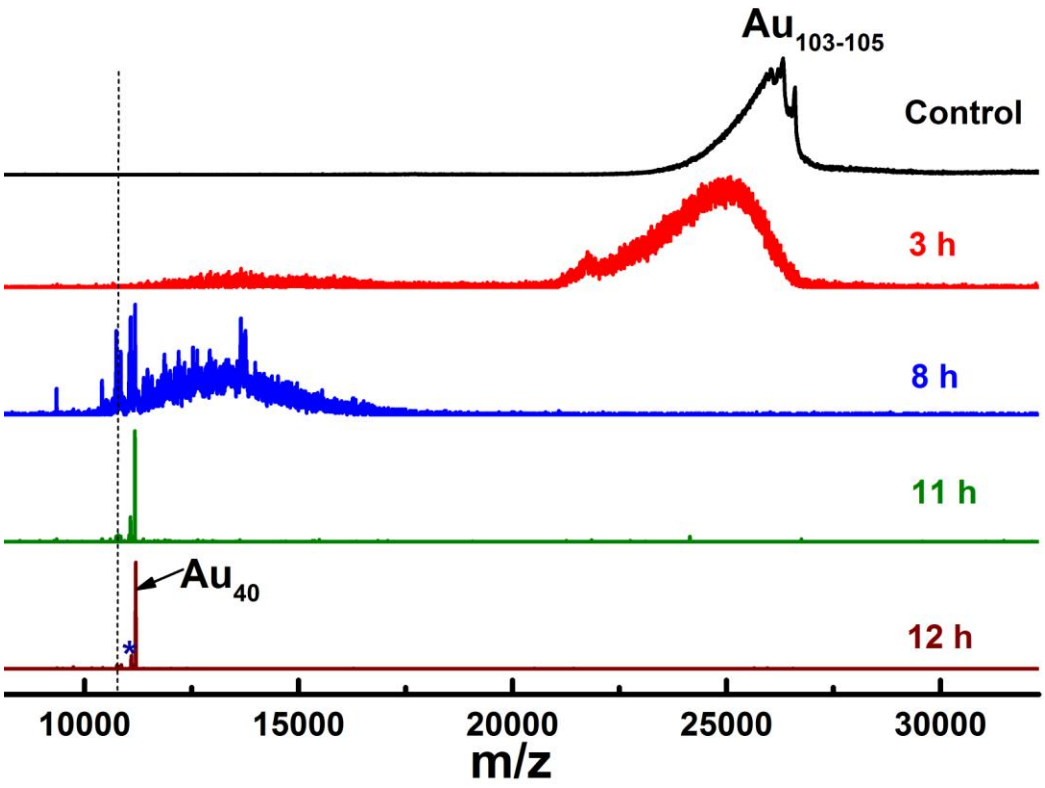

Figure 4.3. Positive MALDI mass spectra of the samples collected from etching of pure $Au_{103-105}$ in the presence of excess thiol.

The top spectrum (in black) in figure 4.3 shows the MALDI mass spectrum of the control material used for etching. The peak is broad as a result of the fragmentation in MALDI. In the ESI-MS, which is a soft ionization technique, single sharp peaks were observed for the same sample. The total etching time was 12 h. The 3 h sample, blue spectrum, metastable species

between 13 and 17 kDa were observed. By 8 h, all the $Au_{103\text{-}105}$ was converted to metastable species. Also in the same spectrum, peaks corresponding to Au_{40} were observed. After 12 h, $Au_{40}(SR)_{24}$ was the only product in the reaction mixture. The peak marked with an asterisk corresponds to $Au_{40}(SR)_{23}S$ with a loss of one $C_6H_5CH_2CH_2$ group from $Au_{40}(SCH_2CH_2C_6H_5)_{24}$. A dotted line is shown at 10778 Da, which is the molecular weight of $Au_{38}(SCH_2CH_2Ph)_{24}$, to denote its absence. Please note that $Au_{40}(SR)_{24}$ was *absent* in the initial sample and no Au_{38} was present in the 12 h sample. This indicates that Au_{40} is *exclusively* formed via a core size conversion process. The yield of Au_{40} in this core conversion was ~31% with respect to the amount of the $Au_{103\text{-}105}$ used. There was always some white insoluble component present at the bottom of the reaction vial in core conversion reactions, which may be Au-SR polymers. This indicates that 100% of the starting material was not core converted to the final product. It is interesting to note that no $Au_{102}(SCH_2CH_2Ph)_{44}$ was observed in the reaction indicating that the combination 102,44 is not stable with phenylethanethiol ligand.

4.4.3. Core conversion of Au_{67} and $Au_{103\text{-}105}$ mixture to Au_{40}

After observing Au_{67} converting to Au_{40} and $Au_{103\text{-}105}$ converting to Au_{40}, we were interesting to learn the results of etching a mixture of Au_{67} and $Au_{103\text{-}105}$. To perform this interesting experiment, we have isolated a crude product that contains Au_{67} and $Au_{103\text{-}105}$ without any other sizes of nanomolecules. Upon etching, $Au_{103\text{-}105}$ and Au_{67} mixture core converted to pure Au_{40}. The results illustrated in figure 4.4 confirm the earlier observations that both Au_{67} and $Au_{103\text{-}105}$ core convert to Au_{40} whether in pure form or in mixtures.

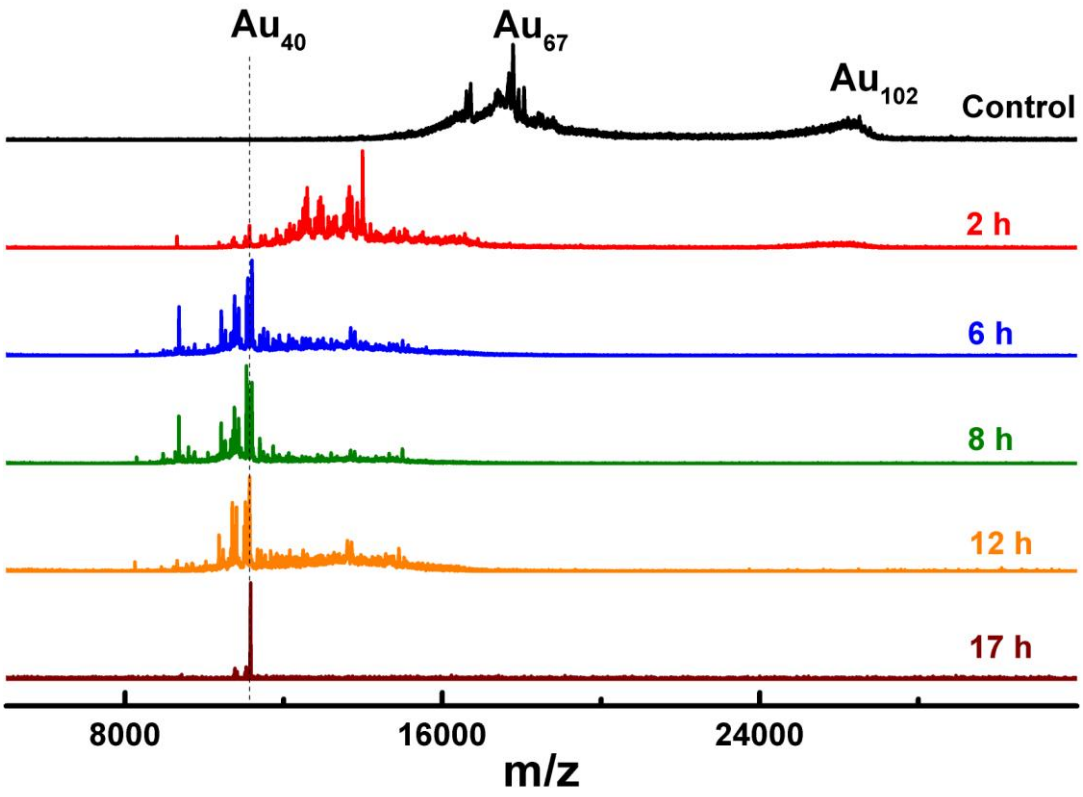

Figure 4.4. MALDI mass spectra of the samples collected from the etching of a mixture of Au_{67} and $Au_{103\text{-}105}$.

4.4.4. Core conversion of polydisperse mixture of lower mass species

We have observed that both Au_{67} and $Au_{103\text{-}105}$ core convert to Au_{40} upon etching. If that is the case, the question arises as to how Au_{38} is formed when the polydisperse mixtures are etched. To investigate this, we have etched nanoclusters in the mass range 10 to 17 kDa, that is nanomolecules smaller than Au_{67} (see bottom spectra in figure 4.1).

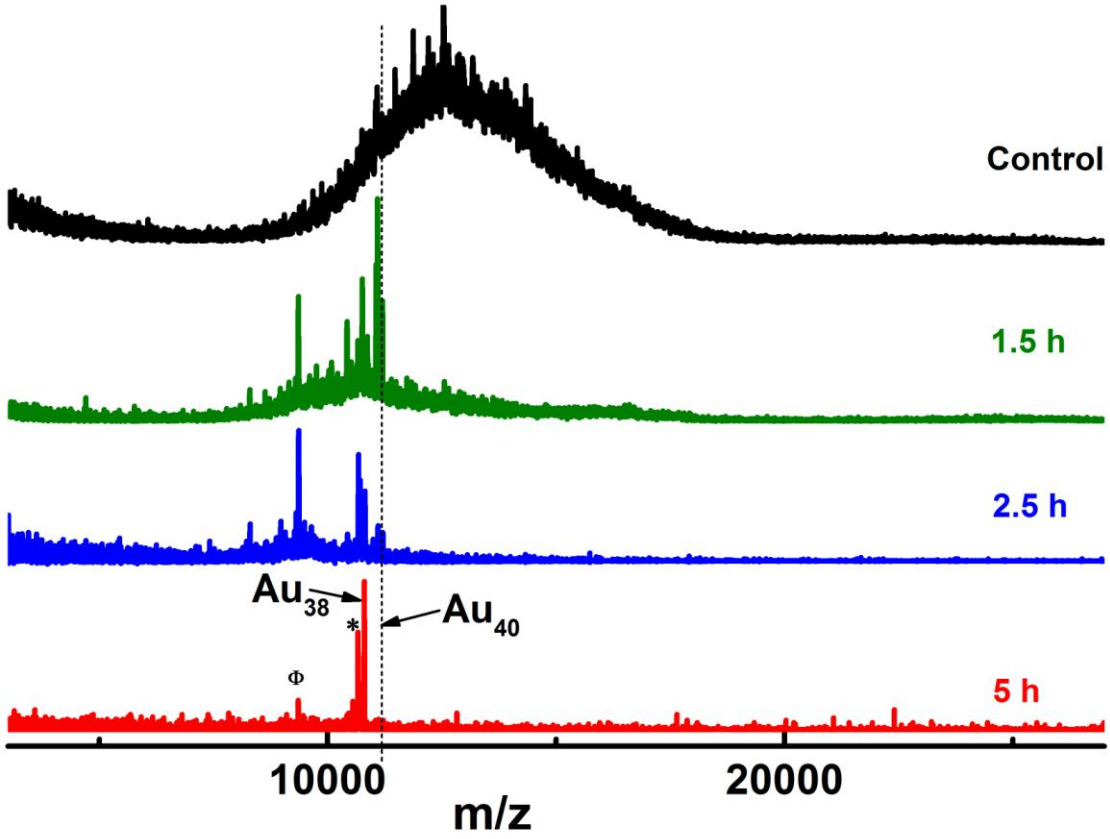

Figure 4.5. MALDI mass spectra of the samples collected from etching of clusters smaller than Au_{67} in the presence of excess thiol. Peaks with * and ϕ indicates the fragments of $Au_{38}(SR)_{24}$ corresponding to a loss of SR and $Au_4(SR)_4$ respectively.

For this experiment, species between 10 and 17 kDa were isolated using SEC. The top spectrum labelled as "Control" was the starting material used for this etching. There were no species above 17 kDa which means Au_{67} and $Au_{103\text{-}105}$ were absent in the sample. The peaks observed below 10 kDa in 1.5 h and 2.5 h samples are for fragments of Au_{38}. After 5 h, $Au_{38}(SR)_{24}$ was the only product in the reaction mixture. Please note that no $Au_{38}(SR)_{24}$ was

present in the initial sample and no Au_{40} was present in the 5 h product. This indicates that $Au_{38}(SR)_{24}$ was exclusively formed via a core size conversion process. For a discussion on the intermediates observed in the core conversion reactions, refer later sections. Peaks with * and ϕ indicate the fragments of $Au_{38}(SR)_{24}$ corresponding to a loss of SR and $Au_4(SR)_4$ respectively. It is also important to note that the presence of Au_{25} in the starting material of $<Au_{67}$ does not affect the core conversion since Au_{25} is not stable thermally. As a control experiment, we have etched monodisperse Au_{25} and showed that it decomposes to lower clusters in 2 h. The yield of this reaction could not be calculated on Au atom basis, as the exact composition of starting material was unknown. On a weight basis, ~40% yield was obtained.

4.5. Mechanism of core size conversion based on mass spectrometry data

The core conversion of larger species occurs by its breakdown during etching reactions. To understand the mechanism of this conversion, mass spectrometry data of reaction aliquots (intermediates) during the etching reaction were analyzed in great detail. The mass spectrometry data of three samples that had multiple peaks corresponding to metastable species were compared with each other. For etching of Au_{67} and $Au_{103\text{-}105}$, samples at 23 h and 8h (from a different reaction) were chosen. For studying the etching of $<Au_{67}$ fraction, starting material from a different etching reaction was chosen. Figure 4.6 shows the assignment of the meta-stable species observed in these samples.

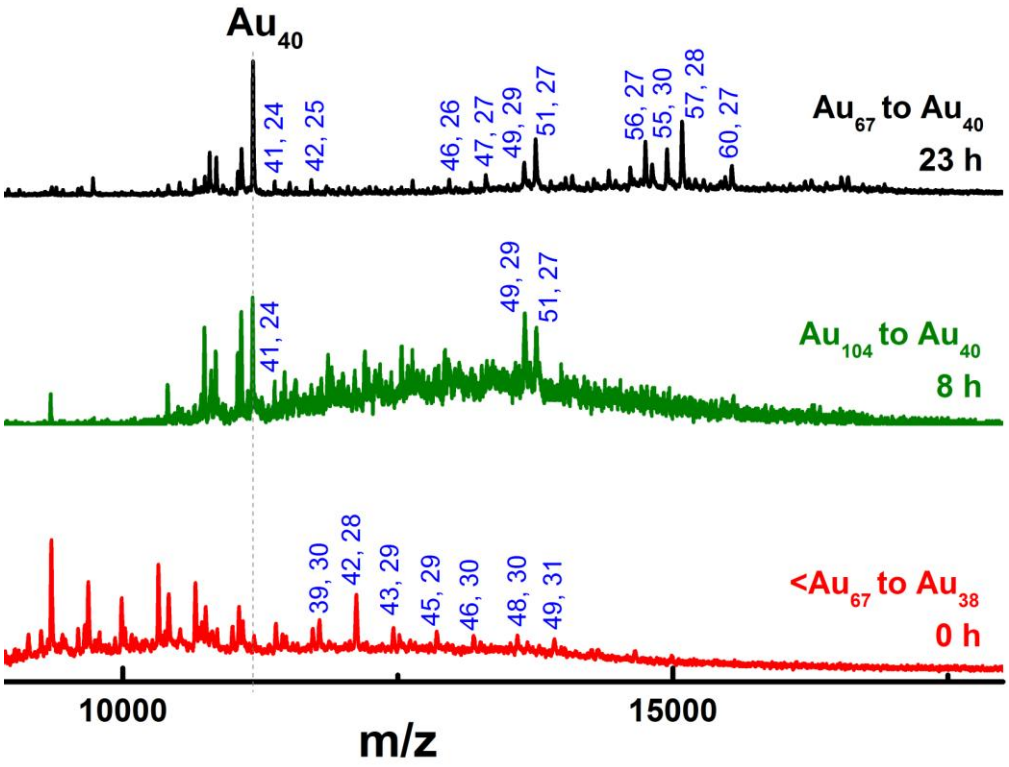

Figure 4.6. Positive MALDI mass spectra of the meta-stable species observed in the core size the core size conversion reactions of Au_{67}, $Au_{103\text{-}105}$ and $<Au_{67}$ clusters.

In the etching of Au_{67} (black curve in figure 4.6), the composition of each species is indicated on top of each peak. Some of the peaks could not be attributed to any reasonable and practical combination of ligands and gold atoms. Of the several species observed, $Au_{57}(SR)_{28}$, $Au_{55}(SR)_{30}$, $Au_{56}(SR)_{27}$, and $Au_{51}(SR)_{27}$ were the most dominant in the mass spectra. Other species include $Au_{60}(SR)_{27}$, $Au_{49}(SR)_{29}$, $Au_{47}(SR)_{27}$, $Au_{46}(SR)_{26}$ and $Au_{41}(SR)_{24}$. Upon closer inspection of these species, it is reasonable to assume that there is a systematic loss of gold atoms and ligands to form $Au_{40}(SR)_{24}$ in the etching of Au_{67}. This mass spectrometric evidence strongly suggest that the larger clusters break down during the core size conversion reactions. In the

earlier reports, where Au_{38} was formed during etching reactions, the process of core size conversion is reported.[23, 6] In the present work, it is systematically shown which particular sizes convert to Au_{38} and Au_{40}.

$Au_{103\text{-}105}$ fraction also converted to Au_{40} via core size conversion reactions. As the final product in both of these etching reactions was Au_{40}, it was likely that the reactions proceed via same or closely related intermediate species, analogous to small molecule organic reactions. To verify this, the meta-stable clusters in the $Au_{103\text{-}105}$ etching reaction were also assigned. In both the cases, Au_{67} and $Au_{103\text{-}105}$ etching reactions, peaks corresponding to $Au_{51}(SR)_{27}$, $Au_{49}(SR)_{29}$ and $Au_{41}(SR)_{24}$ were observed (labelled in green in figure 4.6 and scheme 1). The fact that both the reactions showed the same species in these reactions suggested that these were the intermediates for the formation of $Au_{40}(SR)_{24}$ during the core size conversion reactions.

The fraction < Au_{67} obtained after SEC of the crude product, was similar to the meta-stable species observed in core size conversion of Au_{67} and $Au_{103\text{-}105}$. In that case, the etching of this material should also form $Au_{40}(SR)_{24}$ as the final product. To answer this question, the peaks observed in the <Au_{67} fraction were also assigned using the MALDI mass spectrometry data (red curve in figure 4.6). The species observed in the <Au_{67} fraction were different than the meta-stable intermediates observed in Au_{67} and $Au_{103\text{-}105}$ etching reactions. In the etching experiments, the size distribution of the crude product used affected the yield of Au_{38} obtained. The meta-stable species observed during the core size conversion reactions proved the importance of size distribution of the crude product. It was important to have the clusters that convert to Au_{38} in greater abundance for higher yields of Au_{38} in these etching reactions. This also provided a clear synthetic route for exclusive, formation of Au_{40} via core size conversion process.

4.6. Conclusions

From the number of experiments performed on core conversion of nanomolecules, we can draw a few significant conclusions.

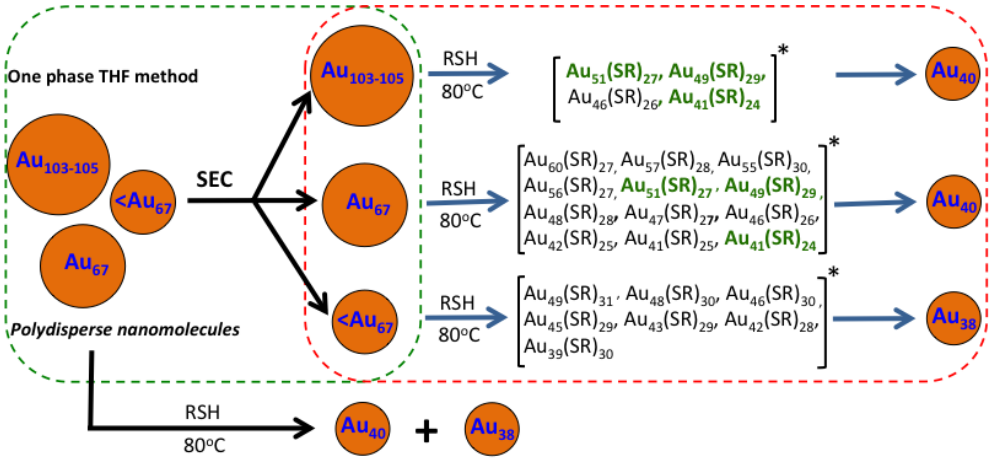

Scheme 2.1. Core size conversion in clusters. One phase THF synthesis typically yields a mixture of $Au_{103\text{-}105}$, Au_{67}, and clusters smaller than Au_{67} including Au_{25}. When this mixture is etched as such, a mixture of Au_{38} and Au_{40} by core size conversion is formed. From the same crude product, fractions containing $Au_{103\text{-}105}$, Au_{67} and clusters smaller than Au_{67} were separated by SEC (shown in the green dotted box in the scheme). Upon etching, $Au_{103\text{-}105}$ and Au_{67} core converts to Au_{40} and clusters smaller than Au_{67} core convert to pure Au_{38} (shown in the red dotted box in the scheme). Each of these core size conversion reactions proceed via several intermediate species identified by MALDI TOF mass spectrometry. Based on the MALDI TOF data we speculate that the core size conversion reactions proceed via these intermediate species. Note that the core conversion is a gradual down sizing phenomenon. Gold atoms and ligands are systematically lost from the larger clusters and smaller sizes are formed.

We showed that Au_{38} and Au_{40} are formed by core size conversion of larger species. The exclusive routes for the synthesis of Au_{40} and Au_{38} were clearly demonstrated as the evidence showed that Au_{67} and $Au_{103\text{-}105}$ converted to Au_{40} and species $<Au_{67}$ converted to Au_{38}. We have also attempted to understand the core size conversion using mass spectrometry data. The results show the importance of the size distribution of the starting crude product in the core size conversion reactions.

CHAPTER FIVE

EFFECT OF AROMATIC LIGANDS ON THE GEOMETRY AND PROPERTIES OF GOLD NANOMOLECULES

Part of the text and figures in this chapter are extracted from the following publications:

Praneeth Reddy Nimmala and Amala Dass

J. Am. Chem. Soc., 2011, 133 (24), pp 9175–9177

Praneeth Reddy Nimmala, Stefan Knoppe, Vijay Reddy Jupally, Jared H. Delcamp, Christine M. Aikens, and Amala Dass

J. Phys. Chem. B, 2014, 118 (49), pp 14157–14167

Praneeth Reddy Nimmala and Amala Dass

J. Am. Chem. Soc., 2014, 136 (49), pp 17016–170

CHAPTER FIVE

EFFECT OF AROMATIC LIGANDS ON THE GEOMETRY AND PROPERTIES OF GOLD NANOMOLECULES

5.1 Abstract

Gold nanomolecules are entities in the nanometer size regime that contain a specific number of gold atoms and passivating organic thiolate ligands. The chemical nature and the polarity of the passivating ligands can be varied to produce nanomolecules with desired solubility based on the end application. They can also impart functionality such as fluorescent, electrochemical and chiral signature.[88] Aliphatic ligands (like hexanethiol and dodecanethiol) and phenylethanethiol are the commonly used ligands in the synthesis of gold nanomolecules. For the first time, a well-defined core size protected completely by an aromatic ligand, $Au_{36}(SPh)_{24}$, was synthesized by etching Au_{67} and $Au_{103\text{-}105}$ capped with phenylethanethiol. The results were interesting as Au_{36} was different from the known stable sizes Au_{38} and Au_{40} in aliphatic and phenylethanethiol systems. The purity was determined by MALDI-MS and molecular composition was assigned using high resolution ESI-MS. The synthesis involves core size conversion, which was monitored by MALDI-MS. The compound was crystallized and its structure determined by X-ray crystallography, and found to have a *fcc* core. The optical and

electrochemical properties have been determined from experimental data using UV-vis spectroscopy, cyclic voltammetry and differential pulse voltammetry. The results from Au_{36} experiments indicated that aromatic ligands protect the gold core in a different way compared to the commonly used aliphatic thiols and phenylethanethiol. Investigation into this by other researchers in the field yielded stable Au_{36} cores with other ligands like p-*tert*-butylbenzenethiol (HSC_6H_4-*t*Bu) and cyclopentanethiol (HSC_5H_9). [28,89] The formation of $Au_{36}(SC_5H_9)_{24}$ rules out the possibility of electronic conjugation effect of the aromatic ligand leading to the formation of $Au_{36}(SPh)_{24}$ or $Au_{36}(SPh\text{-}tBu)_{24}$. The only possible explanation that remains is the bulkiness of these ligands compared to phenylethanethiol ($HSCH_2CH_2Ph$). We further investigated into the effect of aromatic ligands with the core conversion of Au_{144}, a highly stable nanomolecule. Au_{144} capped by phenylethanethiol has been reported by several groups[83,90,91] and is a stable core. But when Au_{144} was etched in aromatic ligands Au_{99} was the product. The product Au_{99} was isolated and characterized using UV-vis, differential pulse voltammetry and mass spectrometry. This conversion was observed in case of various aromatic ligands -SPhX (X= F, CH_3 and OCH_3). We have also etched Au_{144} in extremely bulky ligands of adamantanethiol and cyclohexanethiol and the results are intriguing as no Au_{99} was observed. Analyzing the results from Au_{36} and Au_{99}, we conclude that both a) bulkiness of the ligand and b) the aromaticity of the phenyl ring have effect on the size and structure of the nanomolecules and one them could be dominant as observed in the case of Au_{36} and Au_{99}.

Author contributions

Praneeth Nimmala performed the experiments for synthesis and characterization of Au_{36} as well as Au_{99}. Vijay Jupally performed the crystallization experiments and obtained a single

crystal of Au_{36}. Theoretical calculations on Au_{36} were performed by Stefan Knoppe and Christine Aikens. Jared Delcamp has performed the energy level depiction for the photoexcitation of Au_{36}.

5.2 Introduction

Research on gold-thiolate nanomolecules over the past two decades predominantly uses aliphatic thiol (C_nH_{2n+1}-SH) ligands as capping agents. Murrays early work showed that an acetonitrile extract of $Au_m(SCH_2CH_2Ph)_n$ yielded $Au_{25}(SCH_2CH_2Ph)_{18}$. [82,92] The acetonitrile solubility of $Au_{25}(SCH_2CH_2Ph)_{18}$ facilitated the isolation of highly pure Au_{25} before SEC and PAGE protocols were established for purifications. Subsequently, other larger core sizes such as $Au_{38}(SR)_{24}$, $Au_{144}(SR)_{60}$ were prepared using R=$HSCH_2CH_2Ph$. This was due in part to the fact that phenylethanethiol ligated nanomolecules work better in MALDI with the DCTB matrix. Overall, phenylethanethiol has become the most widely used ligand by researchers worldwide. It was found that both aliphatic ligands and phenylethanethiol yield the same core sizes, including 25-, 38-, 67-, 144-atom nanomolecules. For the purposes of synthesis of Au-SR nanomolecules, it was found that the chemical differences between aliphatic and phenylethanethiol are minimal and does not reflect in the final composition and the core-size of the nanomolecule.

We have studied the effect of aromaticity on the composition and core-size of the gold nanomolecules using benzenethiol and its derivative thiols. We observed from the core size conversion reactions in the previous chapters that when a mixture of Au_{67} and $Au_{103\text{-}105}$ was etched in phenylethanethiol, the product obtained was Au_{40}. When the same starting material was etched in an aromatic thiophenol ligand, the product obtained was $Au_{36}(SPh)_{24}$. The conversion

was interesting in terms of the effect of ligand on the final product. Interestingly, this conversion of Au_{67} and $Au_{103\text{-}105}$ occurs through an intermediate $Au_{38}(SCH_2CH_2Ph)_{14}(SPh)_{10}$. We noticed that when the number of thiophenol ligands reaches a threshold, a change in core size to Au_{36} occurred. In a subsequent study, Jin and coworkers have verified our finiding by converting $Au_{38}(SCH_2CH_2Ph)_{24}$ to $Au_{36}(SPh)_{24}$.[28] Their study varied the R group from -Ph to -*t*Bu-Ph to obtain $Au_{36}(SPh\text{-}tBu)_{24}$. Interestingly, the same group reported that $Au_{25}(SCH_2CH_2Ph)_{18}$ converts to $Au_{28}(SPh\text{-}tBu)_{20}$ on reaction with aromatic ligand.[93] We have observed that $Au_{102}(SPhCOOH)_{44}$ could not be reproduced with phenylethanethiol. Instead, a mixture of sizes in the range $Au_{103\text{-}105}(SCH_2CH_2Ph)_{45\text{-}46}$ were observed.[18,94] To understand the similar effects of aromatic ligands in the larger sizes, we have investigated the effect of aromaticity on the ultra-stable and larger $Au_{144}(SCH_2CH_2Ph)_{60}$ nanomolecule. MALDI and high resolution ESI-MS data showed that $Au_{144}(SCH_2CH_2Ph)_{60}$, upon reacting with HS-Ph at 80°C, converts to a smaller more stable $Au_{99}(SPh)_{42}$. We studied the core size conversion using MALDI and ESI-MS and show that after an exchange of thirteen thiophenol ligands, the 144-atom core is unstable and converts to 99-atom core similar to what was observed in case of Au_{36}. The conversion of Au_{144} to Au_{99} was also observed with thiophenol derivatives of the form HSPhX (where X = F, CH_3, OCH_3)

All these results showed that aromaticity has a clear effect on the core-size and composition of gold nanomolecules. In other words, Au_{25}, Au_{38}, Au_{40} are clearly different than aromatic ligand capped systems like Au_{28}, Au_{36}, Au_{99} and Au_{102}. It is also important to mention at this point that this series is observed in the report by Whetten's group on the direct synthesis of thiophenol-capped nanomolecules.[95] Sizes with core masses of 5.5, 8.7, 22 and 28 kDa were reported by them, but no molecular assignments were made.

5.3 Synthesis and characterization of $Au_{36}(SPh)_{24}$

5.3.1 Experimental

Materials: Thiophenol (SAFC, ≥ 97%), trans-2-[3[(4-tertbutylphenyl)-2-methyl-2-propenylidene]malononitrile (DCTB matrix) (Fluka, ≥ 99%) were purchased from Aldrich. Tetrahydrofuran (no stabilizer) and other solvents like toluene, methanol, acetonitrile and acetone were used from Fisher as received. Biorad BioBeads SX1 were used for size exclusion chromatography (SEC).

Methods: UV-visible absorption spectra were recorded in toluene on a Shimadzu UV-1601 instrument in toluene. ESI-MS and MS-MS spectra were acquired on Waters SYNAPT HDMS instrument in HPLC grade THF, without any additives present. The instrument was calibrated using $Au_{38}(SCH_2CH_2Ph)_{24}$, which is closer to the mass of $Au_{36}(SPh)_{24}$. Electrochemical measurements were performed on a CHI 620 instrument using 5 mg of nanomolecule in 5 mL of 1,2-dichloroethane with 0.5 mM $BTPPATBF_{20}$ (bis(triphenyl phosphoranylidene) ammonium tetrakis (pentafluorophenyl)borate as supporting electrolyte under nitrogen atmosphere. Powder XRD measurements were performed on a Bruker D8-Focus XRD instrument on a quartz substrate. 10 mg of sample was dissolved in minimal amount of toluene and deposited on the substrate and air-dried.

Crystallization: 1 mg of $Au_{36}(SPh)_{24}$ was dissolved in 100 μL of toluene for some unrelated experiments. 20 μL of this solution was used for experiments, while the rest of the solution was left unattended in an uncapped vial in the fume hood over a period of few days. After ~2 weeks, dried crystals were observed in the bottom and side of the vial. The formation of crystals was serendipitous, but the crystals obtained were of sufficiently high quality for

acquiring X-ray diffraction data.

Single crystal X-ray analysis: A black needle like crystal was selected in oil under ambient conditions and attached to the tip of a MiTeGen MicroMount. The crystal was mounted in a stream of cold nitrogen at 100 K and centered in the X-ray beam with aid of a video camera. The crystal evaluation and data collection were performed on a Bruker APEX II diffractometer with Mo Kα (λ = 0.71073 Å) radiation. The initial cell constants were obtained from three series of ω scans at different starting angles. Each series consisted of 12 frames collected at intervals of 0.5º in a 6º range about ω with the exposure time of 20 seconds per frame. The reflections were successfully indexed by an automated indexing routine built in the APEXII program suite. The solution and refinement was carried out in Olex2[96] using the program SHELXTL.

Crystal data: For $Au_{36}S_{24}C_{144}H_{120}$: triclinic, space group $P\bar{1}$ (no.2), a=18.554(12) Å, b=20.370(13)Å, c=30.482(20)Å, α=95.488(7)°, β=94.821(8) °, γ=110.991(7) °, V=10620(12) $Å^3$, z=2, μ(Mo Kα) = 25.02 mm^{-1}; ρ_{calc} = 3.037 mg/mm^3, F(000)=8424, T = 100K, $2\theta_{max}$ = 41.9°, 22386 reflections, R(int) = 0.1178; Data/restraints/parameters = 22386/276/709; GooF = 1.057, R_1=0.0681, wR_2(all data) =0.2329; -2.54 <Δρ< 2.19 e/$Å^3$. CCDC number 996171.

*Computational details***:** Computations were performed using the grid-projected augmented-wave method as implemented in the GPAW package including scalar-relativistic effects for gold atoms.[97,98] If not indicated otherwise, all calculations were done at the GGA-PBE level of theory.[64,99] Optimizations ($Au_{36}(SH)_{24}$; convergence criterion 0.05 eV/Å for each atom) and electronic structure analysis were performed using a grid spacing of h = 0.2 Å. Bader Charge (BC) analysis was performed using the program provided by the Henkelmann group.[100,101] Angular-momentum resolved Projected Density of States (PDOS) analysis was done by

projecting the Kohn-Sham (KS) wavefunctions into the center-of-mass of the cluster including a radius of 3.0 Å.[102] Atom-resolved PDOS-decomposition was performed by projecting the KS-wavefunctions into each atom including a radius of 1.4 Å.[103] KS orbitals were plotted using an isosurface cut-off of 0.05.

Additional computations were run using density functional theory as implemented in the code ADF2012.01.[104] In the ADF program, the LB94 model potential[105] was used to calculate 500 excited states using linear response time-dependent density functional theory (TDDFT). A double-zeta (DZ) basis set with the frozen core approximation was used for all calculations. Relativistic effects were considered using the zeroth order regular approximation (ZORA).[106,107] Excitation spectra were convoluted using a Lorentzian with a FWHM value of 30 nm.

5.3.2. Synthesis

Briefly, the synthesis of $Au_{36}(SPh)_{24}$ involved three steps. The first step was the synthesis of a crude product using phenylethanethiol ligand, which was a polydisperse mixture of nanoclusters dominated by 14 kDa and 22 kDa nanoclusters, $Au_{67}(SR)_{35}$ and $Au_{103\text{-}105}(SR)_{44\text{-}46}$, respectively. The second step was etching the polydisperse mixture in thiophenol. The third and final step was the purification of the product from the second step by size exclusion chromatography.[22]

Step 1: Synthesis of a crude product.[12] For the synthesis of the crude product, 1 mmol of $HAuCl_4{\cdot}3H_2O$ was dissolved in 20 ml of tetrahydrofuran and 6 mmol of phenylethanethiol ($HSCH_2CH_2Ph$) was added. The reaction mixture was allowed to stir at 500 rpm for 30 min when the yellow solution became turbid white mixture. To this solution, 10 mmol of $NaBH_4$ was added and the color changed from turbid to black instantly. The reaction was stirred for 5 min

before the solvent was removed via rotary evaporation. The resulting product was washed three times to remove the excess ligand and dried.[12]

Step 2: Etching the crude product in thiophenol. The MALDI mass spectrum of the product from step 1 showed a polydisperse mixture of nanoclusters with $Au_{67}(SR)_{35}$ and $Au_{103\text{-}105}(SR)_{44\text{-}46}$ as dominant clusters.[35] The mixture was dissolved in 1 ml of thiophenol and heated at 80° C for 3 h. The stirring was kept low and constant at 300 rpm. The resulting product was washed with methanol 5× times to remove the excess thiophenol.

Step 3: Purification of the product. The high laser MALDI mass spectrum of the product from step 2 showed a dominant peak in the mass range 9-10 kDa for $Au_{36}(SPh)_{24}$ with some minor peaks in the higher mass region. From the product obtained after step 2, the higher mass clusters were removed using size exclusion chromatography was performed on the above product. The monodispersity of Au_{36} was confirmed by MALDI mass spectrometry performed at high laser fluence.

5.3.3 Characterization of Au_{36}

5.3.3.1 Mass spectrometry

The first mass spectrometric analysis of the new all-aromatic thiol capped nanomolecule Au_{36} was performed on MALDI-MS using DCTB matrix in positive linear mode. The MALDI mass spectrometry of the compound gave a parent peak at 9601 Da, which corresponds to $Au_{36}(SPh)_{23}$. The parent peak was accompanied by two fragment peaks corresponding to $Au_{32}(SPh)_{19}$ and $Au_{32}(SPh)_{20}$ due to fragmentation at threshold laser. The synthesis and MALDI were reproduced more than 20 times.

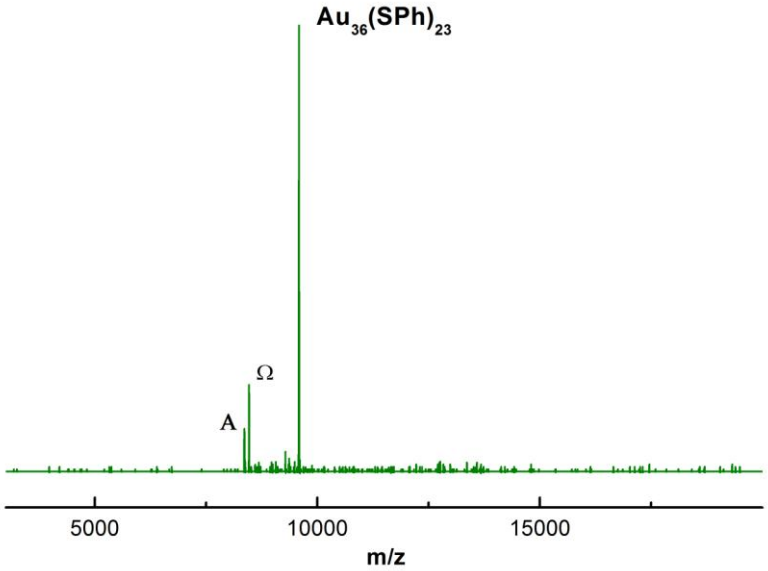

Figure 5.1. MALDI-TOF mass spectrum of $Au_{36}(SPh)_{23}$ using DCTB matrix in positive linear mode. The fragment peaks denoted by A and Ω are $Au_{32}(SPh)_{19}$ and $Au_{32}(SPh)_{20}$ respectively.[35]

The purity of the compound was also confirmed by MALDI mass spectrometry. Jin and co-workers reported the crystal structure of $Au_{36}(SPh\text{-}tBu)_{24}$ following the publication of $Au_{36}(SPh)_{23}$.[28,35] Since -SPh-*t*Bu gives similar chemical effect as that of -SPh, we later analyzed our compound using high-resolution electrospray ionization mass spectrometry. ESI MS being a softer ionization technique did not show any fragmentation and confirmed the assignment of the nanomolecule to be $Au_{36}(SPh)_{24}$ and not $Au_{36}(SPh)_{23}$. However, MALDI MS analysis always resulted in the loss of one ligand and such a scenario was never observed before. We have corrected this assignment in our subsequent publication on Au_{36}.[29]

The ESI spectrum of Au_{36} is shown in figure 5.2. The peak at 4855 Da corresponds to the 2+ of $Au_{36}(SPh)_{24}$. No peak was observed for 2+ of $Au_{36}(SPh)_{23}$ at 4800 Da. The isotopic pattern of the nanomolecule showed a good match between the experimental and calculated mass of

$Au_{36}(SPh)_{24}$.

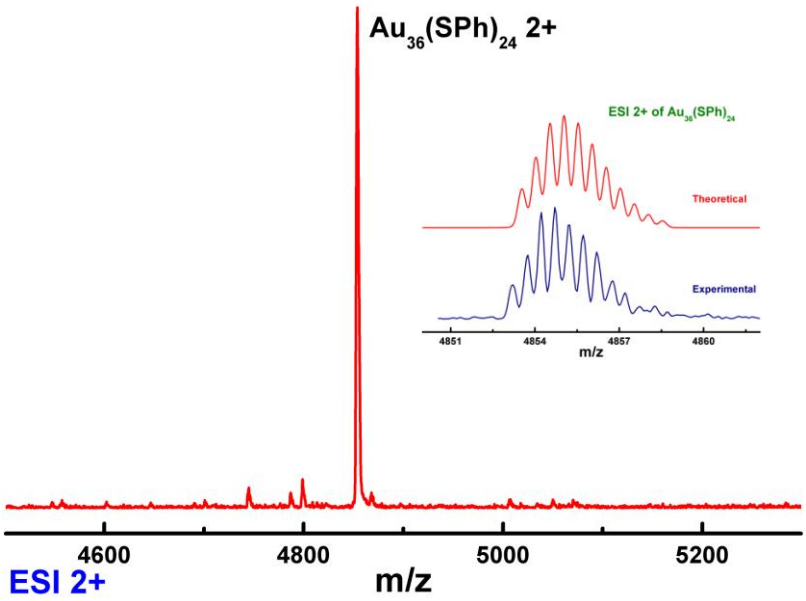

Figure 5.2. ESI-MS of 2+ peak of $Au_{36}(SPh)_{24}$ at *m/z* 4854. Inset shows the isotopic pattern match for the theoretically obtained and experimentally derived mass of $Au_{36}(SPh)_{24}^{2+}$.[29]

We have studied the fragmentation pattern of the compound $Au_{36}(SPh)_{24}$ using MS/MS, where it is possible to select a single peak in the mass spectrometer and fragment it. Interestingly, no fragment loss of one ligand to $Au_{36}(SPh)_{23}$ was observed as shown in figure indicating that fragmentation to (36,23) is specific to MALDI-MS.

5.3.3.2. Optical properties of Au_{36}

Nanomolecules > 2 nm in size show a surface plasmon resonance (SPR) peak centered around 530 nm. In the larger (>2 nm) nanomolecules, the SPR peak is the only dominant absorption feature observed and redshifts with increasing size. On the other hand, smaller

nanomolecules with <75 gold atoms show distinct and prominent absorption features in the UV-vis region due to the quantization effects.

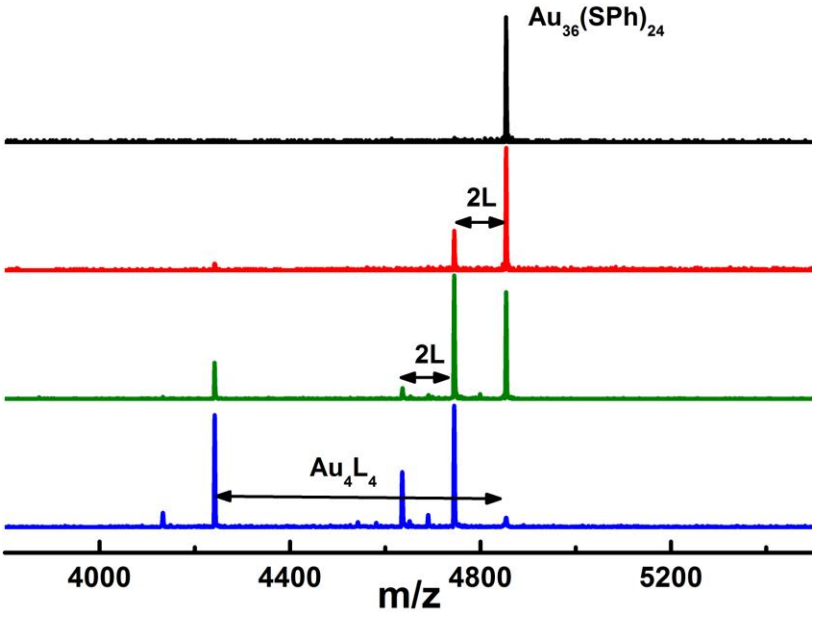

Figure 5.3. ESI Q-TOF MS-MS analysis on $Au_{36}(SPh)_{24}$ peak at *m/z* 4854 showing the systematic fragment loss of 2 L (L = PhS-, MW = 110 Da), 4 L, and Au_4L_4 loss with increasing extraction cone voltage.[29]

The optical spectrum of Au_{36} has distinct features in the UV-vis region at 575, 373 (intense peaks) and 408 nm (shoulder peak). The compound shows an absorption onset at ~725 nm (1.71 eV), which is in close agreement with the PBE-calculated HOMO-LUMO gap (1.65 eV).

5.3.3.3. Electrochemistry

The electrochemical characterization of $Au_{36}(SPh)_{24}$ was performed for the first time using differential pulse voltammetry (DPV). The electrochemical gap, given by the potential difference between the first oxidation and first reduction peaks, was calculated to be 1.96 eV from the DPV

measurements.

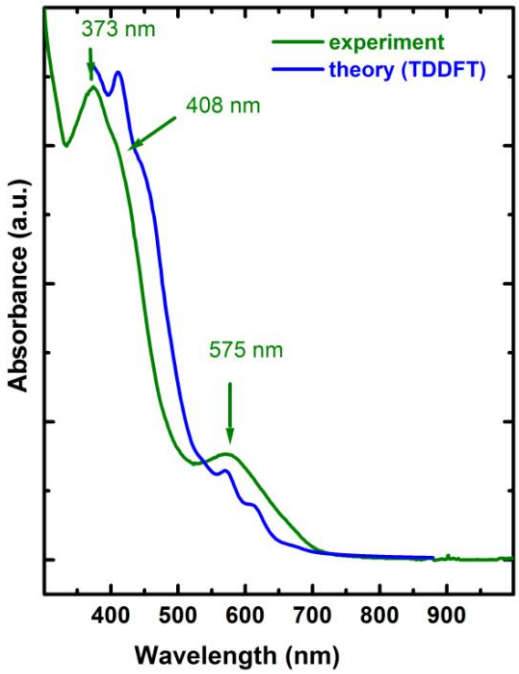

Figure 5.4. Experimental (green) and calculated (blue) UV-vis spectra of $Au_{36}(SPh)_{24}$ showing the intense absorption peaks at 575 and 373 nm. It is also interesting to see that the optical spectrum of Au_{36} is completely different from that of Au_{38} (although they differ by two Au atoms) highlighting the size sensitive properties in gold nanomolecules.

When corrected for the charging energy (0.23 eV)[108], the HOMO-LUMO gap for Au_{36} is 1.73 eV which is in close agreement with the theoretically calculated HOMO-LUMO gap. It is interesting to note that this gap is considerably higher than the HOMO-LUMO gap of $Au_{38}(SCH_2CH_2Ph)_{24}$ which is 1.33 eV.[84]

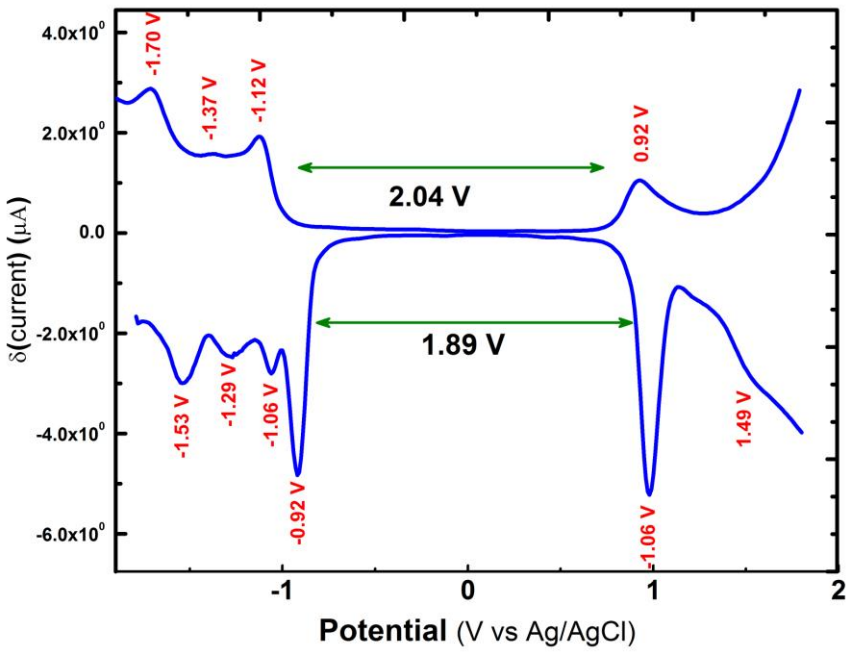

Figure 5.5. Differential pulse voltammetry (DPV) curve of $Au_{36}(SPh)_{24}$ in dichloroethane/0.5M $BTPPATBF_{20}$ as supporting electrolyte.

5.3.3.4. Crystal structure of Au_{36}

X-ray quality crystals of compound were solved to an R1 value of 6.8% to yield the composition $Au_{36}(SPh)_{24}$. The total structure of $Au_{36}(SPh)_{24}$ is shown in figure 5.6 a. The heavy atoms, Au and S, were anisotropically refined as shown by the thermal ellipsoids in Figure 5.6 b. The size of the thermal ellipsoids is a good crystallographic indicator of correct atom assignment. Figure 5.6 c shows the unit cell containing two molecules (Z=2). Figure 1 d-f show the $Au_{36}S_{24}$ motif. The four $–Au_2SR_3–$ motifs are shown in blue and are rotated by 90° in figures 5.6 e and 5.6 f. Figure 5.6 g shows the Au_{28} core with fcc-like atomic arrangement. Twelve

sulfur atoms bond with the Au_{28} core to form four $–Au_2SR_3–$ like motifs with this core, as seen in 0 and 90° views in Figure 5.6 h and 5.6 i. Figures 5.6 j-l shows how the Au_{28} core is protected by the additional four $–Au_2SR_3–$ motifs shown in blue. See below for an alternative charge state analysis based Au_{20} core. The cubic close-packing of the Au_{28} motif is illustrated in both ball and stick (figure 5.6 m) and space filling (figure 5.6 n) models, where the various layers (Au_3-Au_7-Au_{12}-Au_6 = Au_{28}) of atoms are shown by different colors. The layers of atoms are artificially stretched out in Figure 5.6 o to display the cubic close-packing in the Au_3(green)-Au_7(orange)-Au_{12}(blue)-Au_6(red) layers. Smaller gold nanomolecules (Au_{25} and Au_{38}) are found to have icosahedral cores, intermediate sized nanomolecules (Au_{67} and Au_{144}) are expected to have decahedral cores and as the size further increases (Au_{329} or larger) the nanomolecule cores are expected to take fcc structures. It is important to note that this proposal was made at the time when the capping ligands used were aliphatic and phenylethanethiol. In contrast to this popular belief by a majority of the nanomolecule research community, the structure of $Au_{36}(SPh)_{24}$ was found to have fcc lattice with a Au_{28} core and bridging thiophenol ligands. These unprecedented crystallographic results suggest that the ligands play a significant role in determining the structure of nanomolecules. The recent crystallographic analysis of $Au_{28}(SPh\text{-}tBu)_{20}$, which also possess an fcc core supports the above point that the ligands play a key role in determining the atomic arrangement of the nanomolecule[27-29,89,93]. This discovery calls for a new proposal that does not rule out the possibility of fcc cores in smaller sizes. Whether the formation of fcc core in Au_{36} and Au_{28} is due to aromaticity or bulkiness of the ligands is not clear. To investigate this, we tried to study the effect of aromatic ligands on larger Au_{144} nanomolecule. When the stable $Au_{144}(SCH_2CH_2Ph)_{60}$ nanomolecules were reacted with aromatic ligands, 99-gold atom

nanomolecules were observed and the results are presented in the following section on Au_{99}.

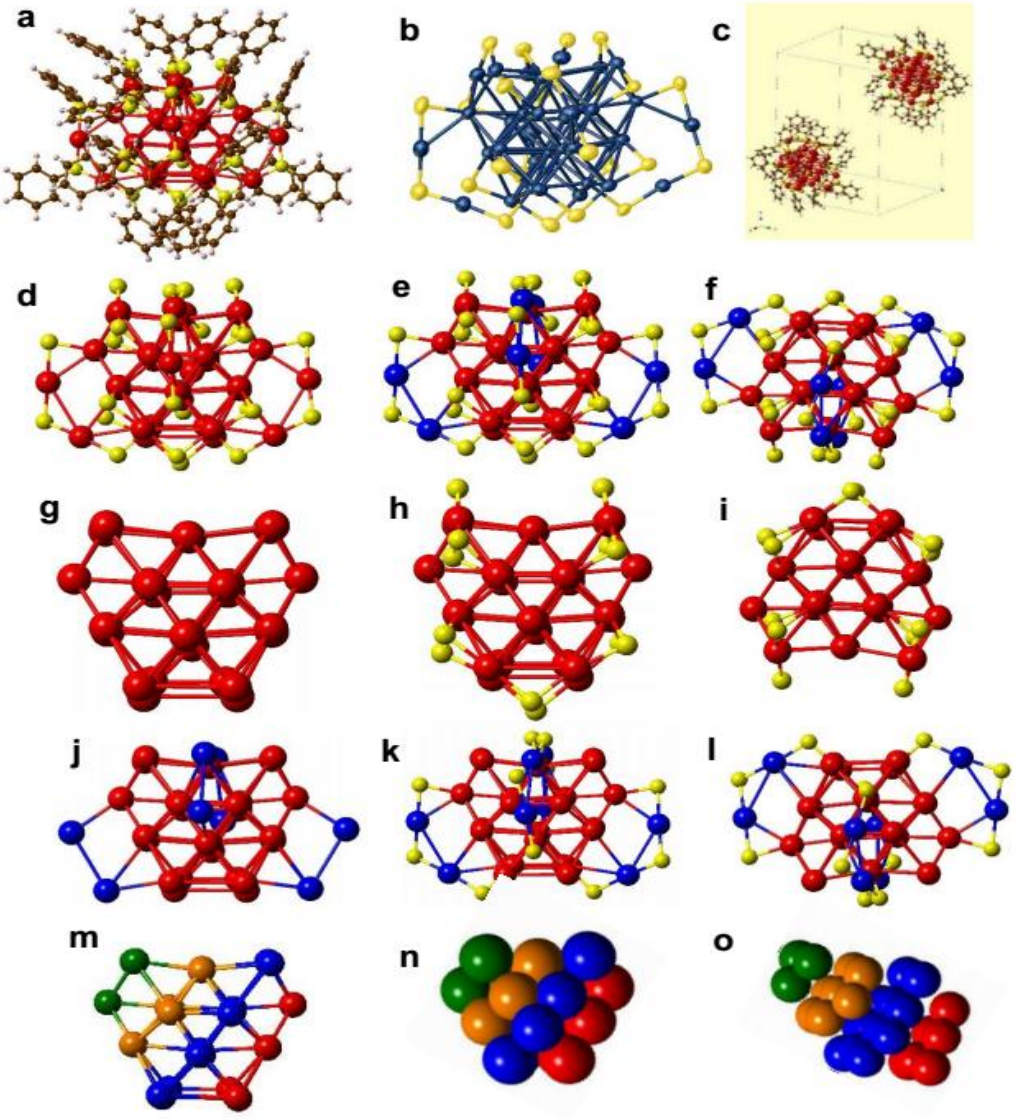

Figure 5.6. X-ray crystal structure of $Au_{36}(SPh)_{24}$. a) Total structure of $Au_{36}(SPh)_{24}$; b) $Au_{36}S_{24}$ motif shown as thermal ellipsoids, illustrating the quality of the structure; C) Unit cell showing two $Au_{36}(SPh)_{24}$ molecules; d) $Au_{36}S_{24}$ motif only; e) $Au_{36}S_{24}$ motif with the two -Au_2SR_3- motifs shown in blue; f) the structure in (e) rotated by 90° rotation; g) Au_{28} motif only; h) The

$Au_{28}S_{12}$ motif, where the four Au_2SR_3-type motif is observed; i) the structure in (h) rotated by 90°; j) Au_{36} motif; k) Au_{28} motif with the four Au_2SR_3 motif is highlighted in blue; l) 90° rotation of structure in (k); Au_{28} motif in ball and stick; (m) space filling model; (n) displaying various layers of atoms in different colors to illustrate cubic close-packing; o) The space filling model in (n) where the various layers of atoms are artificially stretched-out to display the cubic close-packing; structures in (a) and (c) to (l) are shown in ball and stick models. Coloring scheme is as follows: Au-red or blue; S-yellow; C-brown; H-pink.

5.4 Effect of ligands on the size and geometry of nanomolecules : A case of $Au_{99}(SPh)_{42}$

5.4.1 Experimental

Chemicals: Phenylethanemercaptan (Sigma aldrich, ≥ 99%), sodium borohydride (Acros, 99%), *trans*-2-[3-(4-*tert*-butylphenyl)-2-methyl-2-propenylidene]malononitrile (DCTB matrix) (Fluka, ≥ 99%), benzenethiol (Aldrich 97%), 4-methoxybenzenethiol (Aldrich 97%), 4-fluorobenzenethiol (Aldrich 97%), 4- bromobenzenethiol (Aldrich 95%), 5-chloro-2-methyl-benzenethiol and tert-butylbenzenethiol (Aldrich 95%) were purchased from Aldrich and used as received. Tetrahydrofuran (Acros anhydrous, stabilized 99.9%) and other solvents like toluene, methanol, acetonitrile and acetone were used from Fisher as received.

Equipment: UV-visible absorption spectra were recorded in toluene on a Shimadzu UV-1601 instrument. Matrix assisted laser desorption time-of-flight (MALDI-TOF) mass spectra were collected on a Bruker Autoflex II mass spectrometer in linear positive mode using a nitrogen laser (337 nm) with DCTB as a matrix. ESI-MS spectra were acquired on Waters SYNAPT mass spectrometer using THF. No supporting electrolyte was used. Electrochemical measurements were performed on a CHI 620 instrument using 5 mg of title compound in DCE

solution with 0.5 mM $BTPPATBF_{20}$ as supporting electrolyte under nitrogen atmosphere.[109] Powder XRD measurements were performed on Bruker D8-Focus XRD instrument for 48h on a quartz substrate. 5 mg of sample was dissolved in minimal amount of toluene and deposited on the substrate and air-dried.

5.4.2. Synthesis of $Au_{99}(SPh)_{42}$

The synthesis of Au_{99}, similar to Au_{36}, involves two stages. The first stage involves the synthesis of $Au_{144}(SCH_2CH_2Ph)_{60}$ using a two phase Brust-Schiffrin synthesis, and the second stage involves etching Au_{144} with thiophenol. The details of the two stages are described here.

Step 1 - Synthesis of Au_{144}: The synthesis of Au_{144} can be done using different protocols reported in the literature.[70,110] Here, for the synthesis of Au_{144}, 0.35 g (0.88 mmol) of $HAuCl_4$ dissolved in 30 ml of distilled water was added to 0.6 g (1.1 mmol) TOABr in 30 ml toluene. The contents were mixed for 30 min at 500 rpm until the gold salt transferred to the organic phase. The organic layer was then transferred into a separate round bottom flask and 0.45 ml (0.88 × 4 mmol) of phenylethanethiol was added. The reaction mixture was stirred for 60 min at 500 rpm. Then, 0.34 g (8.8 mmol) of $NaBH_4$ in 20 ml ice-cold distilled water was added to the reaction mixture in one portion. Upon addition of $NaBH_4$, the reaction mixture turned dark, indicating the formation of nanoparticles. The reaction was stopped after 1 h of sodium borohydride addition. The aqueous layer was pipetted out and the contents were dried by rotary evaporation. The resulting product was washed with methanol three times by centrifugal precipitation to remove the excess ligand and dried by rotary evaporation. The resulting products were analyzed by MALDI-TOF MS to find the composition. There was a mixture of Au_{144} and Au_{25} in the product. From this mixture, Au_{25} was separated by solvent fractionation using toluene and methanol

mixtures. Occasionally, an SEC purification step was involved to separate Au_{144}. Pure Au_{144} obtained after solvent fraction was used for etching in stage 2.

Step 2 - Synthesis of Au_{99}: To 10 mg of Au_{144}, 1 ml of benzenethiol was added and the reaction mixture was heated at 80^0C for about 3 h.[23] MALDI-MS was performed to monitor the progress of the reaction.[61] For complete ligand exchange, a second etching step was sometimes required. Same procedure was employed for the other substituents of benzenethiol including 4-methoxybenzenethiol, 4-fluorobenzenethiol and 4-methylbenzenethiol. The resulting product was passed through a short SEC column (20 cm with Biorad SX1 beads in THF)[86] to remove the excess benzenethiol ligand. This avoids the extremely foul smell and the labor required during processing of this product via methanol precipitation in a centrifuge. The product which was collected as the eluate is $Au_{99}(SPh)_{42}$ and completely free of benzenethiol.

5.4.3 Results and Discussion

5.4.3.1 Core-size conversion of $Au_{144}(SCH_2CH_2Ph)_{60}$ to $Au_{99}(SPh)_{42}$

MALDI monitored conversion of Au_{144} to Au_{99} : Research in nanomolecules has been focussed on capping nanomolecules with aliphatic ligands and phenylethanethiol. With those ligands, $Au_{144}(SR)_{60}$ is highly stable and resistant to chemical etching at elevated temperatures. But when $Au_{144}(SCH_2CH_2Ph)_{60}$ was etched with thiophenol at 80°C, all the phenylethanethiol ligands were exchanged and the core was transformed to form $Au_{99}(SPh)_{42}$. Figure 5.7 below shows the MALDI-MS monitored reaction of $Au_{144}(SCH_2CH_2Ph)_{60}$ converting to $Au_{99}(SPh)_{42}$. The starting material, $Au_{144}(SCH_2CH_2Ph)_{60}$ is shown in black (0 h) indicating the purity of the material. The multiple peaks observed in ~35 kDa region are due to the fragmentation in MALDI. The ESI-MS showed single peak for the 3+ charge state of the parent peak at 12196 Da.

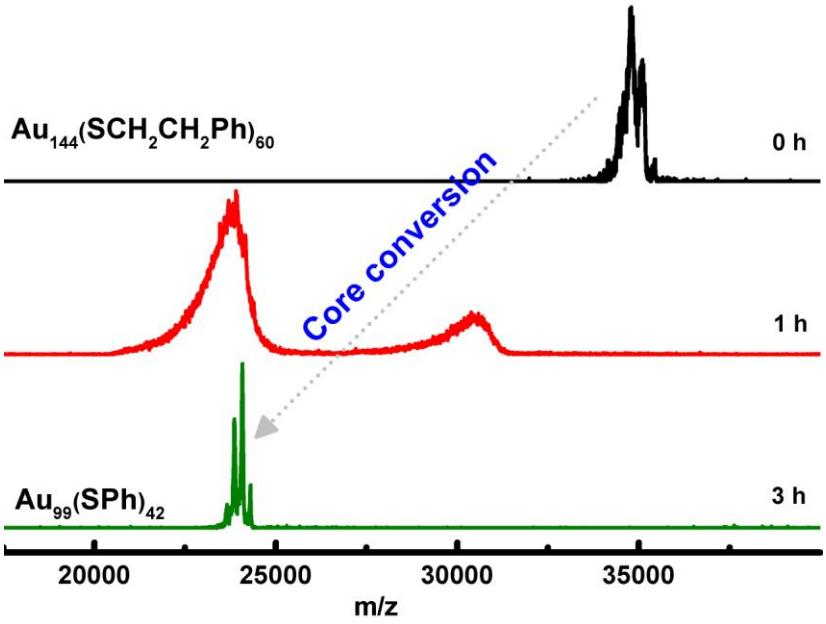

Figure 5.7. MALDI-MS data of the aliquots collected from the thermo-chemical treatment of Au_{144} with benzenethiol to obtain the title compound. $Au_{130}(SPh)_{50}$ is seen in the 1 h sample, which degrades or converts to Au_{99} by the end of the reaction.

The MALDI mass spectrum of 1 h sample in red shows no peak at ~35 kDa indicating that all the $Au_{144}(SCH_2CH_2Ph)_{60}$ from the starting material has been consumed or converted in the reaction. The two peaks at ~30 kDa and 24 kDa correspond to $Au_{130}(SPh)_{50}$ (assigned using ESI-MS) and $Au_{99}(SPh)_{42}$. In the 3 h sample in olive, there is only 24 kDa peak corresponding $Au_{99}(SPh)_{42}$. All the Au_{130} observed in the 1 h sample converted to Au_{99} in the final product suggesting that it is an intermediate in the reaction. The composition of the final product was assigned using high resolution ESI-MS.

5.4.3.2 *Compositional assignment of $Au_{99}(SPh)_{42}$*

ESI-MS is a high resolution mass spectrometry that is capable of yielding multiply charged molecular ion peaks for nanomolecules. High resolution ESI-MS data (blue curve in

figure 5.7) showed peaks at ~12 and ~8 kDa/z, suggesting a charge state of 2+ and 3+ respectively.

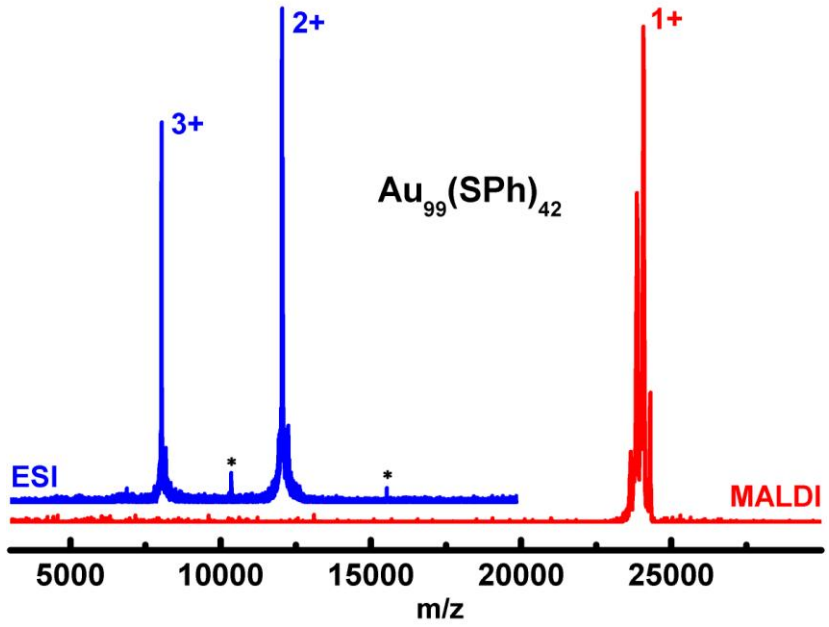

Figure 5.8. ESI (blue) and MALDI-TOF (red) mass spectrum of $Au_{99}(SPh)_{42}$. DCTB was used as matrix. Peaks with asterisks indicate $Au_{130}(SPh)_{50}$ that are formed in minor quantities during etching along with the title compound.

The experimental 12040 and 8027 m/z peaks matched well with that of theoretical values 12041.1 (2+ calc.) and 8026.6 (3+ calc.) corresponding to the composition, $Au_{99}(SPh)_{42}$. We also confirmed the mass assignment by preparing the Au_{99} nanomolecules using another ligand. When $Au_{144}(SCH_2CH_2Ph)_{60}$ was etched with p-methoxybenzenethiol, $HSPhOCH_3$, the same core size conversion phenomenon was observed. The final product obtained from the etching of $Au_{144}(SCH_2CH_2Ph)_{60}$ with p-methoxybenzenethiol was analyzed by ESI-MS. Figure 5.9 shows the ESI-MS (3+ peaks) observed for the product obtained with p- methoxybenzenethiol ($HSPhOCH_3$), in comparison with that of benzenethiol (HSPh). If both of these peaks correspond

to same species, the mass difference between these two peaks should correspond to the difference in the mass of the ligands.[12,111,112]

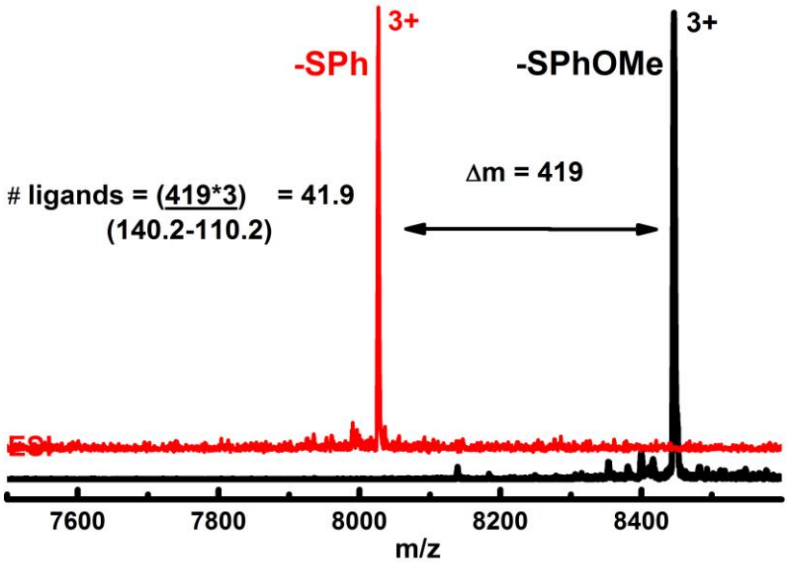

Figure 5.9. ESI mass spectra of $Au_{99}(SPh)_{42}$ nanomolecules protected by benzenethiol (red curve) and p-methoxybenezenethiol (black curve) showing a mass difference of 419 m/z used to calculate the number of ligands in the Au_{99} to be 42.

The mass difference between these two peaks was found to be 419 m/z units. Since this was a 3+ ion, the actual mass difference of the molecular ion would be 1257 (3 × 419) Da. When this mass difference was divided by the difference in the mass of the ligands [140.2 (-SPhOCH3) – 110.2 (-SPh) = 30 Da], the number of ligands was found to be 42. This further confirms the composition of this gold nanomolecule to be $Au_{99}(SPh)_{42}$ and $Au_{99}(SPhOCH_3)_{42}$ with benzenethiol and p-methoxybenzenethiol respectively.

5.4.3.3 Au_{144} → Au_{99} core-size conversion studied by ESI-MS

In the case of Au_{36}, the core conversion of Au_{67} and $Au_{103\text{-}105}$ to Au_{36} occurs via an

intermediate $Au_{38}(SCH_2CH_2Ph)_{14}(SPh)_{10}$. After ten thiophenol ligands were exchanged, the core of Au_{38} was unstable and it converted to a more stable end product $Au_{36}(SPh)_{24}$. We attempted to analyze the core conversion of Au_{144} to Au_{99} by using a high resolution ESI-MS. The multiply charged peaks appear at a lower mass and offer better resolution of the peaks, enabling us to identify the exchanges on Au_{144}.

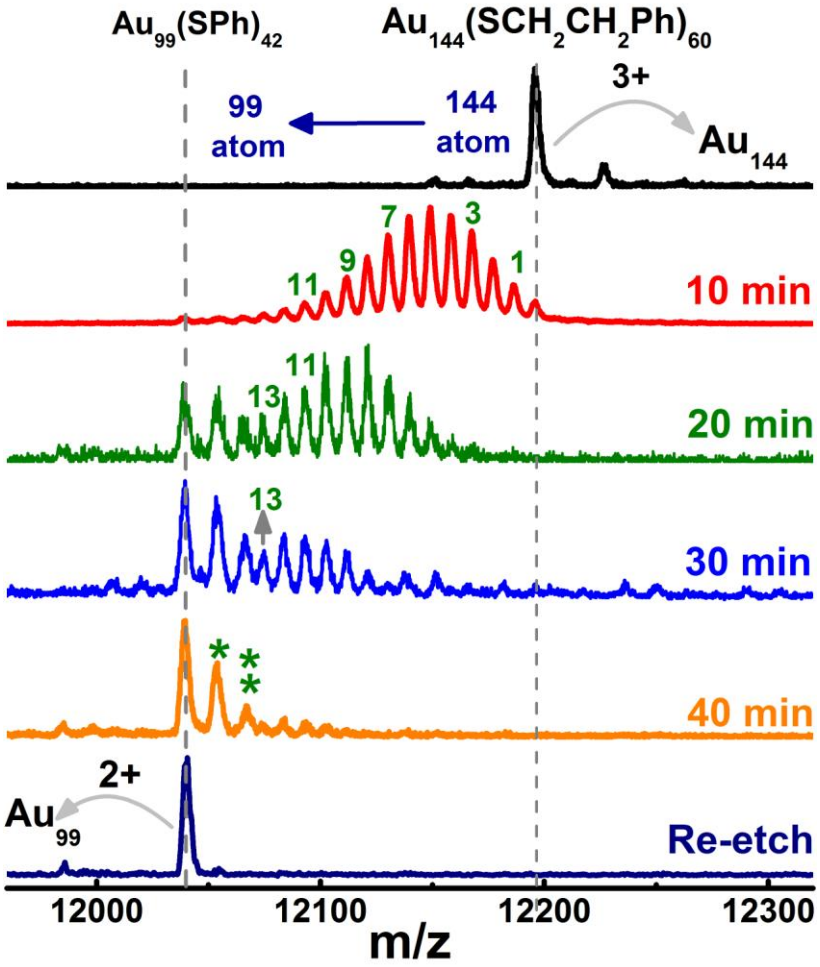

Figure 5.10. ESI-MS monitored thermo-chemical treatment of $Au_{144}(SCH_2CH_2Ph)_{60}$ in benzenethiol. The spectra is zoomed in the 12 kDa mass region to highlight the ligand exchanges

occurring in the early stage of reaction. Note that up to thirteen exchanges, the Au_{144} core is preserved. Further exchanges lead to formation of $Au_{99}(SPh)_{42}$ (2+ at 12,039 m/z). $Au_{99}(SPh)_{41}(SCH_2CH_2Ph)_1$ and $Au_{99}(SPh)_{40}(SCH_2CH_2Ph)_2$ species are denoted by olive asterisks.

Figure 5.10 shows the ESI monitored etching of Au_{144}. The peak at 12195 m/z is for the starting material (3+ of Au_{144}). The reaction is quick compared to other ligand exchanges on Au_{144}. Within10 min, sample shows an average of 13 ligands exchanged. There is no peak corresponding to Au_{144} in the 20 min sample. The spectrum shows a peak for 2+ of Au_{99} emerging at ~12,039 m/z. The 40 min sample shows that the reaction is almost complete with only two unexchanged ligands; $Au_{99}(SPh)_{40}(SCH_2CH_2Ph)_2$. These last two ligand exchanges are tough and typically required a re-etching process, where the product of first etching was washed and reacted with a fresh addition of benzenethiol for 30 min at 80°C to drive the reaction to completion. The same observation was made in the case of synthesis of Au_{36}, where a second etching was needed for complete exchange with benzenethiol. Careful observation showed that after about 13 ligand exchanges, the Au_{144} core became unstable and converted to an entirely different core, Au_{99}. That is, as the value of x in $Au_{144}(SCH_2CH_2Ph)_{60-x}(SPh)_x$, becomes larger than 13, the aromaticity induced by the 13 ligands reached a threshold value, at which point the Au_{144} core starts converting to Au_{99} core. We believe that the core size conversion after 13 ligands is a consequence of the aromaticity associated with the benzenethiol.

5.4.3.4 Substituent effects on the core conversion of $Au_{144} \rightarrow Au_{99}$

We have performed the ligand exchange of Au_{144} with substituted benzenethiols, of the form HSPhX, to study the effect of the substituent on the Au_{144} to Au_{99} reaction.[113] In this study,

we have used 4-methoxybenzenethiol, 4-fluorobenzenethiol and 4-methylbenzenethiol in addition to benzenethiol. All the four ligands have shown core conversion of Au_{144} to Au_{99}. 4-methoxybenzenethiol resulted in $Au_{99}(SPhOMe)_{42}$ which was analyzed by ESI-MS and MALDI-MS.

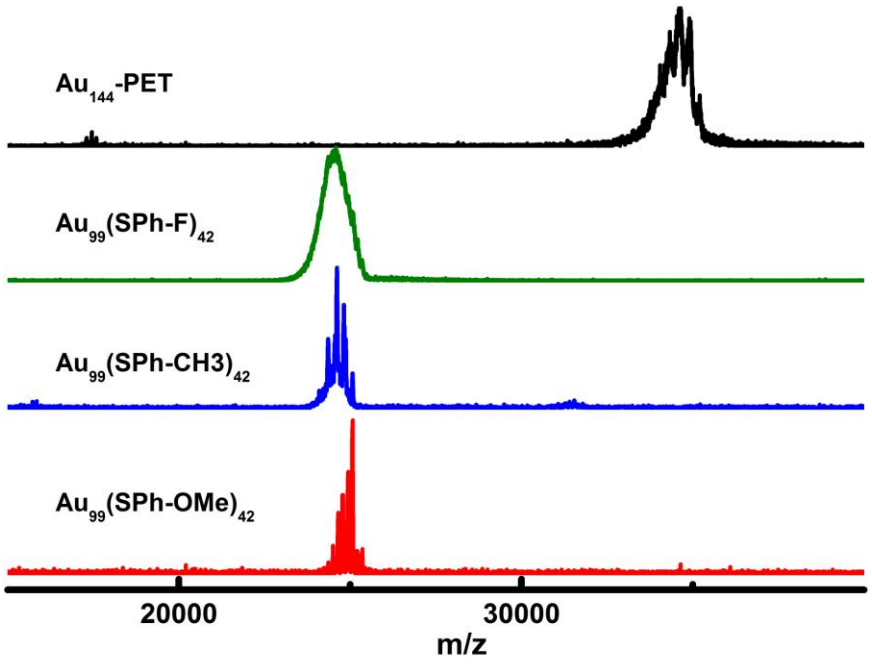

Figure 5.11. MALDI-MS of a products obtained by core conversion of Au_{144} using various substituents of benzenethiol including 4-flourobenzenethiol, 4-methylbenzenethiol and 4-methoxybenzenethiol.

The end products of reactions using 4-fluorobenzenethiol and 4-methylbenzenethiol were analyzed by MALDI-MS in figure 5.11. Although the exact assignments could not be made using these two ligands, the experimentally observed masses were close to the predicted mass for $Au_{99}(SPh\text{-}F)_{42}$ (calc. 24,667 Da) and $Au_{99}(SPh\text{-}CH_3)_{42}$ (calc. 24,834 Da). We did not attempt to assign the composition for these two products due to the low resolution of MALDI-MS at this

mass range. For the ligands considered here, the 144→99 core-size conversion is due to aromaticity; with the electronic effects due to substituents' on the aromatic ring, imposing only minimal influence.

5.4.3.5 Effect of conjugation of ligands on the 144 → 99 core conversion

We have also studied the effect of linker length between benzene ring and thiol group on the Au_{144} → Au_{99} core size conversion. The thermochemical stability of Au_{144} is known for nearly two decades now.[1,23,70,114] $Au_{144-x}Ag_x(SR)_{60}$ was also prepared by silver doping, suggesting the high stability of the 144-atom species.

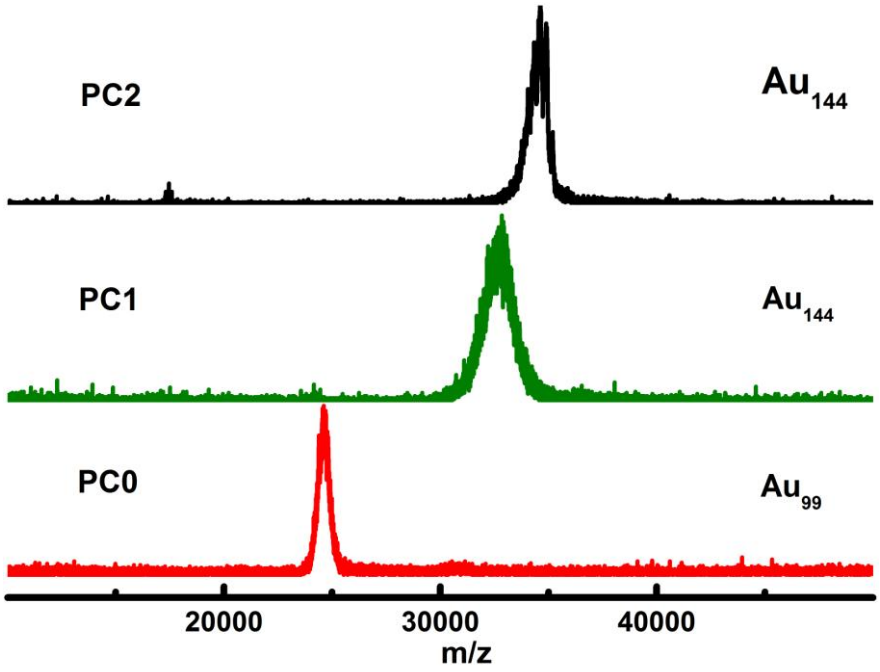

Figure 5.12. ESI-MS of products obtained by etching $Au_{144}(SCH_2CH_2Ph)_{60}$ in $PhCH_2CH_2SH$ (black), $PhCH_2SH$ (olive) and PhSH (red).

When $Au_{144}(SCH_2CH_2Ph)_{60}$ was etched in phenylethanethiol at 80^0C, it was stable and remained as 144-atom core for over 24 h as shown in Figure 5.12, black spectrum. Etching of

$Au_{144}(SC_nH_{2n+1})_{60}$ in $HSCH_2CH_2Ph$ also yields $Au_{144}(SCH_2CH_2Ph)_{60}$ without affecting the 144-atom core. In this study, we have etched $Au_{144}(SCH_2CH_2Ph)_{60}$ with $HSCH_2CH_2Ph$, $HSCH_2Ph$, and HSPh. In other words, the effect of linker length, n in $HS(CH_2)_nPh$ was varied by one methylene group at a time from n=2, 1 and 0. We observed that both $HSCH_2CH_2Ph$, $HSCH_2Ph$ maintained the 144-metal atom core and do not convert it to 99-metal atom core. This is shown in the black and olive MALDI spectra in Figure 5.11. However, when Ph is directly connected to the thiol group, it converts to Au_{99}, as shown in red curve in Figure 5.11. It is clear from these results that a direct conjugation of benzene ring with thiol group is necessary for the $Au_{144} \rightarrow Au_{99}$ conversion. In addition to etching of Au_{144} in aromatic ligands, we have investigated the etching of higher clusters[115] (between 50 and 150 kDa). The results were interesting in that this mixture of higher clusters core converted to Au_{99} in 3 h. These results combined with the reports on Au_{36} show that Au_{99} and Au_{36} are the core-sizes stabilized by aromatic ligands under etching, where Au_{36} is stable in lower mass region, and Au_{99} is stable in higher mass region.

5.5 Conclusions

In summary, we have synthesized and characterized $Au_{36}(SPh)_{24}$ and $Au_{99}(SPh)_{42}$ as part of our investigation on the role of ligands in influencing the structure and properties of gold nanomolecules. There are important conclusions we can draw based on the results of this study. Firstly, the aromatic ligands on gold core yield sizes that are different from the aliphatic thiol capped nanomolecules. The series of stable sizes formed with aliphatic ligand capping are Au_{25}, Au_{38}, Au_{67}, $Au_{103\text{-}105}$ and Au_{144} while in case of aromatic thiol capping, we found so far that Au_{28}, Au_{36} and Au_{99} are the stable sizes. Secondly, the geometry of nanomolecules is significantly affected by the aromatic ligand capping. $Au_{38}(SCH_2CH_2Ph)_{24}$ has a bi-icosahedral geometry

while $Au_{36}(SPh)_{24}$ possess an fcc geometry with new bridging thiolate ligands[28,116]. Thirdly, the properties of nanomolecules are affected significantly by the choice of capping ligands. The HOMO-LUMO gap increases from 1.3 eV to 1.7 eV from $Au_{38}(SCH_2CH_2Ph)_{24}$ to $Au_{36}(SPh)_{24}$. Whether the above conclusions are a result of aromaticity of the benzenethiol and its derivatives or the bulkiness of the same ligands is still debatable.

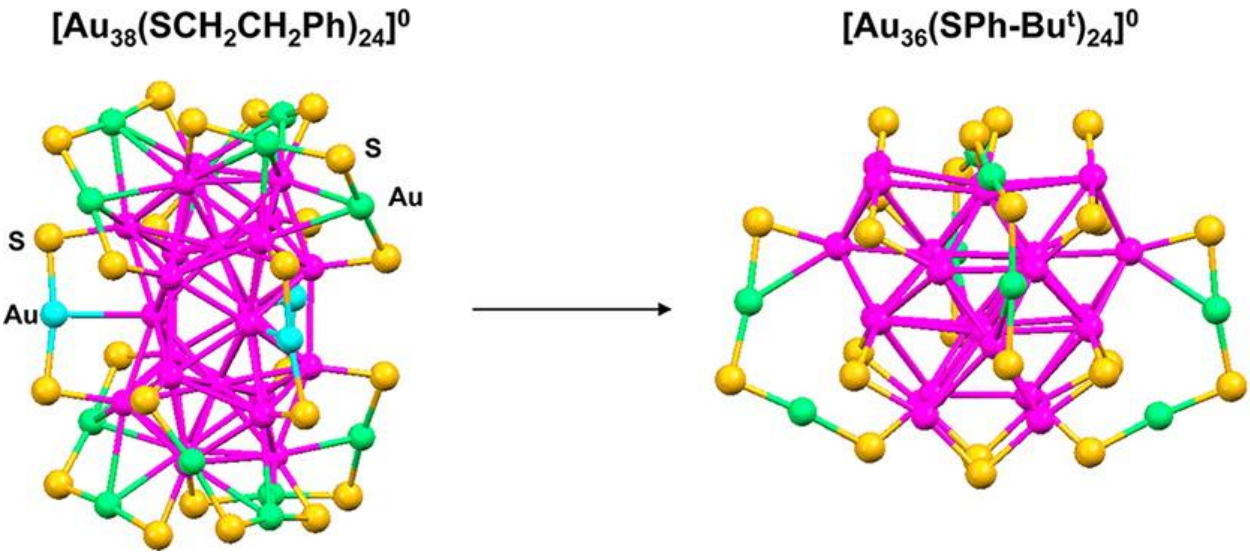

Scheme 3.1 The scheme illustrating the transformation of bi-icosahedral geometry in $Au_{38}(SCH_2CH_2Ph)_{24}$ to fcc geometry in $Au_{36}(SPh\text{-}t\text{Bu})_{24}$ upon ligand exchange. Reprinted with permission from ref 112. Copyright American Chemical Society 2013.

The first discovery of $Au_{36}(SPh)_{24}$ by our group lead us to propose that the conjugation of benzenethiol was the reason for this transformation. The theory was supported by the subsequent report by Jin and coworkers on the crystal structure of $Au_{36}(SPh\text{-}tBu)_{24}$. Then came the report on the crystal structure of $Au_{36}(SC_5H_{11})_{24}$ with a non-aromatic ligand, questioning the theory of aromaticity induced transformation. But in the same report, it was mentioned that the yield of Au_{36} with cyclopentanethiol was less compared to that with an aromatic thiol (50% vs 90%). To

explain this, the report came up with a proposal that bulkiness of the ligand is the triggering agent for the initial ligand exchange/transformation while the electronic conjugation of aromatic ligands is the reason for the formation of stable sizes like Au_{36}. We cannot undermine the effect of electronic conjugation, as Au_{36} is not formed with other bulkier ligands like cyclopentanethiol or adamantanethiol. With the evidence known so far, it is to be concluded that both aromaticity and the bulkiness of the ligands are vital in determining the structure and properties of the gold nanomolecules.

CHAPTER SIX

CONTRIBUTIONS AND FUTURE DIRECTIONS

In this chapter, contributions of my dissertation research and future directions to the work are summarized. The one-phase protocol for the synthesis of nanomolecules was investigated in detail; sizes like Au_{67} and $Au_{103\text{-}105}$ were isolated for the first time. It was also the first time a gold-thiolate nanomolecules were isolated in 50+ mg quantities in its monodisperse form using solvent fractionation techniques. The high yields enabled characterization of nanomolecules using techniques like powder-XRD and electrochemistry which were otherwise hindered by the availability of large quantities of monodisperse material. Size exclusion chromatographic technique was developed by me for the purpose of isolating pure $Au_{103\text{-}105.}$ The technique is since then being used in our laboratory for isolation and purification purposes. It has become the method of choice for separation of nanomolecules like Au_{67} and $Au_{\sim 103}$. The isolation techniques proved successful for large scale synthesis of Au_{67} and $Au_{103\text{-}105}$ and paved way for comparing the stability of various sizes of nanomolecules using core conversion reactions. We showed that Au_{38} and Au_{40} were formed from core conversion of larger species. The core conversion

experiments clearly how smaller, more stable sizes of nanomolecules are formed from the larger sizes. A decade ago, there was a popular notion that the size, geometry and properties of these nanomolecules were not influenced by the choice of ligand used in the synthesis or etching reactions. We have investigated the effect of ligands by using aromatic ligands instead of traditionally used aliphatic ligands on gold nanomolecules. The experimental results suggested that ligands have an influence on the size, geometry and properties of nanomolecules. All these interesting results have contributed and progressed the research in this field by a great deal in the past five years.

The chapter 2 of the dissertation describes the synthesis and characterization of $Au_{67}(SCH_2CH_2Ph)_{35}$ nanomolecules. It is interesting and important to mention that Au_{67} is only produced in a one-phase Brust-Schiffrin synthesis protocol. It was observed in the mass spectrometry for years then but was never assigned or characterized due to a) difficulty to capture Au_{67} in one-phase synthesis and b) lack of techniques to isolate the compound. I have investigated the one-phase synthesis in detail, studied the size evolution of nanomolecules in the reaction and developed a protocol to capture the Au_{67} and $Au_{103\text{-}105}$ species. After these species were produced in the synthesis, I have developed solvent fractionation technique to systematically separate Au_{67} from the rest of the species in the polydisperse mixture of various sizes. Although the protocol was laborious, it proved fruitful in isolating ~50 mg quantities of nanomolecules. Such high yields have enabled the use of characterization techniques like powder-XRD, NMR and electrochemistry which were otherwise restricted due to low yields.

$Au_{103\text{-}105}(SCH_2CH_2Ph)_{45\text{-}46}$ is one other size nanomolecule that is produced only in a one-phase synthesis along with $Au_{67}(SCH_2CH_2Ph)_{35}$ and not characterized due to lack of isolation

techniques. I have worked on the isolation of $Au_{103\text{-}105}$ which yielded 50+ mg quantities of the pure compound. For the isolation of $Au_{103\text{-}105}$, we have employed size exclusion chromatographic technique. SEC offers more control, high reproducibility and more effective separation compared to the previously employed solvent fractionation technique. It was also interesting to see that $Au_{102}(SCH_2CH_2Ph)_{44}$ was absent in the mass spectrum as expected from the $Au_{102}(SPh\text{-}COOH)_{44}$ crystal structure reported in 2007.[18] Instead, a set of peaks $Au_{103}(SCH_2CH_2Ph)_{45}$, $Au_{104}(SCH_2CH_2Ph)_{45}$, $Au_{104}(SCH_2CH_2Ph)_{46}$ and $Au_{105}(SCH_2CH_2Ph)_{46}$ were observed in the high resolution mass spectrum. The results gave interesting positive leads on the influence of ligand on the composition of the nanomolecules. We pursued this lead by studying the aromatic ligand capping and its influence on the size, geometry and properties of nanomolecules.

I have shown core size conversion in gold nanomolecules for the first time. These studies can be used as an indicator for the stability of nanomolecules. The isolation of Au_{67} and $Au_{103\text{-}105}$ using SEC have enabled the core size conversion reactions using them as starting materials. I showed that smaller, more stable nanomolecules (Au_{38}, Au_{40} etc) could be formed from the cores of larger, less stable sizes (Au_{67}, $Au_{103\text{-}105}$ etc). Prior to the discovery of these reactions, it was not possible to synthesize stable Au_{38} and Au_{40} nanomolecules exclusively but with the core size conversion reactions, I showed that controlling the size distribution of the starting material can influence the end product.

As described in chapter 5 of this dissertation, I have investigated the role of ligands on the size, geometry and its electronic properties. Prior to our study, it was assumed that ligands have a minor role in influencing the properties of nanomolecules. I have first synthesized $Au_{36}(SPh)_{24}$ nanomolecule using an aromatic ligand thiophenol. The size Au_{36} was observed for

the first time and it was different from the expected Au_{38} and Au_{40} sizes which are traditionally formed stable sizes using aliphatic ligands. Besides the size, the geometry and properties of Au_{36} were completely different from that of Au_{38}. Au_{36} was found to possess an fcc geometry while Au_{38} had a bi-icosahedral geometry. The electrochemical gap in Au_{36} significantly increased when compared to Au_{38} (1.72 vs 1.33 eV). I had continued studies using aromatic ligands and observed a stable size $Au_{99}(SPh)_{42}$ in the larger mass region instead of $Au_{144}(SR)_{60}$ as observed with aliphatic ligands. There were several other groups in the fields that reported similar sizes with aromatic ligands. It is now established that the sizes of Au_{28}, Au_{36} and Au_{99} are stable with aromatic capping while the sizes like Au_{25}, Au_{67}, $Au_{103\text{-}105}$, Au_{130} and Au_{144} that are stable with aliphatic ligands. I performed studies using some bulky ligands like adamantanethiol and cyclohexanethiol to see if the above effect was due to the conjugation of the ligands or just the bulkiness. The results so far suggest that it is a combined effect of conjugation and bulkiness. But it is important to investigate further the effect of ligands on the properties of nanomolecules. Obtaining the crystal structure of $Au_{99}(SPh)_{42}$ can give valuable insights into why that size is preferred over the well-known stable $Au_{144}(SR)_{60}$.

I would like to put forward a few more ideas in a) developing synthetic protocols and b) synthesis of aromatic ligand capped nanomolecules.

a) It is important to expand our synthetic protocols beyond the two-phase Brust-Schiffrin synthesis and the one-phase THF synthesis. From our preliminary experiments, we learned that use of solvents with different polarity yields different products. For example, one-phase synthesis using THF gives products different in size from one-phase synthesis using dichloromethane. It is important to explore different solvents (based on the ligand polarity and

solubility) when nanomolecules are synthesize. We have established the two-phase and one-phase synthesis for phenylethanethiol. It is time to explore the possibility of using these protocols to prepare functionalized gold nanoparticles. One strategy to conjugate biomolecules to gold nanomolecules is through esterification. We can prepare gold nanomolecules capped by mercaptocarboxylic acids and use them as reactant in esterification reaction with -OH groups containing functional biomolecules.[117,118]

Table 6.1. The list of biomolecules proposed as capping ligands on gold nanomolecules.

Ligand	**Application**
Polyethylene glycol	Adheres to cell membrane, hence useful in targeting application
DNA	Bioimaging, gene delivery
Antibodies	Treatment and diagnosis
Peptides	Cellular and intracellular targeting

Tuning of nanomolecules is the key factor that raises enthusiasm about the practical applications. It is possible to demonstrate the tuning of nanomolecules in case of $Au_{36}(SR)_{24}$. In this regard, we can synthesize Au_{36} with derivatives of thiophenol ranging in electronegativity from -SPhF to -$SPhOCH_3$. Based on the reports of Murray et al[113], it is fair to derive a hypothesis where the electrochemical gap will be constant but shift systematically. We can also extend this studies where we can prepare $Au_{36}(SCH_2CH_2Ph)_{24}$ or $Au_{36}(SC_6H_{13})_{24}$ via ligand exchange and compare its electrochemical properties with $Au_{36}(SPh)_{24}$.

To conclude, we established protocols for synthesis and characterization of ultra-small, ultra-stable nanomolecules. We can extend these protocols to prepare functionalized nanomolecules and tune them to practical applications.

BIBLIOGRAPHY

(1) Whetten, R. L.; Khoury, J. T.; Alvarez, M. M.; Murthy, S.; Vezmar, I.; Wang, Z. L.; Stephens, P. W.; Cleveland, C. L.; Luedtke, W. D.; Landman, U. *Adv. Mater.* **1996**, *8*, 428.

(2) Ho, S. Y.; Cheng, E. C.-C.; Tiekink, E. R. T.; Yam, V. W.-W. *Inorganic Chemistry* **2006**, *45*, 8165.

(3) Kimling, J.; Maier, M.; Okenve, B.; Kotaidis, V.; Ballot, H.; Plech, A. *The Journal of Physical Chemistry B* **2006**, *110*, 15700.

(4) Faraday, M. *Philosophical Transactions of the Royal Society of London* **1857**, *147*, 145.

(5) Mie, G. *Annalen der Physik* **1908**, *330*, 377.

(6) Jain, P. K.; Huang, X.; El-Sayed, I. H.; El-Sayed, M. A. *Accounts of Chemical Research* **2008**, *41*, 1578.

(7) Lin, C.-A. J.; Yang, T.-Y.; Lee, C.-H.; Huang, S. H.; Sperling, R. A.; Zanella, M.; Li, J. K.; Shen, J.-L.; Wang, H.-H.; Yeh, H.-I.; Parak, W. J.; Chang, W. H. *ACS Nano* **2009**, *3*, 395.

(8) Tsunoyama, H.; Ichikuni, N.; Sakurai, H.; Tsukuda, T. *Journal of the American Chemical Society* **2009**, *131*, 7086.

(9) Chen, W.; Chen, S. *Angewandte Chemie International Edition* **2009**, *48*, 4386.

(10) Schmid, G.; Baumle, M.; Geerkens, M.; Heim, I.; Osemann, C.; Sawitowski, T. *Chemical Society Reviews* **1999**, *28*, 179.

(11) de Heer, W. *Reviews of Modern Physics* **1993**, *65*, 611.

(12) Nimmala, P. R.; Yoon, B.; Whetten, R. L.; Landman, U.; Dass, A. *J. Phys. Chem. A.* **2013**, *117*, 504.

(13) Qian, H.; Zhu, M.; Wu, Z.; Jin, R. *Acc. Chem. Res.* **2012**, *45*, 1470.

(14) Schaaff, T. G.; Shafigullin, M. N.; Khoury, J. T.; Vezmar, I.; Whetten, R. L.; Cullen, W. G.; First, P. N.; Gutiérrez-Wing, C.; Ascensio, J.; Jose-Yacamán, M. J. *The Journal of Physical Chemistry B* **1997**, *101*, 7885.

(15) Alvarez, M. M.; Khoury, J. T.; Schaaff, T. G.; Shafigullin, M. N.; Vezmar, I.; Whetten, R. L. *J. Phys. Chem. B.* **1997**, *101*, 3706.

(16) Schaaff, T. G.; Shafigullin, M. N.; Khoury, J. T.; Vezmar, I.; Whetten, R. L.; Cullen, W. G.; First, P. N.; Guti√©rrez-Wing, C.; Ascensio, J.; Jose-Yacam√°n, M. J. *The Journal of Physical Chemistry B* **1997**, *101*, 7885.

(17) Jiang, D.-e.; Tiago, M. L.; Luo, W.; Dai, S. *Journal of the American Chemical Society* **2008**, *130*, 2777.

(18) Jadzinsky, P. D.; Calero, G.; Ackerson, C. J.; Bushnell, D. A.; Kornberg, R. D. *Science* **2007**, *318*, 430.

(19) Brust, M.; Walker, M.; Bethell, D.; Schiffrin, D. J.; Whyman, R. *Journal of the Chemical Society, Chemical Communications* **1994**, 801.

(20) Wu, Z.; Suhan, J.; Jin, R. *J. Mater. Chem.* **2009**, *19*, 622.

(21) Mori, S.; Barth, H. G. *Size exclusion chromatography*; Springer, 1999.

(22) Knoppe, S.; Boudon, J.; Dolamic, I.; Dass, A.; Bürgi, T. *Anal. Chem.* **2011**, *83*, 5056.

(23) Schaaff, T. G.; Whetten, R. L. *J. Phys. Chem. B.* **1999**, *103*, 9394.

(24) Daniel, M.-C.; Astruc, D. *Chemical Reviews* **2003**, *104*, 293.

(25) Hostetler, M. J.; Templeton, A. C.; Murray, R. W. *Langmuir* **1999**, *15*, 3782.

(26) Song, Y.; Murray, R. W. *Journal of the American Chemical Society* **2002**, *124*, 7096.

(27) Qian, H.; Eckenhoff, W. T.; Zhu, Y.; Pintauer, T.; Jin, R. *J. Am. Chem. Soc.* **2010**, *132*, 8280.

(28) Zeng, C.; Qian, H.; Li, T.; Li, G.; Rosi, N. L.; Yoon, B.; Barnett, R. N.; Whetten, R. L.; Landman, U.; Jin, R. *Angewandte Chemie* **2012**, *124*, 13291.

(29) Nimmala, P. R.; Knoppe, S.; Jupally, V. R.; Delcamp, J. H.; Aikens, C. M.; Dass, A. *The Journal of Physical Chemistry B* **2014**, *118*, 14157.

(30) Schaaff, T. G.; Knight, G.; Shafigullin, M. N.; Borkman, R. F.; Whetten, R. L. *The Journal of Physical Chemistry B* **1998**, *102*, 10643.

(31) Dass, A.; Stevenson, A.; Dubay, G. R.; Tracy, J. B.; Murray, R. W. *Journal of the American Chemical Society* **2008**, *130*, 5940.

(32) Negishi, Y.; Nobusada, K.; Tsukuda, T. *Journal of the American Chemical Society* **2005**, *127*, 5261.

(33) Creighton, J. A.; Eadon, D. G. *Journal of the Chemical Society, Faraday Transactions* **1991**, *87*,

3881.
(34) Perenboom, J. A. A. J.; Wyder, P.; Meier, F. *Physics Reports* **1981**, *78*, 173.
(35) Nimmala, P. R.; Dass, A. *J. Am. Chem. Soc.* **2011**, *133*, 9175.
(36) Chen, S. W.; Ingram, R. S.; Hostetler, M. J.; Pietron, J. J.; Murray, R. W.; Schaaff, T. G.; Khoury, J. T.; Alvarez, M. M.; Whetten, R. L. *Science* **1998**, *280*, 2098.
(37) Murray, R. W. *Chem. Rev.* **2008**, *108*, 2688.
(38) Schaaff, T. G.; Shafigullin, M. N.; Khoury, J. T.; Vezmar, I.; Whetten, R. L.; Cullen, W. G.; First, P. N.; GutierrezWing, C.; Ascensio, J.; JoseYacaman, M. J. *J. Phys. Chem. B* **1997**, *101*, 7885.
(39) Wyrwas, R. B.; Alvarez, M. M.; Khoury, J. T.; Price, R. C.; Schaaff, T. G.; Whetten, R. L. *European Physical Journal D* **2007**, *43*, 91.
(40) Walter, M.; Akola, J.; Lopez-Acevedo, O.; Jadzinsky, P. D.; Calero, G.; Ackerson, C. J.; Whetten, R. L.; Gronbeck, H.; Hakkinen, H. *Proc. Natl. Acad. Sci. U.S.A.* **2008**, *105*, 9157.
(41) Dass, A. *Nanoscale* **2012**, *4*, 2260.
(42) Dass, A. *J. Am. Chem. Soc.* **2011**, *133*, 19259.
(43) Qian, H.; Zhu, Y.; Jin, R. *Proc. Natl. Acad. Sci.* **2012**, *109*, 696.
(44) Faraday, M. *Philos. Trans. R. Soc. London* **1857**, *147*, 145.
(45) Jadzinsky, P. D.; Calero, G.; Ackerson, C. J.; Bushnell, D. A.; Kornberg, R. D. *Science* **2007**, *318*, 430.
(46) Heaven, M. W.; Dass, A.; White, P. S.; Holt, K. M.; Murray, R. W. *J. Am. Chem. Soc.* **2008**, *130*, 3754.
(47) Akola, J.; Walter, M.; Whetten, R. L.; Hakkinen, H.; Gronbeck, H. *J. Am. Chem. Soc.* **2008**, *130*, 3756.
(48) Zhu, M.; Aikens, C. M.; Hollander, F. J.; Schatz, G. C.; Jin, R. *J. Am. Chem. Soc.* **2008**, *130*, 5883.
(49) Dass, A.; Stevenson, A.; Dubay, G. R.; Tracy, J. B.; Murray, R. W. *J. Am. Chem. Soc.* **2008**, *130*, 5940.
(50) Qian, H.; Zhu, Y.; Jin, R. *ACS Nano* **2009**, *3*, 3795.
(51) Hakkinen, H. *Nat Chem* **2012**, *4*, 443.
(52) Pei, Y.; Pal, R.; Liu, C.; Gao, Y.; Zhang, Z.; Zeng, X. C. *J. Am. Chem. Soc.* **2012**, *134*, 3015.
(53) Jiang, D. E.; Dai, S. *Inorg. Chem.* **2009**, *48*, 2720.
(54) Aikens, C. M. *J. Phys. Chem. C.* **2008**, *112*, 19797.
(55) Pei, Y.; Gao, Y.; Zeng, X. C. *J. Am. Chem. Soc.* **2008**, *130*, 7830.
(56) Jin, R. *Nanoscale* **2010**, *2*, 343.
(57) Levi-Kalisman, Y.; Jadzinsky, P. D.; Kalisman, N.; Tsunoyama, H.; Tsukuda, T.; Bushnell, D. A.; Kornberg, R. D. *J. Am. Chem. Soc.* **2011**, *133*, 2976.
(58) Schaaff, T. G.; Whetten, R. L. *J. Phys. Chem. B* **1999**, *103*, 9394.
(59) Cleveland, C. L.; Landman, U.; Schaaff, T. G.; Shafigullin, M. N.; Stephens, P. W.; Whetten, R. L. *Phys. Rev. Lett.* **1997**, *79*, 1873.
(60) Dass, A. *Journal of the American Chemical Society* **2009**, *131*, 11666.
(61) Dharmaratne, A. C.; Krick, T.; Dass, A. *Journal of the American Chemical Society* **2009**, *131*, 13604.
(62) Barnett, R. N.; Landman, U. *Physical Review B* **1993**, *48*, 2081.
(63) Troullier, N.; Martins, J. L. *Physical Review B* **1991**, *43*, 1993.
(64) Perdew, J. P.; Burke, K.; Ernzerhof, M. *Phys. Rev. Lett.* **1997**, *78*, 1396.
(65) Tsunoyama, H.; Negishi, Y.; Tsukuda, T. *J. Am. Chem. Soc.* **2006**, *128*, 6036.
(66) Nimmala, P. R.; Dass, A. *Journal of the American Chemical Society*, *133*, 9175.
(67) Chaki, N. K.; Negishi, Y.; Tsunoyama, H.; Shichibu, Y.; Tsukuda, T. *J. Am. Chem. Soc.* **2008**, *130*, 8608.
(68) *Even though the Au4L4 loss in MALDI-TOF remains valid as discussed in our earlier report, we believe that the previous assignment was erroneous due to calibration error in MALDI TOF MS.*
(69) Alvarez, M. M.; Khoury, J. T.; Schaaff, T. G.; Shafigullin, M. N.; Vezmar, I.; Whetten, R. L. *J. Phys. Chem. B* **1997**, *101*, 3706.
(70) Ingram, R. S.; Hostetler, M. J.; Murray, R. W.; Schaaff, T. G.; Khoury, J. T.; Whetten, R. L.;

Bigioni, T. P.; Guthrie, D. K.; First, P. N. *J. Am. Chem. Soc.* **1997**, *119*, 9279.
(71) Hicks, J. F.; Templeton, A. C.; Chen, S. W.; Sheran, K. M.; Jasti, R.; Murray, R. W.; Debord, J.; Schaaf, T. G.; Whetten, R. L. *Anal. Chem.* **1999**, *71*, 3703.
(72) Hicks, J. F.; Miles, D. T.; Murray, R. W. *J. Am. Chem. Soc.* **2002**, *124*, 13322.
(73) Guo, R.; Georganopoulou, D.; Feldberg, S. W.; Donkers, R.; Murray, R. W. *Anal. Chem.* **2005**, *77*, 2662.
(74) Su, B.; Zhang, M.; Shao, Y.; Girault, H. H. *J. Phys. Chem. B.* **2006**, *110*, 21460.
(75) Holm, A. H.; Ceccato, M.; Donkers, R. L.; Fabris, L.; Pace, G.; Maran, F. *Langmuir* **2006**, *22*, 10584.
(76) Terrill, R. H.; Postlethwaite, T. A.; Chen, C.-h.; Poon, C.-D.; Terzis, A.; Chen, A.; Hutchison, J. E.; Clark, M. R.; Wignall, G. *Journal of the American Chemical Society* **1995**, *117*, 12537.
(77) Whetten, R. L.; Shafigullin, M. N.; Khoury, J. T.; Schaaff, T. G.; Vezmar, I.; Alvarez, M. M.; Wilkinson, A. *Accounts of Chemical Research* **1999**, *32*, 397.
(78) Cleveland, C. L.; Landman, U. *J. Chem. Phys.* **1991**, *94*, 7376.
(79) Tracy, J. B.; Crowe, M. C.; Parker, J. F.; Hampe, O.; Fields-Zinna, C. A.; Dass, A.; Murray, R. W. *J. Am. Chem. Soc.* **2007**, *129*, 16209.
(80) Negishi, Y.; Chaki, N. K.; Shichibu, Y.; Whetten, R. L.; Tsukuda, T. *J. Am. Chem. Soc.* **2007**, *129*, 11322.
(81) Pei, Y.; Zeng, X. C. *Nanoscale* **2012**, *4*, 4054.
(82) Donkers, R. L.; Lee, D.; Murray, R. W. *Langmuir* **2004**, *20*, 1945.
(83) Qian, H.; Jin, R. *Nano Lett.* **2009**, *9*, 4083.
(84) Qian, H.; Zhu, M.; Andersen, U. N.; Jin, R. *The Journal of Physical Chemistry A* **2009**, *113*, 4281.
(85) Knoppe, S.; Dolamic, I.; Dass, A.; Bürgi, T. *Angew. Chem. Int. Ed.* **2012**, *51*, 7589.
(86) Knoppe, S.; Boudon, J.; Dolamic, I.; Dass, A.; BuÃàrgi, T. *Analytical Chemistry* **2011**, *83*, 5056.
(87) Dass, A.; Stevenson, A.; Dubay, G. R.; Tracy, J. B.; Murray, R. W. *J. Am. Chem. Soc.* **2008**, *130*, 5940.
(88) Templeton, A. C.; Hostetler, M. J.; Warmoth, E. K.; Chen, S. W.; Hartshorn, C. M.; Krishnamurthy, V. M.; Forbes, M. D. E.; Murray, R. W. *J. Am. Chem. Soc.* **1998**, *120*, 4845.
(89) Das, A.; Liu, C.; Zeng, C.; Li, G.; Li, T.; Rosi, N. L.; Jin, R. *The Journal of Physical Chemistry A* **2014**, *118*, 8264.
(90) Qian, H.; Jin, R. *Chemistry of Materials* **2011**, *23*, 2209.
(91) Lopez-Acevedo, O.; Akola, J.; Whetten, R. L.; Grönbeck, H.; Häkkinen, H. *The Journal of Physical Chemistry C* **2009**, *113*, 5035.
(92) Chen, S.; Murray, R. W. *Langmuir* **1998**, *15*, 682.
(93) Zeng, C.; Li, T.; Das, A.; Rosi, N. L.; Jin, R. *J. Am. Chem. Soc.* **2013**, *135*, 10011.
(94) Dass, A.; Nimmala, P. R.; Jupally, V. R.; Kothalawala, N. *Nanoscale* **2013**.
(95) Price, R. C.; Whetten, R. L. *Journal of the American Chemical Society* **2005**, *127*, 13750.
(96) Dolomanov, O. V.; Bourhis, L. J.; Gildea, R. J.; Howard, J. A. K.; Puschmann, H. *J. Appl. Crystallogr.* **2009**, *42*, 339.
(97) Mortensen, J.; Hansen, L.; Jacobsen, K. *Physical Review B* **2005**, *71*.
(98) Enkovaara, J.; Rostgaard, C.; Mortensen, J. J.; Chen, J.; Dulak, M.; Ferrighi, L.; Gavnholt, J.; Glinsvad, C.; Haikola, V.; Hansen, H. A.; Kristoffersen, H. H.; Kuisma, M.; Larsen, A. H.; Lehtovaara, L.; Ljungberg, M.; Lopez-Acevedo, O.; Moses, P. G.; Ojanen, J.; Olsen, T.; Petzold, V.; Romero, N. A.; Stausholm-Moller, J.; Strange, M.; Tritsaris, G. A.; Vanin, M.; Walter, M.; Hammer, B.; Hakkinen, H.; Madsen, G. K.; Nieminen, R. M.; Norskov, J. K.; Puska, M.; Rantala, T. T.; Schiotz, J.; Thygesen, K. S.; Jacobsen, K. W. *Journal of physics. Condensed matter : an Institute of Physics journal* **2010**, *22*, 253202.
(99) Perdew, J. P.; Burke, K.; Ernzerhof, M. *Phys. Rev. Lett.* **1996**, *77*, 3865.
(100) Suzuki, N.; Shiba, K.; Tsukuda, T.; Nakamura, T. *Ieice Transactions on Electronics* **2002**, *E85C*, 93.
(101) Tang, W.; Sanville, E.; Henkelman, G. *Journal of physics. Condensed matter : an Institute of Physics journal* **2009**, *21*, 084204.
(102) Walter, M.; Akola, J.; Lopez-Acevedo, O.; Jadzinsky, P. D.; Calero, G.; Ackerson, C. J.; Whetten, R. L.; Gronbeck, H.; Hakkinen, H. *Proc Natl Acad Sci U S A* **2008**, *105*, 9157.

(103) Lopez-Acevedo, O.; Tsunoyama, H.; Tsukuda, T.; Hakkinen, H.; Aikens, C. M. *J Am Chem Soc* **2010**, *132*, 8210.

(104) te Velde, G.; Bickelhaupt, F. M.; Baerends, E. J.; Fonseca Guerra, C.; van Gisbergen, S. J. A.; Snijders, J. G.; Ziegler, T. *Journal of Computational Chemistry* **2001**, *22*, 931.

(105) van Leeuwen, R.; Baerends, E. J. *Physical Review A* **1994**, *49*, 2421.

(106) van Lenthe, E.; Baerends, E. J.; Snijders, J. G. *The Journal of Chemical Physics* **1994**, *101*, 9783.

(107) van Lenthe, E.; Ehlers, A.; Baerends, E.-J. *J. Chem. Phys.* **1999**, *110*, 8943.

(108) Chen, S.; Murray, R. W. *The Journal of Physical Chemistry B* **1999**, *103*, 9996.

(109) Quinn, B. M.; Liljeroth, P.; Ruiz, V.; Laaksonen, T.; Kontturi, K. s. *J. Am. Chem. Soc.* **2003**, *125*, 6644.

(110) Alvarez, M. M.; Khoury, J. T.; Schaaff, T. G.; Shafigullin, M.; Vezmar, I.; Whetten, R. L. *Chem. Phys. Lett.* **1997**, *266*, 91.

(111) Chaki, N. K.; Negishi, Y.; Tsunoyama, H.; Shichibu, Y.; Tsukuda, T. *J. Am. Chem. Soc.* **2008**, *130*, 8608.

(112) Gies, A. P.; Nonidez, W. K.; Ellison, S. T.; Ji, H. L.; Mays, J. W. *Anal. Chem.* **2005**, *77*, 780.

(113) Guo, R.; Murray, R. W. *Journal of the American Chemical Society* **2005**, *127*, 12140.

(114) Schaaff, T. G.; Shafigullin, M. N.; Khoury, J. T.; Vezmar, I.; Whetten, R. L. *J. Phys. Chem. B* **2001**, *105*, 8785.

(115) Dass, A. *Journal of the American Chemical Society*, *133*, 19259.

(116) Zeng, C.; Liu, C.; Pei, Y.; Jin, R. *ACS Nano* **2013**, *7*, 6138.

(117) Tiwari, P.; Vig, K.; Dennis, V.; Singh, S. *Nanomaterials* **2011**, *1*, 31.

(118) DeLong, R. K.; Reynolds, C. M.; Malcolm, Y.; Schaeffer, A.; Severs, T.; Wanekaya, A. *Nanotechnology, Science and Applications* **2010**, *3*, 53.

VITA

VITA

Praneeth Reddy Nimmala [PhD]

1903 Anderson Rd, Apt B6, Oxford, MS. 38655.
Phone: 601-594-9197
Email: praneeth0210@gmail.com

EDUCATION/PROFESSIONAL BACKGROUND

- **Degrees**

- Industrial experience : Internship (Lam research corp, Fremont, CA)
- 2010-May, 2014 (Dec) : Ph.D Chemistry, University of Mississippi, MS
- 2009-2010 : MS Chemistry Mississippi College, MS.
- 2005-2009 : Bachelor's in Pharmacy, Osmania University, India

- **Awards and Honors**

Award	Venue	Time	Type
3rd prize	Lam Research corp-Interns poster competition	Aug, 2013	Poster
3rd prize	Mississippi Academy of Sciences	Feb, 2013	Oral
3rd prize	ACS-local section	Nov, 2012	Poster
3rd prize	NSF-EPSCoR	Apr, 2012	Poster
1st prize	Graduate School Council	Apr, 2012	Poster
3rd prize	ACS-local section	Oct, 2011	Poster
Travel	To Univ of Geneva, Switzerland	Oct, 2011	Collaboration
Travel	To Univ of Geneva, Switzerland	Nov, 2013	Collaboration

SCIENTIFC PUBLICATIONS

- **Published (8 articles)**

- "$Au_{36}(SPh)_{23}$ Nanomolecules", **Praneeth Reddy Nimmala** and Amala Dass, *Journal of American Chemical Society*, **2011**, *133*, 9175-9177.
- "$Au_{67}(SR)_{35}$ Nanomolecules: Characteristic Size-Specific Optical, Electrochemical, Structural Properties and First-Principles Theoretical Analysis", **Praneeth Reddy Nimmala** ,Yoon B, Whetten RL, Landman U, Dass A, *Journal of Physical Chemistry A*, **2013**, *117*, 504-517.
- "$Au_{103}(SR)_{45}$, $Au_{104}(SR)_{45}$, $Au_{104}(SR)_{46}$, $Au_{105}(SR)_{46}$ nanoclusters", Amala Dass, **Praneeth Reddy Nimmala**, Vijay Jupally and Nuwan Kothalawala. *Nanoscale***,** **2013,***5***,** 12082-12085.
- "Isolation of Bright Blue Light-Emitting CdSe Nanocrystals with 6.5 kDa Core in Gram Scale: High Photoluminescence Efficiency Controlled by Surface Ligand Chemistry", Sukanta Dolai, **Praneeth R. Nimmala**, Manik Mandal, Barry B. Muhoberac, Karl Drial, Amala Dass and Rajesh Sardar. *Chemistry of Materials,* **2014**, *26 (2),* pp 1278–1285.
- "Core size conversion: Route for exclusive synthesis of Au_{38} and Au_{40}", **Praneeth Reddy Nimmala**, Vijay Jupally and Amala Dass. *Langmuir*. **2014** *Mar 11;30(9):2490-7*.
- "$Au_{137}(SR)_{56}$ nanomolecules: composition, optical spectroscopy, electrochemistry and electrocatalytic reduction of CO_2" Vijay Reddy Jupally, Asantha C Dharmaratne, David Crasto, Aron J Huckaba, Chanaka Kumara, **Praneeth Reddy Nimmala**, Nuwan Kothalawala, Jared H. Delcamp and Amala Dass. *Chem. Commun.*, **2014**,*50*, 9895-9898.
- "$Au_{36}(SPh)_{24}$ Nanomolecules: X-ray Crystal Structure, Optical Spectroscopy, Electrochemistry and Theoretical Analysis" **Nimmala, Praneeth**; Knoppe, Stefan; Jupally, Vijay; Delcamp, Jared; Aikens, Christine; Dass, Amala. *J. Phys. Chem. B*, **2014**, 118 (49), pp 14157–14167.
- "$Au_{99}(SPh)_{42}$ Nanomolecules: Aromatic Thiolate Ligand Induced Conversion of $Au_{144}(SCH_2CH_2Ph)_{60}$" **Praneeth Reddy Nimmala** and Amala Dass. *J. Am. Chem. Soc.*, **2014**, 136 (49), pp 17016–17023.

SUMMARY OF TECHNICAL SKILLS

- As an analytical chemist, effectively handled following sophisticated analytical instruments on a daily basis:
    a. Mass spectrometry (MALDI-MS Autoflex 1 and 2, Waters QTOF ESI-MS)
    b. Powder X-ray diffraction of nanoparticles
    c. Separation techniques like Chromatography (HPLC and SEC)
    d. Optical microscopy, Scanning electron microscopy and Atomic force microscopy
    e. Electrochemical plating of semiconductors, Electroless depostion,

Electrochemical analysis (cyclic voltammetry and differential pulse voltammetry)

- **PhD Dissertation**

  Title: "Gold nanomolecules : Developing synthetic protocols, characterization and investigating the ligand effects on structure and properties"

  Advisor: Amala Dass

- **Summary:** My PhD research in Nanotechnology was focussed on development of new synthetic protocols for improving the yield and purity of Gold nanoparticle which are chemical molecules comprising of gold atoms and organic ligands. The typical size range of these particles is 1-5 nm with potential applications in catalysis, energy storage devices and drug delivery.

INDUSTRIAL EXPOSURE (LAM)

- **Internship** : Lam Research Corporation (Fremont, California) **May-August 2013**
- Quick learning, focussed work, adjusting with colleagues, and other members at higher levels of the hierarchy.
- Worked in glove box in wet chemistry lab on alternate metallization using Electroless deposition (ELD) of cobalt on W/WN substrate.
- I had the opportunity to observe how the plating experiments were scaled up on tools after successful R&D experiments on small scale.
- At the end, I have competed with other student interns in Interns poster competition (with 63 interns) and got 4th place.

RECOMMENDATIONS

- Dr. Amala Dass (my PhD research advisor), Assosiate Professor and faculty of analytical chemistry, University of Mississippi (amal@olemiss.edu, 662-915-1826)
- Dr. James Cizdziel (my PhD committee member), Associate Professor and faculty of analytical chemistry, University of Mississippi (cizdziel@olemiss.edu, 662-915-1814)